CGSN Site Characterization: Pioneer Mid-Atlantic Bight Array

Control Number: 3210-00007
Version: 2-00
Date: 2024-02-13
Author: A. Plueddemann, A. Macdonald, A. Ramsey

Coastal and Global Scale Nodes
Ocean Observatories Initiative
Woods Hole Oceanographic Institution

Template 3101-00100 Version 1-01

Revision History

Version	Description	ECR No.	Release Date
0-01	Initial draft		
0-02	Review, edits		
1-00	Initial Release	ECR-947	2023-02-07
1-01	Addition of Reference list to Section 5.0	ECR-1102	2023-09-28
2-00	Updates to Offshore site locations, modifications to figures, additions to Tide section	ECR-1163	2024-02-13

Table of Contents

List of Figures

List of Tables

1.0 Introduction

1.1. Scope

This report describes sea surface, seafloor and ocean conditions in the vicinity of the Pioneer Mid-Atlantic Bight (MAB) Array. The configuration of moored and mobile assets for the Pioneer MAB Array are described in OOI document 3210-00008 CGSN Site Design: Pioneer Mid-Atlantic Bight Array (Buffitt, et al., 2023). Seafloor conditions are described first - assessment of regional bathymetry was necessary in order to adjust the proposed mooring locations to obtain the desired geographic layout and water depths. Oceanographic conditions, focusing on currents, temperature-salinity (T-S) properties, and stratification, are described next. Finally, surface conditions, including wind, waves, storm events, and solar radiation are presented.

1.2. Background

The Pioneer Array is a multi-scale array utilizing fixed and mobile assets to provide observations spanning the continental shelf and slope (Gawarkiewicz and Plueddemann, 2020). The Array was designed to be relocatable, suitable for moderate wind, wave and current conditions in water depths of approximately 100-600 m. After initial deployment on the New England Shelf (NES), the Pioneer Array will be relocated in the spring of 2024 to a location off the coast of North Carolina. The proposed site is in the southern part of the MAB, typically defined as encompassing the continental shelf and slope between Cape Hatteras, NC and Martha's Vineyard, MA.

A review of environmental conditions in the southern MAB region is necessary to refine the array layout, determine mooring locations and depths, assess mooring performance, provide the expected density range for ballasted elements (e.g. gliders, wire following profilers) and inform other aspects of array performance such as power generation by solar radiation.

The consensus concept for the Pioneer MAB array, developed from community input at NSF-sponsored Innovations Labs held during March and June of 2021, was for a moored array within a roughly 60 x 60 km box offshore of Nags Head, North Carolina. There was also a recommendation to extend the reach of observations by utilizing gliders in a larger domain. In order to assess regional environmental characteristics, three regions were defined: (Figure 1-1).

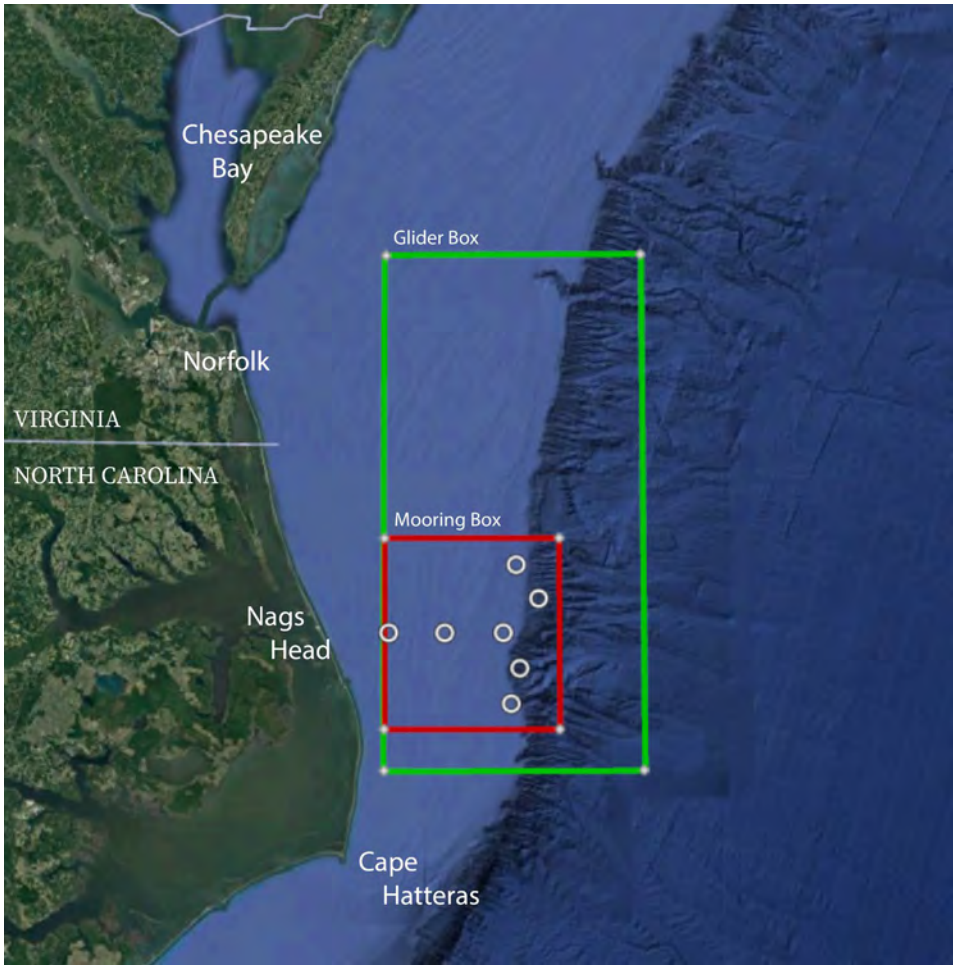

Figure 1-1 – Southern MAB Pioneer Array regions.
The red Mooring Box indicates the region where moorings would be located (originally proposed mooring locations denoted by white circles), and the green Glider Box indicates where the mobile assets (gliders and AUVs) would operate.

The regional bounding box, or "Big Box" includes slightly more (< 1° latitude and longitude) area than that covered by the broadest reaching instrumentation. The Big Box is useful for extracting gridded data, e.g., from a bathymetry database, or a regional model, to ensure there is enough regional coverage and larger scale variability is visible. The Big Box runs from just north of Chincoteague, VA - off Assateague Island at the border between VA and MD – to about 20 miles south of Cape Hatteras. Big Box WESN vertices = [-77.00 -73.00 34.83 38.00].

Table 1-1 – Pioneer Array Big Box Coordinates

Big Box	Lat (°N)	Lon (°E)
NW corner	38.0000	-77.0000
NE corner	38.0000	-73.0000
SE corner	34.8333	-73.0000
SW corner	34.8333	-77.0000

The potential glider operations region, or “Glider Box” is contained within the Big Box, and is where we expect all the Array elements (moorings, gliders, AUVs) to be located. It runs from just north of Chesapeake Bay (Kiptopeke, VA) to just north of Cape Hatteras (CH) – Cedar Island NC. Glider Box WESN vertices = [-75.37 -74.33 35.50 37.17].

Table 1-2 – Pioneer MAB Array Glider Box Coordinates

Glider Box	Lat (°N)	Lon (°E)
NW corner	37.1667	-75.3667
NE corner	37.1667	-74.3333
SE corner	35.5000	-74.3333
SW corner	35.5000	-75.3667

The Mooring Box is contained within the Glider Box, and is the area in which we expect all the mooring sites to be located. Ideally site characterization information for the moored array would come from other observing assets (e.g. NDBC moorings, process study moorings) within the Mooring Box. Mooring Box WESN vertices = [-75.37 -74.67 35.63 36.25].

Table 1-3 – Pioneer MAB Array Mooring Box Coordinates

Mooring Box	Lat (°N)	Lon (°E)
NW corner	36.2500	-75.3667
NE corner	36.2500	-74.6667
SE corner	35.6333	-74.6667
SW corner	35.6333	-75.3667

The Pioneer MAB Moored Array will consist of ten elements: Three Surface Moorings located in 30 m and 100 m water depths, five Profiler Moorings located in 100 m and 300 m water depths, and two Shallow Water Moorings located in 30 m water depths. These elements will be arranged in a sideways “T” shape with seven sites to capture both cross-shelf and along-shelf variability (Figure 1-2). Three of the sites will contain mooring pairs – a Surface Mooring adjacent to a Profiler Mooring. An assessment of regional bathymetry (Section 0) was used to refine the proposed mooring sites and determine latitude, longitude, and depth for each Site Center.

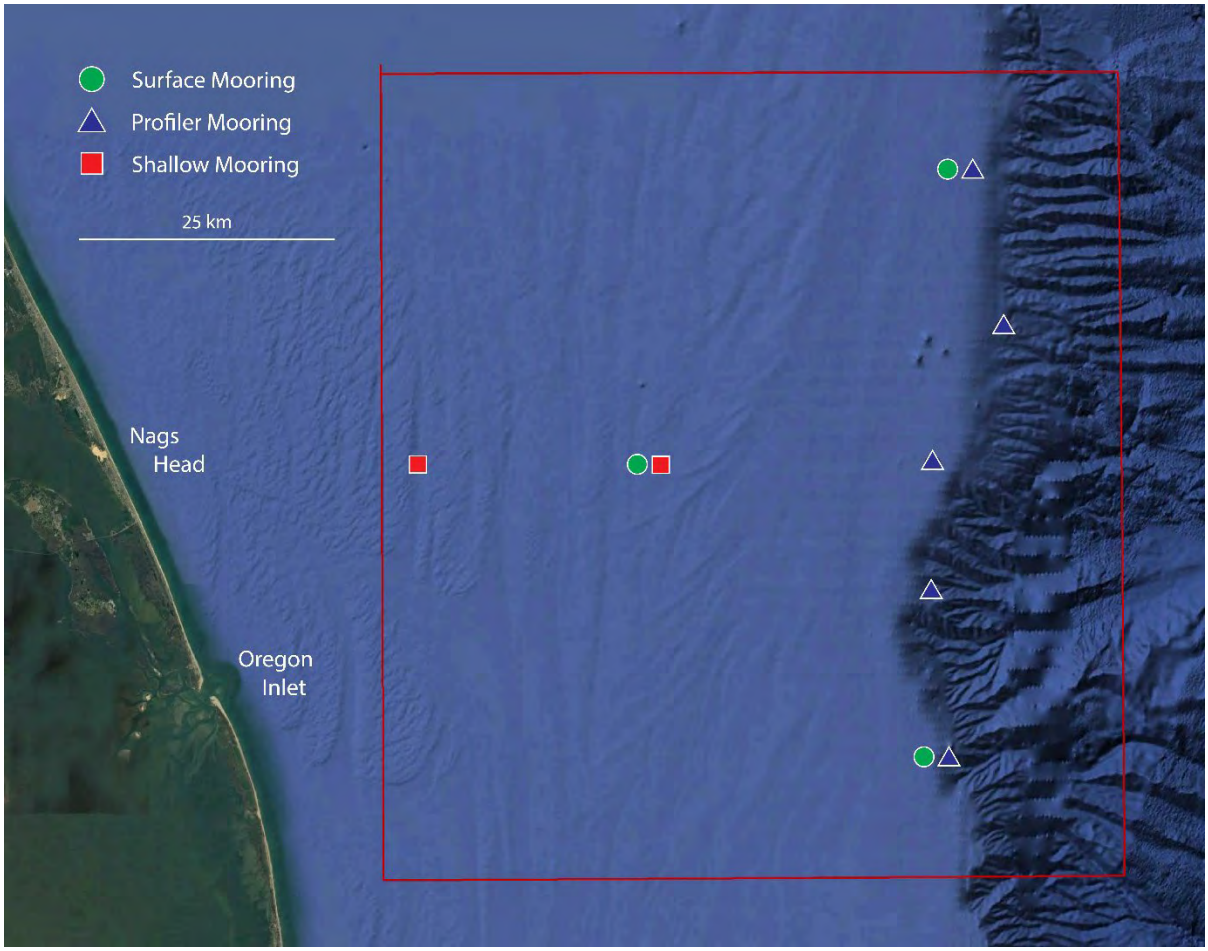

Figure 1-2 –Proposed mooring sites, and mooring types at each site, for the Pioneer MAB Array.

2.0 Seabed

2.1. Bathymetry

The investigation into the bathymetry in the region of the proposed mooring site is based on NOAA National Centers for Environmental Information (2023), Coastal Relief Models (CRMs), Volume 2, which covers the region 31°-40°N, 68°-85°W (Figure 2-1). (These data were formerly part of National Geophysical Data Center (NGDC). It covers the period from January 1999 to present and includes the following data sources: the U.S. National Ocean Service Hydrographic Database, the U.S. Geological Survey (USGS), the Monterey Bay Aquarium Research Institute, the U.S. Army Corps of Engineers. Topographic data are from the USGS and the Shuttle Radar Topography Mission. The CRM product has a grid cell size of 3 arc-seconds, or roughly 90 m. However, one should not assume that grid cell size equals horizontal resolution, at least not everywhere. The website suggests that one should assume a vertical accuracy of no better than 1 m.

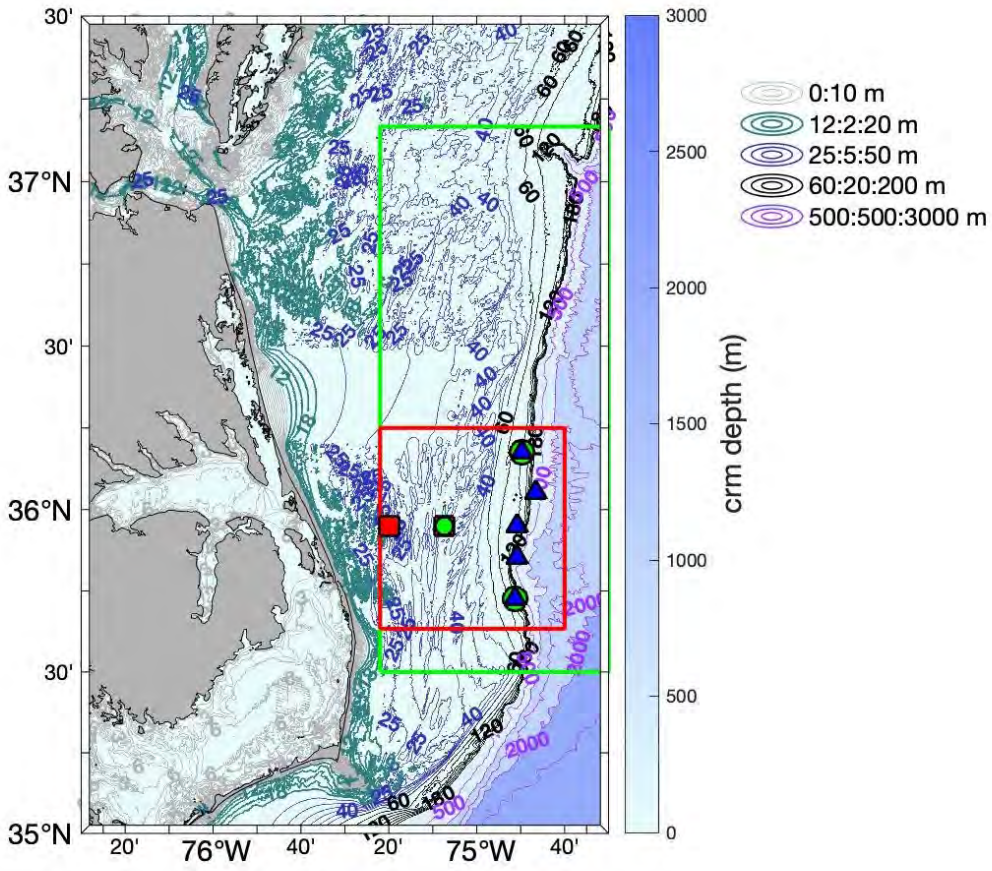

Figure 2-1 – CRM 3-arc second bathymetry (formerly NGDC) in the region of interest including the glider box (green) and mooring box (red). Bathymetry contour lines (grey, green blue, black, and cyan curves) are described in the legend and mooring symbols are defined in Figure 1-2.

Prior to choosing the CRM for examining the characteristics of the local bottom topography to determine “best” locations for the mooring deployments, several bathymetric products were considered. These included the NOAA soundings (Figure 2-2), as well as the Global bathymetry and topography at 15 arc sec: SRTM15+ (Tozer, 2019) and the General Bathymetric Chart of the Oceans (GEBCO) 2022 Grid (GEBCO, 2022) products (Figure 2-3). Both SRTM15+ and GEBCO-2022 have global extent. The former includes some 3.6 million

ship soundings and more than six years of non-repeat altimetry measurements (Tozer et al., 2019). The latter begins with SRTM15+, uses predicted depths based on the V31 gravity model (Sandwell et al., 2019), and is augmented with multibeam data from the Seabed 2030 Regional Centers. Multibeam image mosaics are available from NCEI, with output in the form of image (.tiff) files. A search of “NASA Bathymetry” produces the NASA GEBCO page on mapping near-shore shallows to a horizontal scale of 10 m available in three specific areas. However as of this writing this site did not include our area of interest.

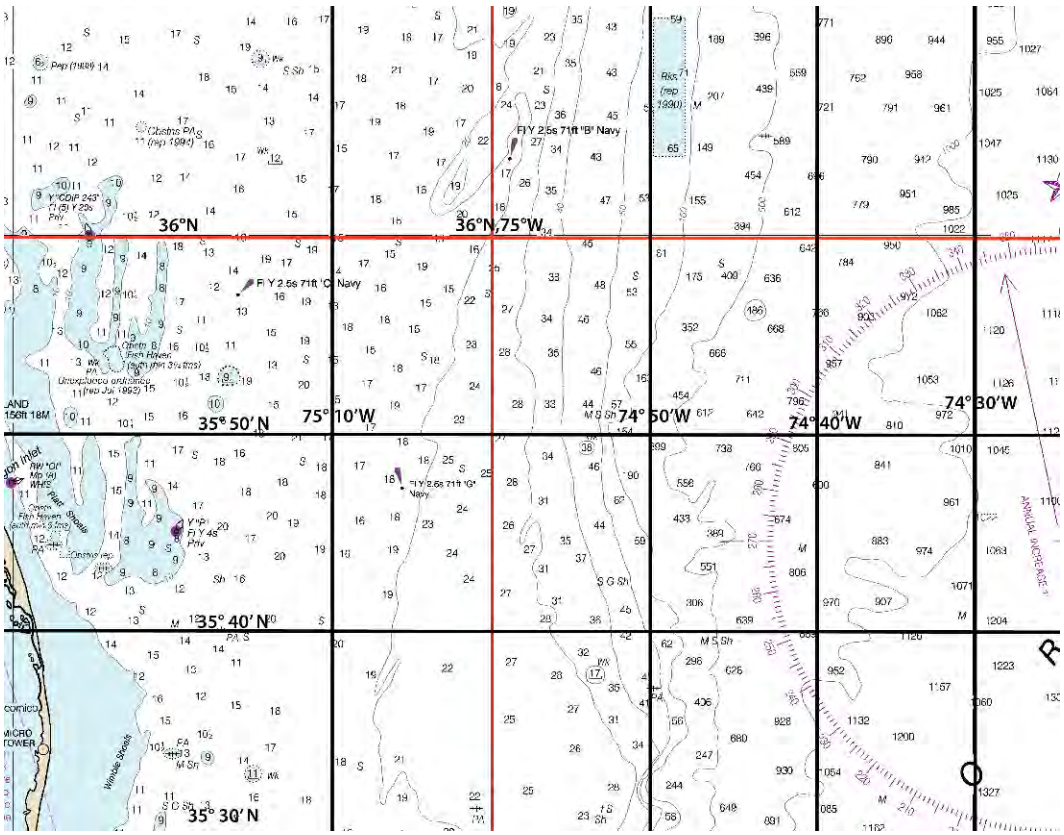

Figure 2-2 – A zoomed-in, cropped version of NOAA Soundings (m) Chart 12200 in the region of the Mooring Box (NOAA Office of Coast Survey, 2023).

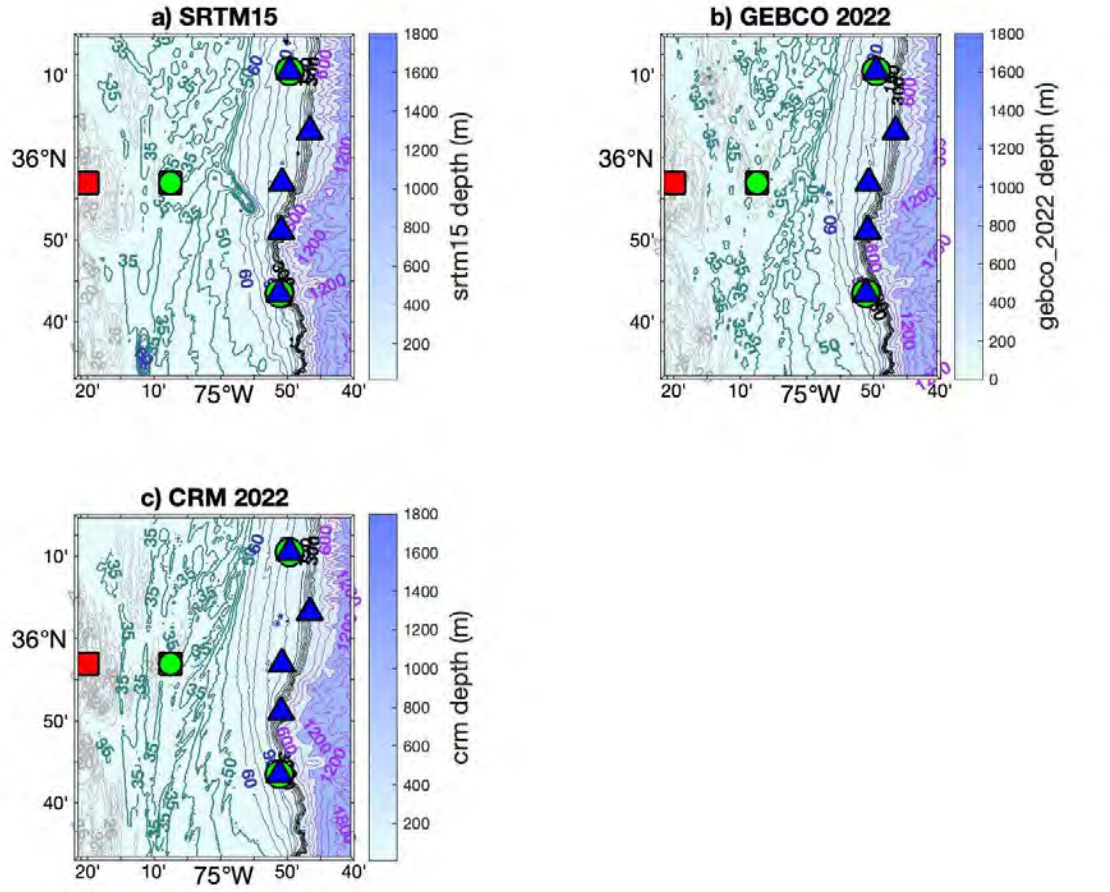

Figure 2-3 – Comparison of bathymetry products in region of the mooring box (red outline) with the preliminary mooring sites labeled as in Figure 1-2: a) Global bathymetry and topography at 15 arc sec: SRTM15+, (Tozer et al., 2019); b) GEBCO-2022 15 arc-second (GEBCO Group, 2022); and c) CRM-2022 3 arc-second (formerly NGDC). All panels have the same bathymetry contours (20:2:30 m grey, 35:5:50 green, 60:10:100 blue, 150:50:400 black, and 600:200:2000 purple).

Besides apparent resolution, the choice of bathymetric product was based on noting the peninsula-like feature running to the southeast of 35° 56'N, 75°W in SRTM15+ (Figure 2-3a) along what was determined to be a satellite track. In the GEBCO-2022 product (Figure 2-3b) that is an update of SRTM15+, this feature while still visible is less apparent, possibly because there is multibeam section that runs along this same track. In the coastally focused CRM product, the peninsula is not seen at all (Figure 2-3c). We also note that while the resolution is low, the soundings in the region (Figure 2-2) do not indicate any such peninsula-like feature.

Determining the location of the moored array Site Centers was an iterative process starting from the schematic array drawing (Figure 1-2), and then considering the desired site separations and depths on the regional bathymetry maps, along with potential water space conflicts (e.g. military operating areas, ship traffic fairways, offshore wind lease blocks, submarine cables and potential coral habitats; see OOI document 3210-00008, Buffitt et al., 2023). The optimal east-west line for the sideways "T" shaped array was determined to be 35° 57'N. The longitudes of the WE and CN sites were constrained by marine navigation fairways; the site depths were determined from the CRM depths at the desired latitude and longitude. The EA, NO and SO sites were planned to be along the 100 m isobath with a north-south separation of about 25 km. The site locations were determined from the location of the CRM 100 m isobath at 35° 57.0'N, 36° 10.5'N and 35° 43.5'N, respectively. The NE and SE sites

were planned to be along the 600 m isobath, with north-south separation of about 12.5 km from the moorings along the 100 m isobath. Based on input during the public comment period for the Supplemental Site Specific Environmental Assessment, the offshore moorings were shifted to 300 m. In-situ bathymetric surveys during the At-Sea Test 3 recovery cruise resulted in revised site centers. The desired north-south separation of about 12.5 km from the 100 m moorings was retained for the NE site. In order to avoid undesirable bathymetric features, the SE site was shifted to the north relative to the half-way point between CN and SO.

The resulting proposed Site Centers are shown in the table below (final site locations are controlled in 3210-00008). Sites are henceforth denoted by their two-letter code.

Table 2-1 – Proposed Mooring Site Center Locations

Mooring Site	Code	Lat (°N)	Lon (°E)
Western	WE	35.9500	-75.3333
Central	CN	35.9500	-75.1250
Eastern	EA	35.9500	-74.8457
Northern	NO	36.1750	-74.8267
Southern	SO	35.7250	-74.8530
Northeastern	NE	36.0536	-74.7776
Southeastern	SE	35.8514	-74.8482

The bathymetry in the region can be described as a broad coastal area with depths of less than 20 m, an inner shelf with depths to ~20 m, and a mid-shelf that extends depths of ~50 m. The shelf break is seen near 100 m with a precipitous drop to > 1000 m (Figure 2-4). The mooring box covers the region offshore of the inner shelf (25 – 30 m, moorings WE and CN) extending to the beginning of the slope to accommodate the 300 m moorings (NE and SE). Moorings NO, EA and SO are aligned along the 100 m isobath at the shelf break. For a sense of scale, the distance from WE to CN is about 19 km, from CN to EA about 25 km, and from NO to SO about 50 km.

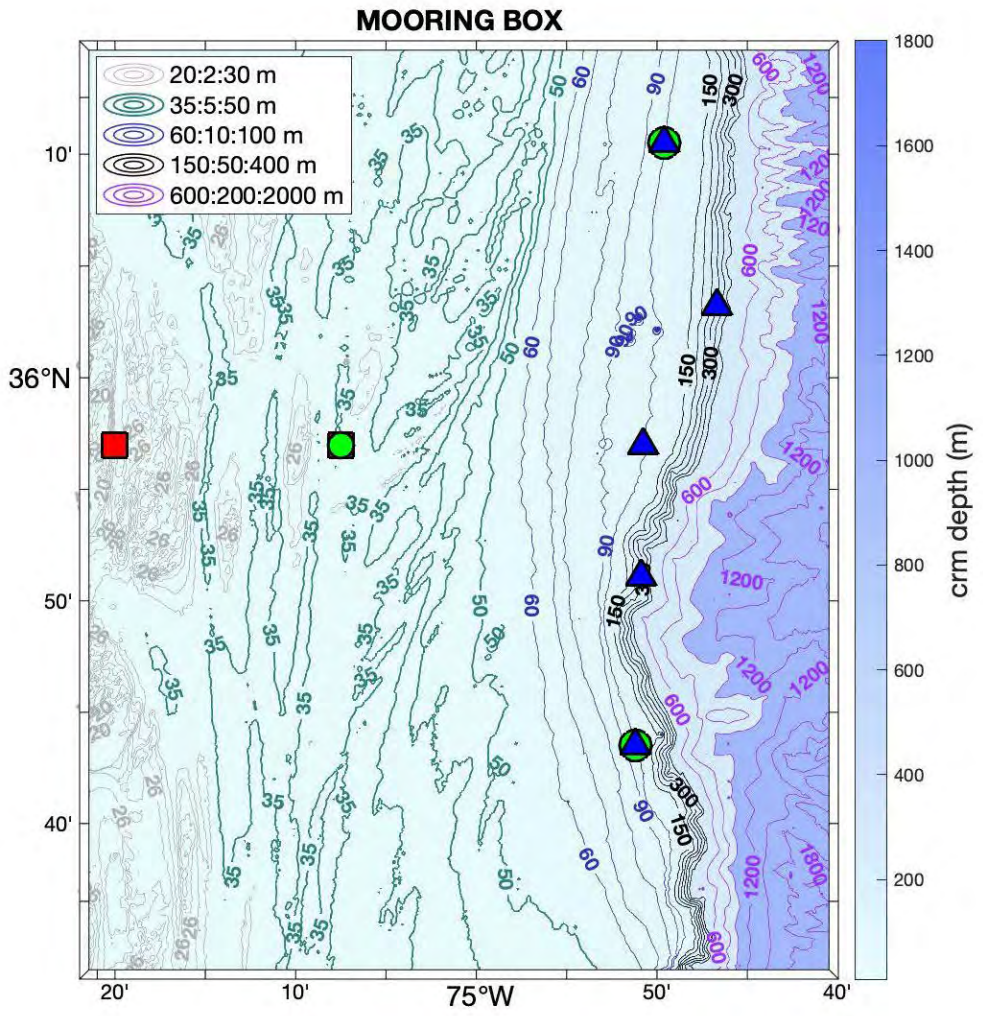

Figure 2-4 – The same as Figure 2-3c but zoomed in to provide a clearer illustration of the mooring box.

To visualize and compare the variability in bathymetry near the moorings (WE, CN, EA, NO, SO, NE and SE) as well as to determine longitudes to go with the latitudinal target positions assigned to all but the shallowest moorings (WE and CN), transects along the latitude of each mooring site were created using the CRM database (Figures 2-5a-e).

Figures 2-5 – East-West Transects across the mooring locations (a-e)

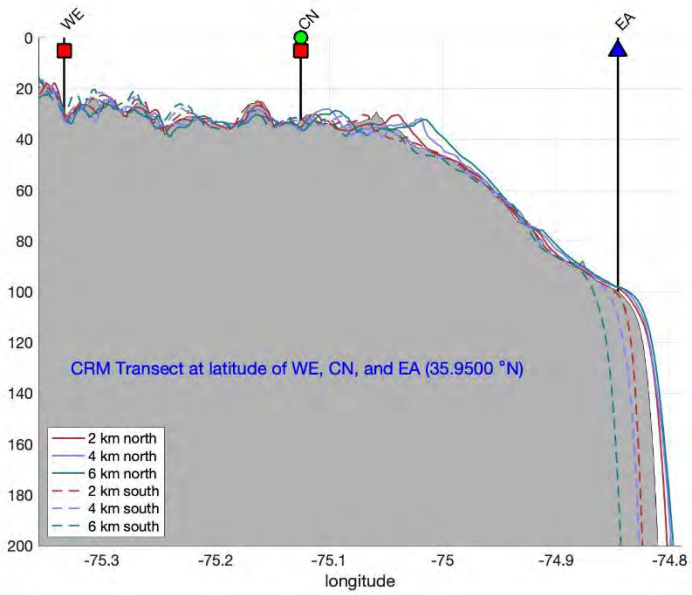

a) Transect along the latitude of the WE, CN and EA moorings (35° 57.00'N) based on CRM 3-arc second bathymetry (formerly NGDC). The longitude of WE and EA sites were chosen based on water space usage considerations; the resulting depths were determined from the bathymetry. The longitude of EA was determined by finding the first instance of a grid cell along this zonal line greater than 100 m and then using linear interpolation to find the longitude at 100 m.

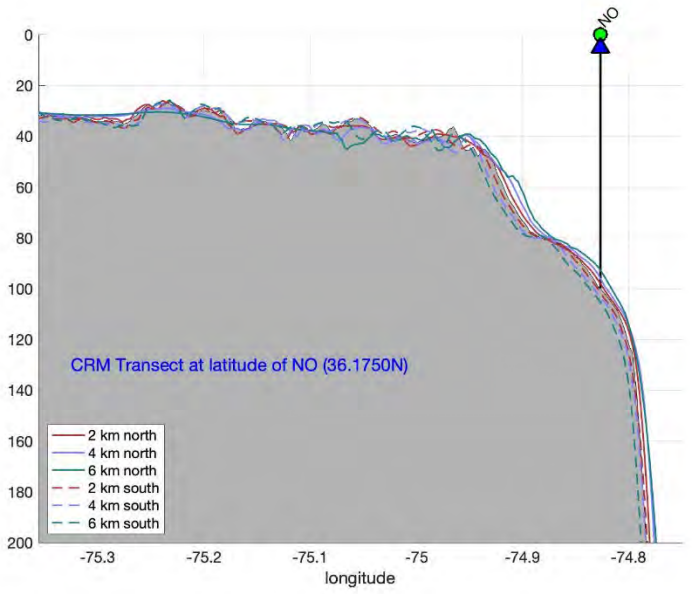

b) Transect along the latitude of the NO mooring (36° 10.50'N) based on CRM 3-arc second bathymetry (formerly NGDC). The longitude of NO was determined by finding the first instance of a grid cell along this zonal line greater than 100 m and then using a linear interpolation to find the longitude at 100 m.

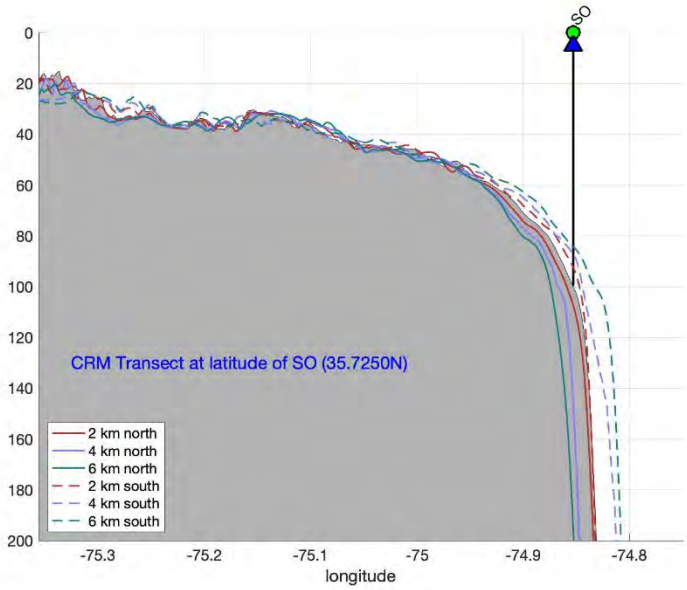

c) Transect along the latitude of the SO mooring (35° 43.50'N) based on CRM 3-arc second bathymetry (formerly NGDC). The longitude of SO as determined by finding the first instance of a grid cell along this zonal line greater than 100 m and then using a linear interpolation to find the longitude at 100 m.

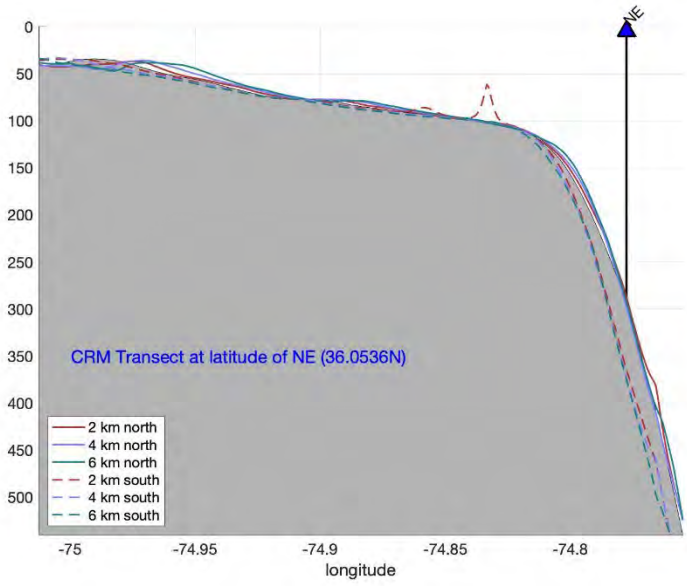

d) Transect along the latitude of the NE mooring (36° 3.217'N) based on CRM 3-arc second bathymetry (formerly NGDC). The longitude of NE as determined by finding the first instance of a grid cell along this zonal line greater than 300 m and then using a linear interpolation to find the longitude at 300 m.

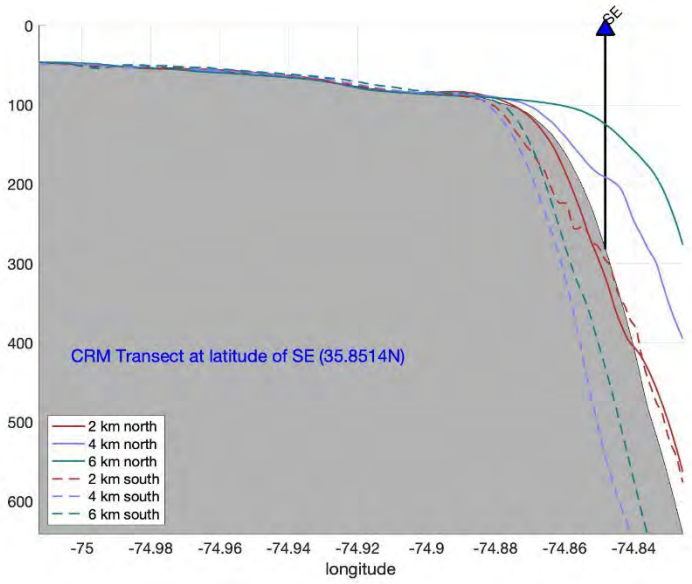

e) Transect along the latitude of the SE mooring (35° 51.083'N) based on CRM 3-arc second bathymetry (formerly NGDC). The longitude of SE as determined by finding the first instance of a grid cell along this zonal line greater than 300 m and then using a linear interpolation to find the longitude at 300 m

Site Maps – regional bathymetric maps in the vicinity (±2 km in latitude and longitude) of each mooring site - were made to illustrate the local depth characteristics (Figures 2-6a-g). It is useful to define the Site Center and Site Radius. The Site Center is the central location for a given mooring site. The Site Center is listed in array location tables and plotted on maps. However, the moorings are not typically located at the Site Center (although they should be within the Site Radius). The Site Radius for the Pioneer Array is a circular region within a radius of 1 km from the Site Center. A region, rather than an exact location, is necessary to allow for local-scale bathymetric features unresolved on available maps, uncertainties in "anchor-over" position, anchor fall-back during deployment, and to allow space for a replacement mooring to be deployed before the deployed mooring is recovered. These plan-view maps are centered on the Site Center and show the depth ranges to be encountered within the Site Radius. The maps also provide information on the likely impact, in terms of depth variation, of deployment targets being missed. Maps were created using the CRM database. (Figures 2-6a-e).

For the NO, EA and SO sites, the CRM bathymetric maps were used to assign a location at 100 m depth along the desired latitude line. Thus, the mapped locations for these sites appear exactly on the desired isobath. The WE and CN sites were located along the desired latitude based on water space constraints (e.g. shipping fairways), and are near the target depth of 30 m. The NE and SE sites were chosen based on multibeam swath bathymetry surveys conducted on the R/V *Armstrong* during the At-Sea Test 3 cruise. The steep, variable bathymetry at the NE and SE sites relative to the accuracy and resolution of the CRM bathymetry results in mapped locations that appear to be different from the target depths (e.g. NE at 295 m and SE at 280 m).

Figures 2-6 – Site Maps for each mooring location (a-g)

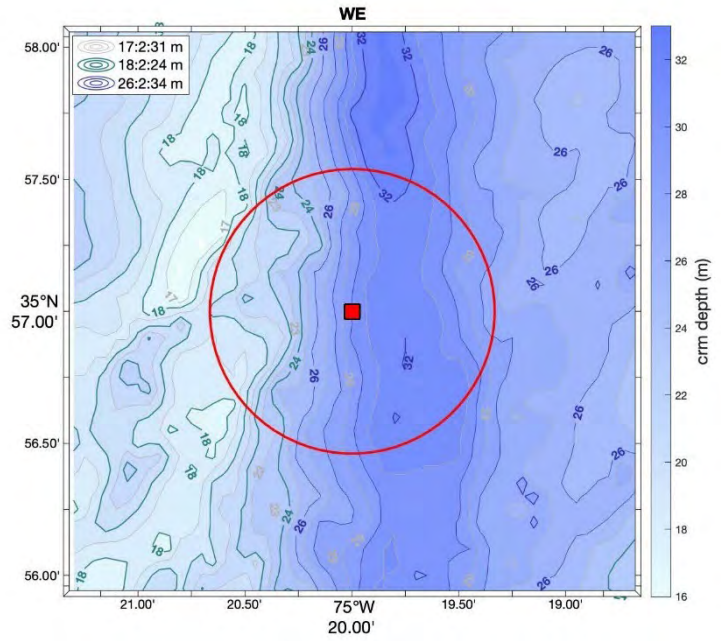

a) Map of the CRM 3-arc second bathymetry (formerly NGDC) in the mid-shelf region within ±2 km of the shallow (~30 m) westernmost mooring WE (red square). Red circle is the 1 km site radius from the site center. Bathymetric contour intervals are shown in the legend.

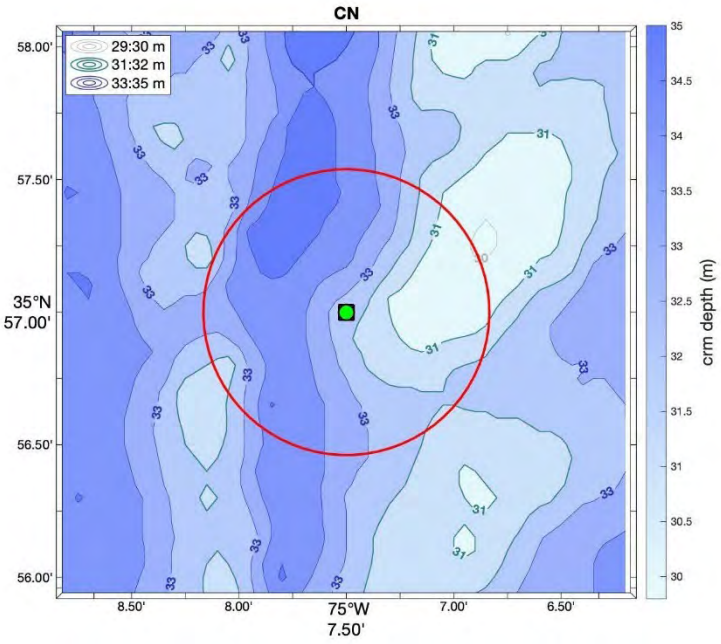

b) Map of the CRM 3-arc second bathymetry (formerly NGDC) in the mid-shelf region within ±2 km of shallow/surface mooring CN (red square/green circle). Red circle is the 1 km site radius from the site center. Bathymetric contour intervals are shown in the legend.

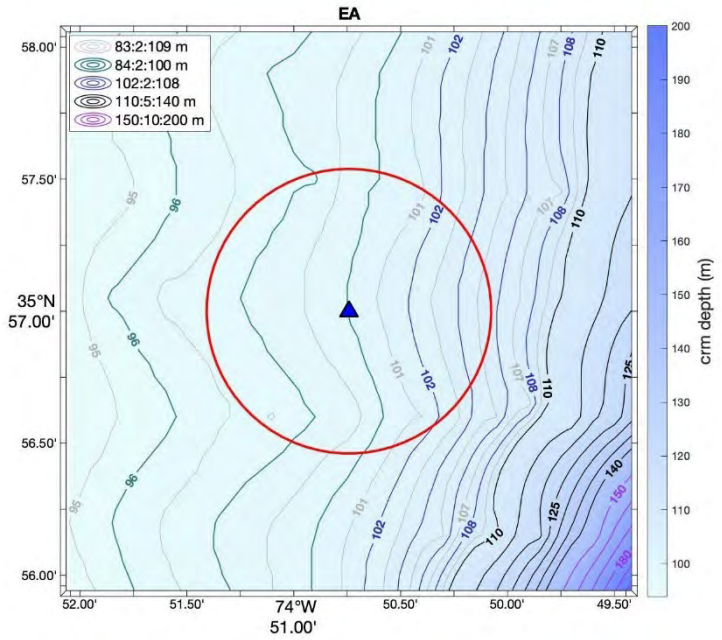

c) Map of the CRM 3-arc second bathymetry (formerly NGDC) in the shelf break region within ±2 km of the profiler mooring EA (blue triangle) located on the 100 m isobath. Red circle is the 1 km site radius from the site center. Bathymetric contour intervals are shown in the legend.

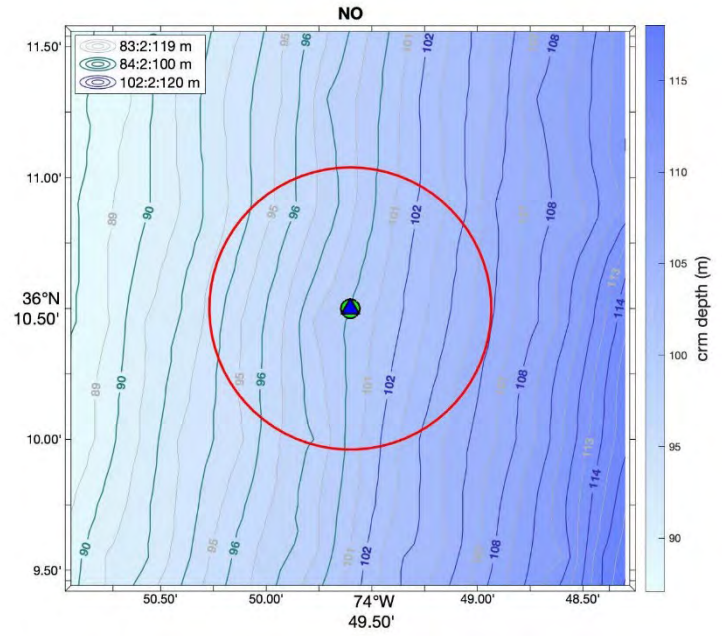

d) Map of the CRM 3-arc second bathymetry (formerly NGDC) in the shelf break region within ±2 km of the northern surface/profiler mooring NO (green circle/blue triangle) located on the 100 m isobath. Red circle is the 1 km site radius from the site center. Bathymetric contour intervals are shown in the legend.

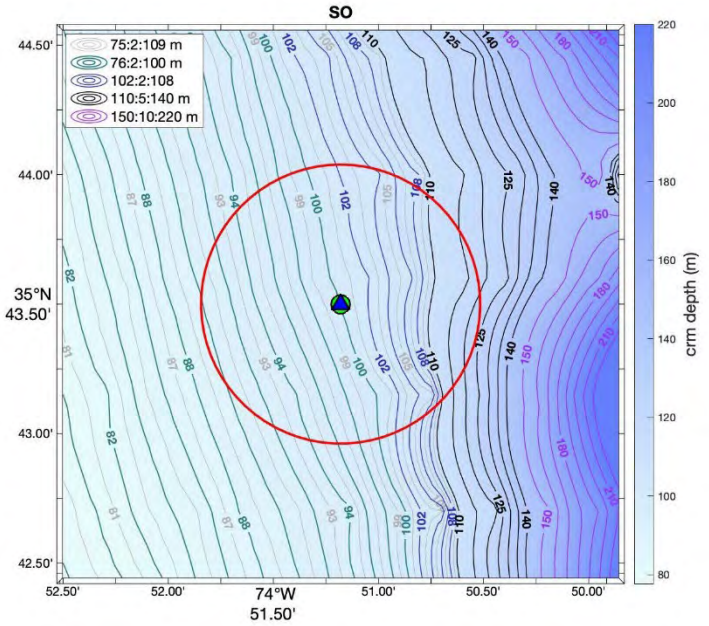

e) Map of the CRM 3-arc second bathymetry (formerly NGDC) in the shelf break region within ±2 km of the southern surface/profiler mooring SO (green circle/blue triangle) located on the 100 m isobath. Red circle is the 1 km site radius from the site center. Bathymetric contour intervals are shown in the legend.

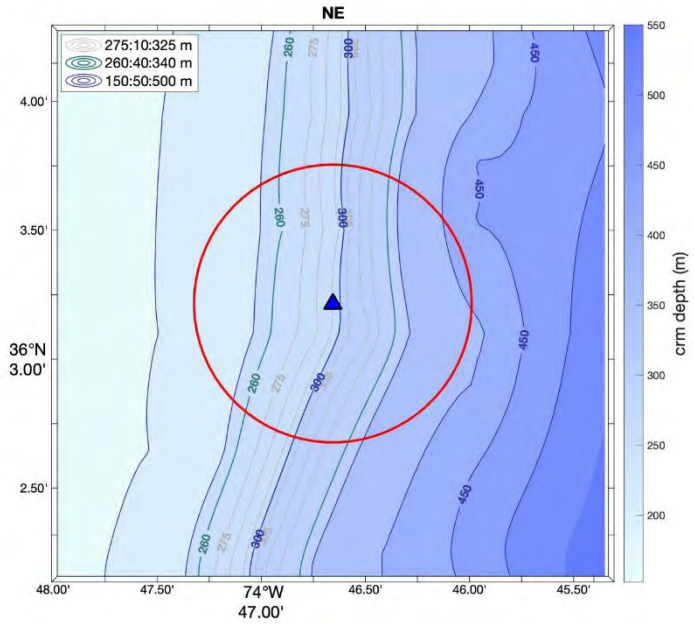

f) Map of the CRM 3-arc second bathymetry (formerly NGDC) in the slope region within ±2 km of the most northern and eastern profiler mooring NE (blue triangle) located near the 300 m isobath. Red circle is the 1 km site radius from the site center. Bathymetric contour intervals are shown in the legend.

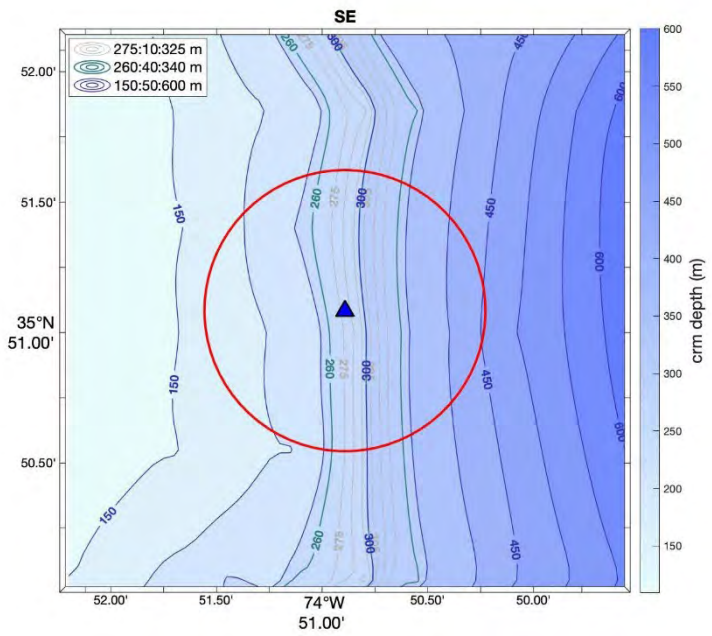

g) Map of the CRM 3-arc second bathymetry (formerly NGDC) in the slope region within ±2 km of the most southern and eastern profiler mooring SE (blue triangle) located near the 300 m isobath. Red circle is the 1 km site radius from the site center. Bathymetric contour intervals are shown in the legend.

Mooring WE lies toward the eastern edge of the inner shelf. With isobaths running meridionally, WE (at ~30 m) appears to lie near the bottom of a short slope (22 to 32 m). The slope appears as a divot in the transect (Figures 2-5a) and is more clearly a slope in the site map (Figures 2-6a). Mooring CN (at ~32.5 m) lies well onto the mid-shelf where the isobaths to the west are oriented in the N/S direction, while those to east appear more as circular hillocks. CN lies halfway up a short 35 to 30 m slope which is far more apparent in the site map (Figures 2-6b) than in the transect (Figures 2-5a). Neither WE nor CN would be greatly affected by a location choice to the north or south (Figures 2-5a).

Mooring EA (at 100 m) lies at the shelfbreak on the same line of latitude as WE and CN. Moving the target location for EA to north would require moving it further east to keep it at 100 m on and on the shelfbreak. As the 100 m isobath at this site center forms a shallow “<”, moorings placed to the north by any distance within 6 km, would require changing in the target longitude to a position further east to keep the 100 m depth. Placement to the south by less than ~1 km, would also require an eastward change in longitude, but any further south than 1 km, would require a compensating shift to westward (Figures 2-5a, Figures 2-6c).

At the location of Mooring NO, the isobaths are fairly regularly spaced and tilted slightly from northeast to southwest (Figures 2-5b). Therefore, NO placement to the north (south) of the site center would require a compensating westward (eastward) shift to remain on the 100 m isobath. Siting the mooring with 6 km without a compensation in longitude would change the target depth by ~10 m (Figures 2-6d). At Mooring SO, the isobaths are again quite regular, but are tilted in the opposite direction from northwest to southeast and are more tightly packed than at SO (Figures 2-5c). The opposite tilt means that placing SO to the north (south) of the site center would require a compensation eastward (westward) shift to remain on the 100 m isobath (Figures 2-6e), i.e., the opposite as the compensation at NO. The steeper gradient requires careful placement to avoid undesired change in depth.

The site centers for Moorings NE and SE at 300 m on the slope mean that small changes in east-west position will have a noticeable effect on the resulting mooring depth. The isobaths

within 2 km of Mooring NE are relatively straight to the north, but turn westward to the south of the site such that 2 km to the south depths increase by ~100 m (Figures 2-5d). A shift northward of about 50 m could be accommodated along the same isobath, but a shift to the south would have to be accompanied by a nearly equal shift to the west to remain along the 300 m isobath. Without compensation, a 30 m shift in longitude either direction would result in a 15 to 20 m difference in depth (Figures 2-5d). The SE site has relatively straight isobaths both north and south of the site, but the east-west gradients are somewhat steeper than at NE so that a 30 m shift in longitude would result in a 20 to 30 m difference in depth (Figures 2-5e, Figures 2-6g).

All maps were created using run_cre_all_smab_bathy_map_plots.m, which allows choice of bathymetric product and region. All transects for created using run_cre_all_smab_bathy_map_plots.m, which allows choice of bathymetric product, mooring and axis limits. Both these scripts call run_plot_bathy.m, which relies on three hardwired functions to define the regions and mooring locations, as well as transect and map specifics: define_smab_boxes.m, define_plot_bathy_region_numbers.m, get_hardwired_plot_map_details.m, and plot_smab_boxes.m. Other low level functions used which are not specific to this software set include: amm_weighted_mean_1var.m, find_nearest_pos.m, fixscore.m, plot_bathy.m, plot_sect_bathy.m, reset_longit.m, retrieve_sect_bathy.m, and set_colorbar.m. The software also makes use of the seawater toolbox by Rich Pawlowicz, as well as the m_map toolbox (https://www.eoas.ubc.ca/~rich/map.html) and from GitHub nctoolbox-1.1.3 (https://github.com/nctoolbox/nctoolbox/releases/tag/1.1.3) and ocean-data-tools (https://github.com/lnferris/ocean_data_tools). These scripts can be found in the ooicgsn-site-characterization GitHub repo (https://github.com/WHOIGit/ooicgsn-site-characterization).

2.2. Bottom types

The USGS sediment classification map (Figure 2-7) summarizes bottom characteristics along the Southern mid-Atlantic Bight and suggests that in OOI mooring region there is mainly a sandy bottom, with some gravelly sediment on the inshore shelf and possible sandy clay or silt on the slope (McMullen et al., 2014). This figure provides a useful overview, but to zoom in and explore the seafloor types within the immediate area of the target Southern mid-Atlantic Bight moorings, we relied on information from the Conley et al. (2017) review.

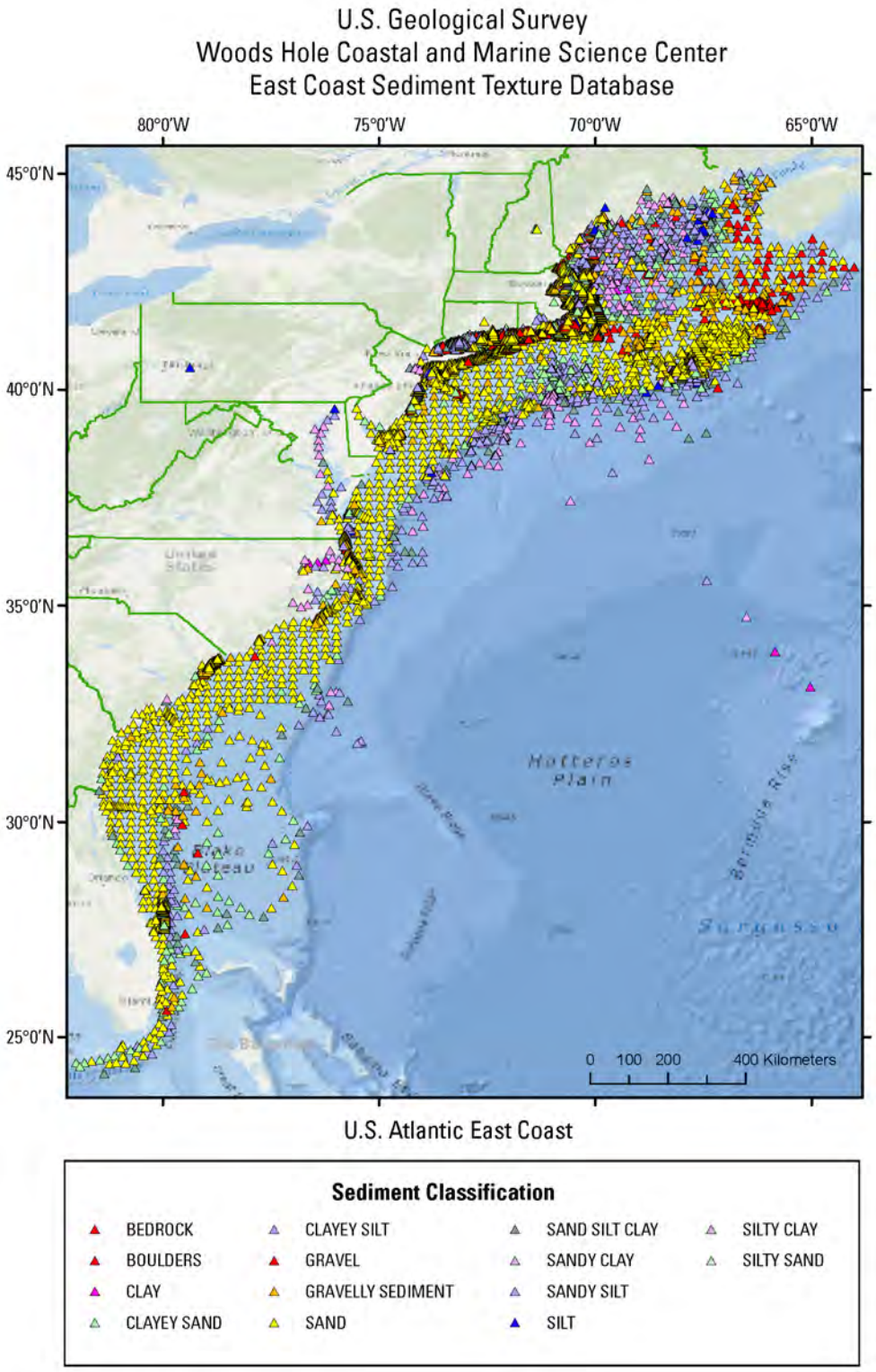

Figure 2-7 – USGS sediment classification map for the U.S. Atlantic East Coast. (Source: U.S. Geological Survey East-Coast Sediment Texture Database, 2014)

Conley et al. (2017) characterized the structure of seafloor geophysics in terms of three variables: bathymetry (depth, which we have described in Section 2.1), seabed forms (topography), and substrate (texture and hardness). Like bathymetry, seabed forms and substrate are important to mooring location decisions. Conley et al. (2017) point out that these three variables are generally more stable than water column parameters which change on

shorter timescales and “have been shown to correlate with the distribution and abundance of demersal fish and benthic organisms.” While OOI does not focus on the latter per se, disturbance of such environments may be a concern in determining mooring locations within the site radii.

Conley et al., (2017) define the varying depth regions in the mid-Atlantic Bight in terms of six littoral zones, four of which concern the target mooring sites (Infralittoral 0-30 m, Shallow Circalittoral 30-70 m, Deep Circalittoral 70-200 m, and Shallow Mesobenthic 200-600 m). See Conley et al. (2017) – their Table 3.1 for a review of the literature on the relationship between seafloor types and biota. Here, we present their figures covering the littoral zones themselves (Figure 2-8), seabed forms (Figure 2-9), soft sediment types (Figure 2-10), and hardbottom types (Figure 2-11) with the target SMAB mooring sites overlaid as open symbols to allow discernment of characteristics at the site centers. Conley et al. (2017) also provide figures which combine these various seabed characteristics (their figure 3.34 combines depth zones with seabed and hardbottom types, and their figure 3.38 shows ecological marine units which combine depth zones with seabed, hardbottom and soft sediment types). However, these figures are somewhat redundant and are also difficult to use to explore the small scales in and around the mooring sites due to their inherent complexity. Further location-specific details may be available through the original databases used by Conley et al. (2017).

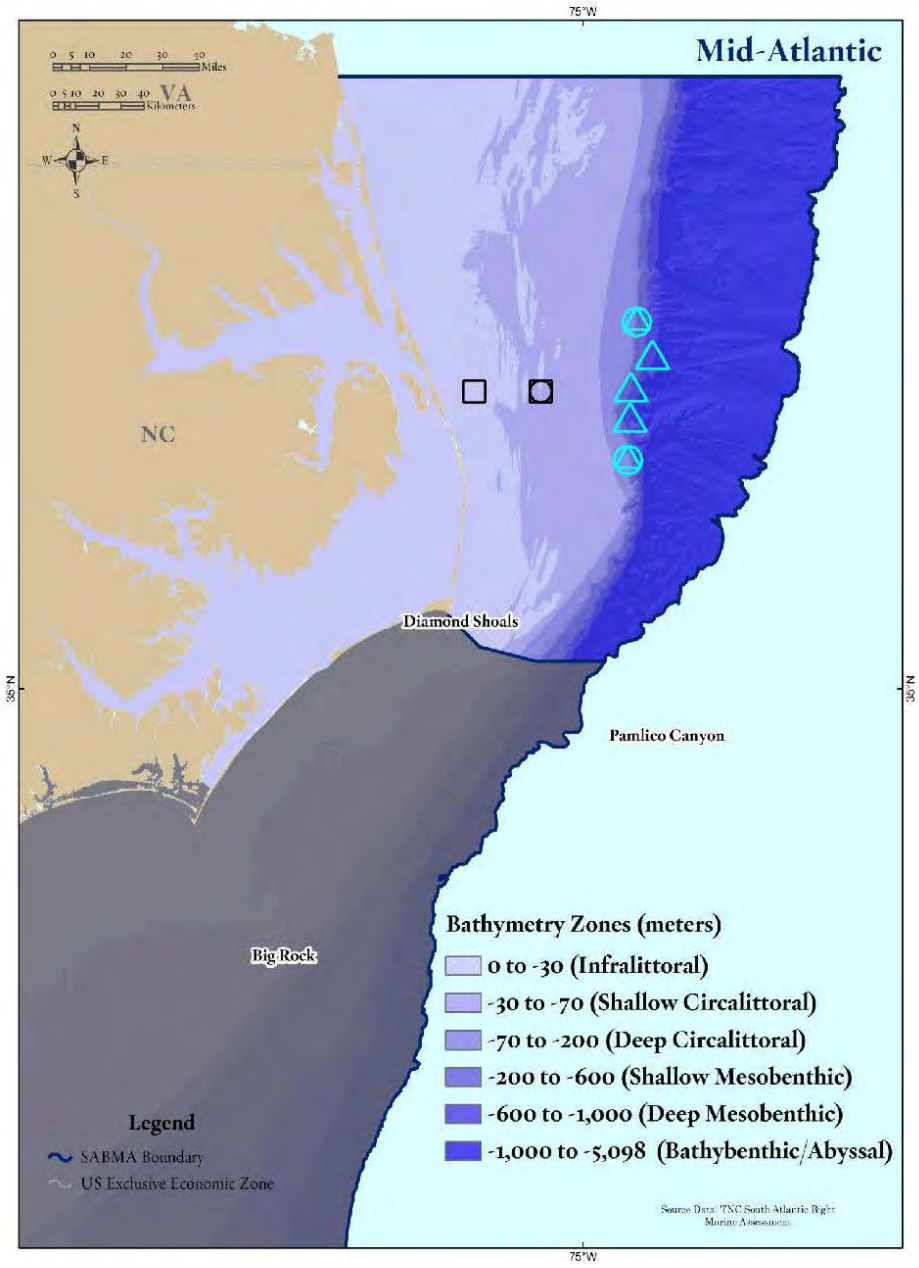

Figure 2-8 – The littoral (Depth) zones according to Conley et al. (2017) in the southern mid-Atlantic Bight. Symbols for target mooring locations as described in Figure 1-2, however the color coding has not been used to allow inspection of bottom characteristics at the site centers. The two symbol colors (black and cyan) have no inherent meaning and were chosen to stand out against all backgrounds in Figure 2-8 through Figure 2-11. (Adapted from Conley et al., 2017, their figure 3.4)

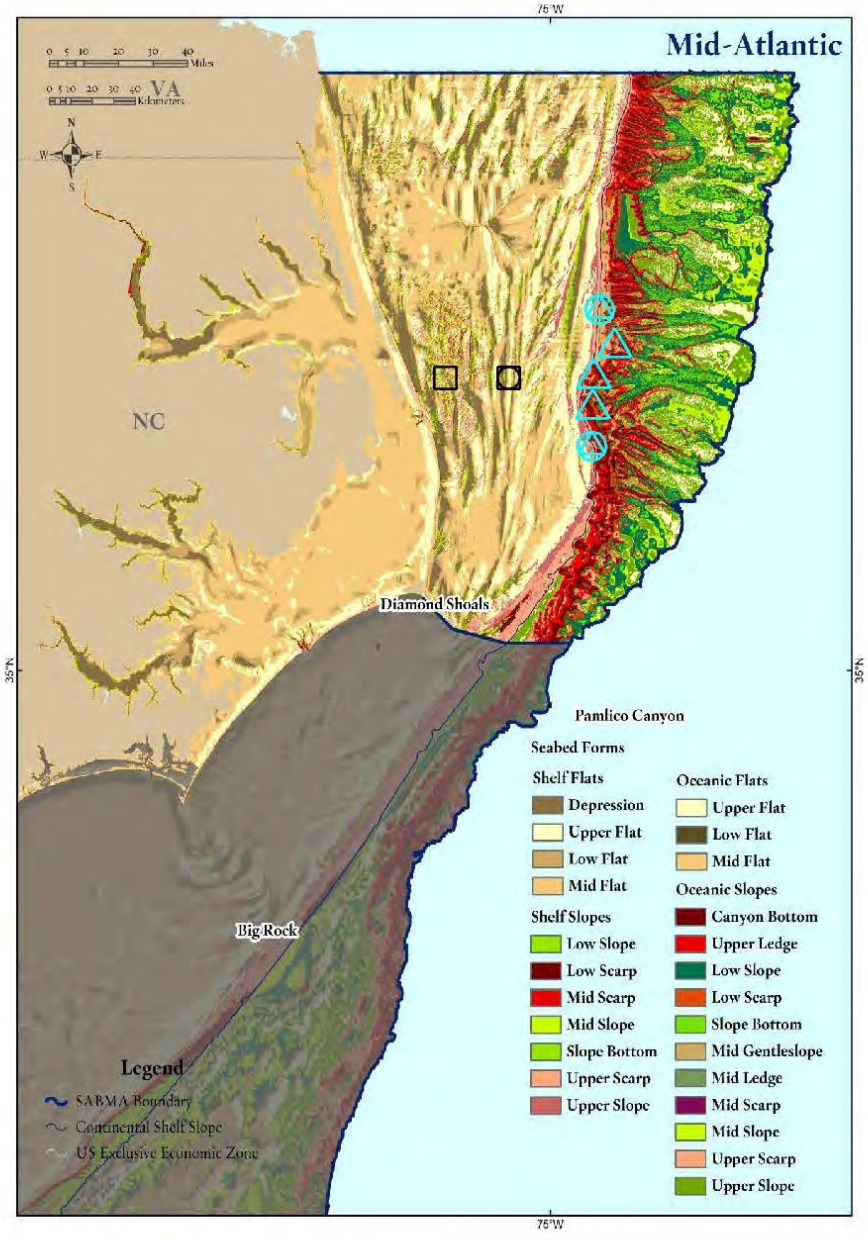

Figure 2-9 – Map of the seabed forms in same region and with same symbols as Figure 2-8. (Adapted from Conley at al., 2017, their figure 3.8)

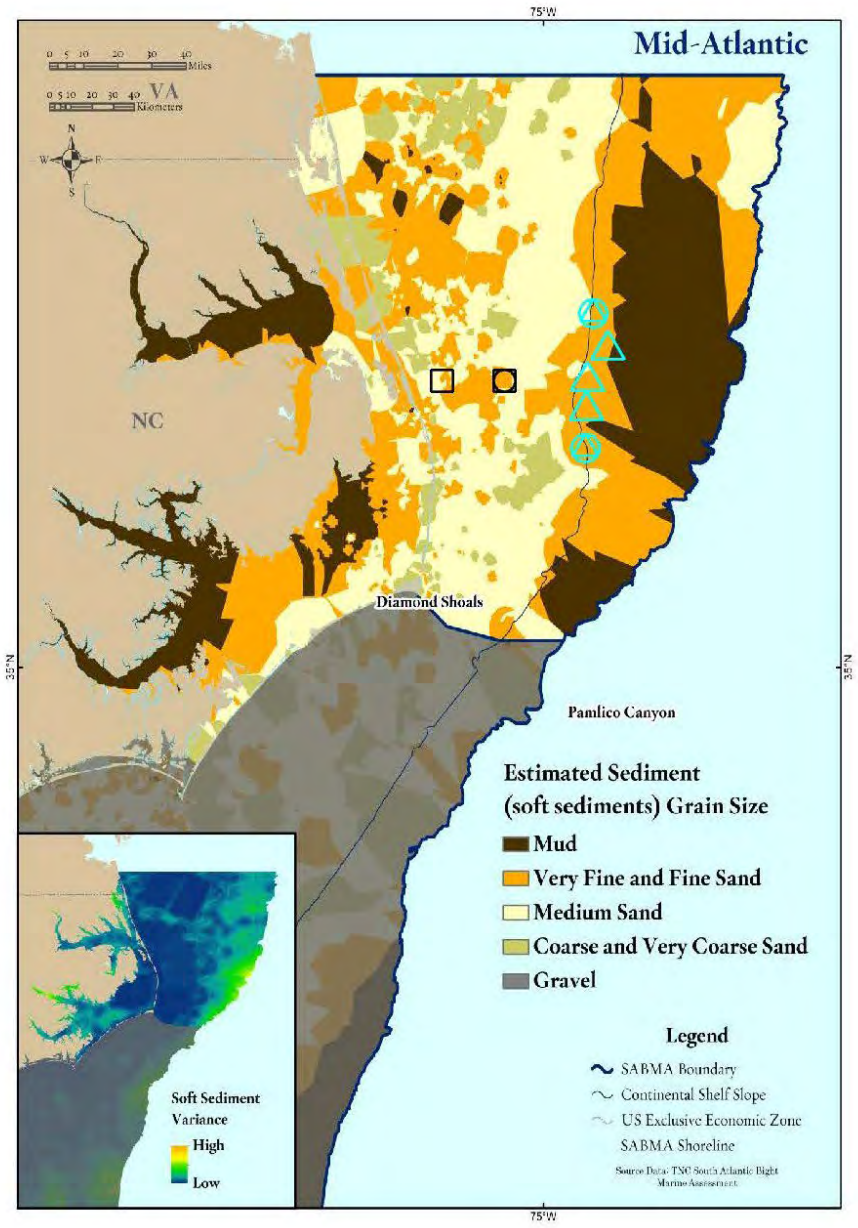

Figure 2-10 – Map of the soft sediment distribution in same region and with same symbols as Figure 2-8. (Adapted from Conley at al., 2017, their figure 3.20)

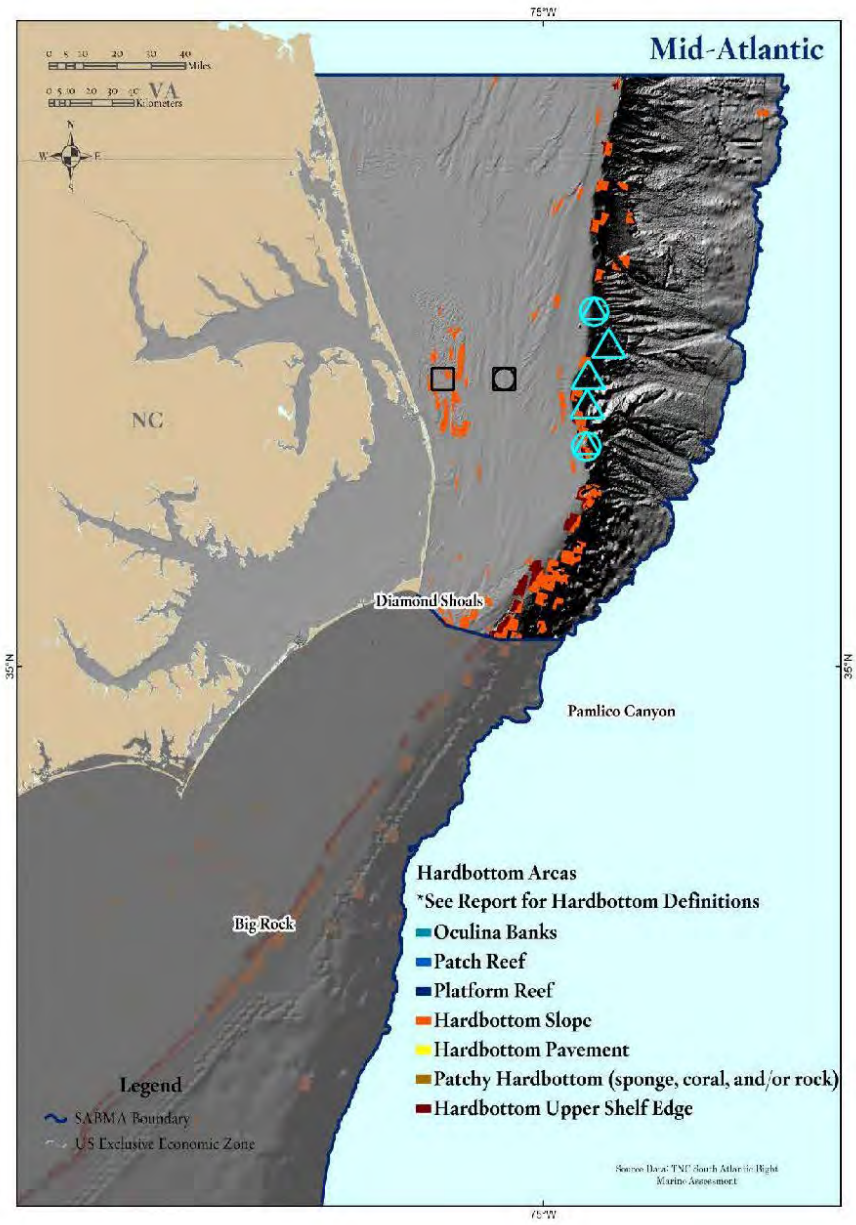

Figure 2-11 – Map of the hardbottom and corals overlaid on shaded topography in same region and with same symbols as Figure 2-8. (Adapted from Conley at al., 2017, their figure 3.25)

An examination of seabed characteristics near the target sites according to these figures is summarized in Table 2-2. We note that while Conley et al. (2017) divided the U.S. east coast area they studied into 7 regions of hardbottom types, only two of these exist in the OOI SMAB region; **Hardbottom Slope**: High relief hardbottom associated with ledges and slopes; **Hardbottom Upper Shelf Edge (HUSE)**: High relief hardbottom associated with the upper shelf edge to -100 m. In particular, the **Patchy Hardbottom (corals, sponges and/or rock)** only exists well south of the intended mooring sites. In addition, the Hardbottom Slope and HUSE regions appear to be patchy; in-situ site surveys will be necessary to augment the seabed characteristics suggested from the Conley et al. (2017) maps.

Table 2-2 – Summary of bottom characteristics in the region of the target mooring sites according to Figure 2-8 through Figure 2-11

Mooring Site	Littoral Zone (m)	Seabed Form	Soft Sediments	Hard Bottom
WE	Infralittoral (0-30)	Variable Shelf Slope	Medium Sand	none
CN	Bordering Infra- & Shallow Circalittoral (0-30-70)	Shelf Upper Flat	Very Fine & Fine Sand	none
EA	Deep Circalittoral (70-200)	Shelf Upper Scarp	Very Fine & Fine Sand	Hardbottom Slope
NO	Deep Circalittoral (70-200)	Shelf Upper Scarp	Very Fine & Fine Sand	none
SO	Deep Circalittoral (70-200)	Shelf Upper Scarp	Very Fine & Fine Sand	Hardbottom Slope/ HUSE
NE	Shallow Mesobenthic (200-600)	Slope Upper Ledge	Very Fine & Fine Sand	none
SE	Shallow Mesobenthic (200-600)	Slope Upper Ledge	Very Fine & Fine Sand	Some Hardbottom Slope

The shallowest westernmost mooring WE target site lies well onto the shelf, but in a region with a variable seabed with rough topography (Figure 2-8). While the site center suggests a medium sand bottom, the intended locations within the site radius could place it in fine or very fine sand or on a hard bottom (but not corals or sponges). CN also lies on the shelf (near the depth break between infralittoral and shallow circa littoral). The site center for CN and the immediate surrounding area is all sand or very fine sand.

EA, NO and SO on the 100 m isobath lie solidly in the deep circalittoral depth zone and are associated with the Shelf Upper Scarp seabed form with fine to very fine sand at the bottom. That said, for SO, mooring placement within the site radius to the north could put it on Hardbottom and placement to south could put it on either Hardbottom or Hardbottom Shelf Edge. There is Hardbottom just to the north of the NO site center, but it is difficult to say whether this region lies within the site radius (Figure 2-11). In neither location (NO or SO) is there any indication of Patchy Hardbottom with corals or sponges.

At 300 m, moorings NE and SE are in the Shallow Mesobenthic zone, but both lie close to the Deep Mesobenthic. The NE site center appears to sit between the Mid-Slope and Mid-Scarp (light green and light red) (bright red, Figure 2-9), and though scale is difficult to discern it appears that both Low and Upper Scarp (deep red and apricot, Figure 2-9) lie within the site radius. This interpretation is consistent with the bathymetric transect (Figures 2-5d). As noted elsewhere, the slope is steep, this representation also indicates that the region is not as smooth as the transect plot suggests. The SE site center is on the Low Scarp (dark red)abuts the Mid Scarp (light red, Figure 2-9)which agrees with what is illustrated in the transect (Figures 2-5e) For SE the ragged topography in region is seen in both transect and Figure 2.9. The seabed sediments at both NE and SE are find and very fine sand (Figure 2-10).

In summary, all target mooring locations except CN and NO lie in regions of patchy seabed characteristics; bathymetric survey will be used to confirm both the depths and seafloor types in the immediate vicinity of each target site.

3.0 Oceanographic Conditions

3.1. Regional Circulation Patterns

The mean circulation patterns over the Mid-Atlantic Bight were analyzed by Lentz et al. (2008a) using moored current observations with records exceeding 200 days. They found a consistent mean circulation pattern with the mean depth-averaged flow along-shelf, towards the equator, increasing linearly with depth (three cm s^{-1} at the 15-meter isobath and 10 cm s^{-1} at the 100-meter isobath). The mean cross shelf circulation was weak but still showed a consistent cross-shelf and vertical structure. Near the surface, the flow was typically offshore, ranging between -2 to 4 cm s^{-1}. The “interior” cross-shelf flow was ~1 cm s^{-1} onshore and was found to be consistent. Mean flow in the near-bottom region increased with water depth from -1 cm s^{-1} (near the coast) to 4 cm s^{-1} (over the slope), switching from onshore to offshore around the 50-meter isobath. The inner shelf showed a two-layer structure, offshore near the top and onshore near the bottom. The mid- and outer shelf had a three-layer structure with offshore flows near the top and bottom and an onshore flow in the “interior”.

3.2. Surface currents

The Mid-Atlantic Regional Association Coastal Ocean Observing System (MARACOOS) has been measuring hourly ocean surface currents (depths > 2.5 m) using High Frequency Radar between Cape Cod, MA and Cape Hatteras, NC, since 2007. Roarty et al. (2020) analyzed 10 years (2007-2016) of High Frequency Radar data in the Mid-Atlantic Bight resulting in a detailed evaluation on the effect of wind forcing and riverine discharge on surface flows over seasonal and annual time periods.

The HF Radar hourly averaged surface currents were de-tided, low-pass filtered using a 30-hour period, and gridded. Three-month seasonal means and 12-month annual means were calculated using only data from grids with more than 50% of measurements available. Decadal means for each season and full year were calculated by taking the mean of the 10 seasonal means so each year was equally weighted.

NOAA weather buoys and Coastal-Marine Automated Network (C-MAN) stations provided hourly wind data using only data with at least 50% coverage included in analysis. Mean seasonal, annual, and decadal wind was calculated using the same method as currents above. River discharge data was provided by the U.S. Geological Survey (USGS) with data from all the smaller tributaries flowing into Chesapeake combined into a single data set.

Results from the analysis found a strong coastal current which turns offshore south of the Chesapeake Bay and merges with Gulf Stream. Steady flow was found along the shelf and the most varied found near shore. As found by Lentz (2008b), the mean along-shelf currents increased with distance offshore. The variability in mean flow was small from year to year but large within any given year, which may be influenced by the Gulf Stream. The largest variability was in fall and winter when the water-column changes from stratified to well mixed with strong winds and freshwater flow driving the variability.

An overview of findings by Roarty et al. (2020), broken down by season, is as follows. Winter: Strong cross shore winds (NW), strong freshwater flow, currents strongest across the entire shelf, mostly offshore (peak velocities 7-12 cm/s), largest along shore currents turning counterclockwise off shelf and into gulf stream, with a cross-shore wind and more mixed water column. Spring: Weak alongshore winds (SW), with nearshore winds from the west, strong

freshwater flow, weaker currents nearshore (3-6 cm/s) and follow same pattern as winter, strongest at shelf break, currents reach similar highs to fall and winter but without wind forcing, and weakest along shore (opposed by wind). Summer: Wind speeds are midrange (1.0-1.9 m/s) and from SW, which is typical response from Bermuda high, weakest wind alongshore, weak freshwater flow, weakest currents overall (3-6 cm/s), weakest along shore (opposed by wind), strongest currents at shelf break, flowing in more cross-shelf direction, then southeast towards gulf stream. Fall: Strong cross shore winds (NW), weak freshwater flow, fastest seasonal currents, driven by wind and directing flow along shore, more mixed water column, coastal current flows to shelf and joins shelf break jet, flowing offshore into one current.

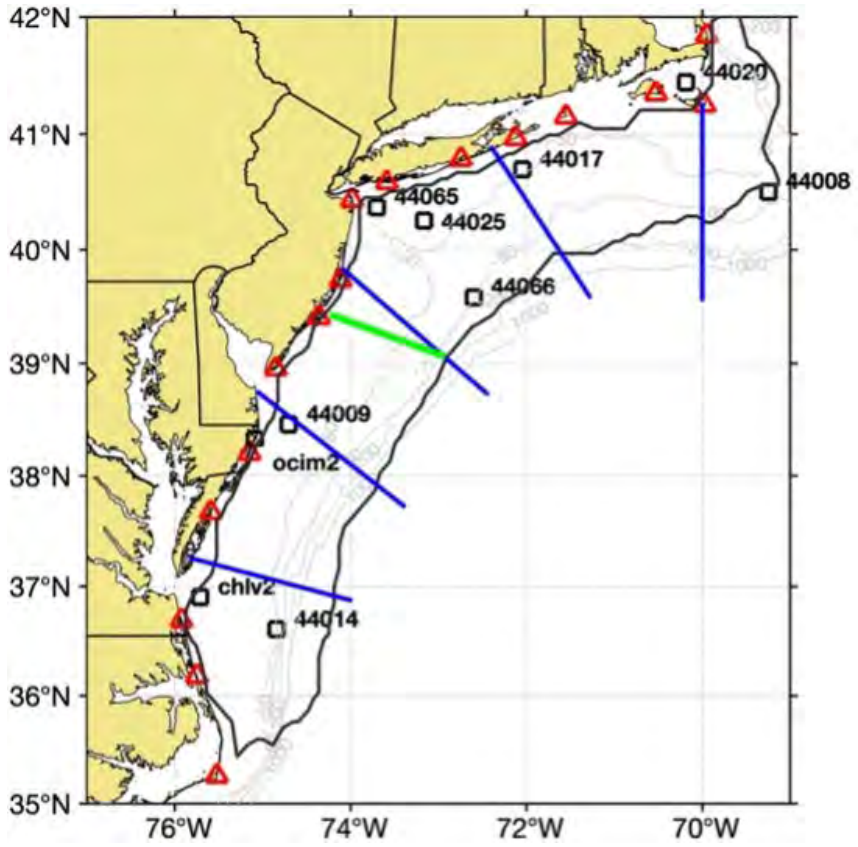

Figure 3-1 – From Roarty et al. (2020). NOAA NDBC stations are marked as black squares and labeled. The 50-, 80-, 200-, and 1,000-m isobaths are marked along with the total vector coverage for the study period shown as the thick black line. The Tuckerton endurance line is marked in green. The continental shelf was divided into six regions following definitions used by Wallace et al. (2018). From north to south, the regions are Eastern New England (ENE), Southern New England (SNE), New York Bight 1 (NYB1), New York Bight 2 (NYB2), Southern Shelf 1 (SS1), and Southern Shelf 2 (SS2).

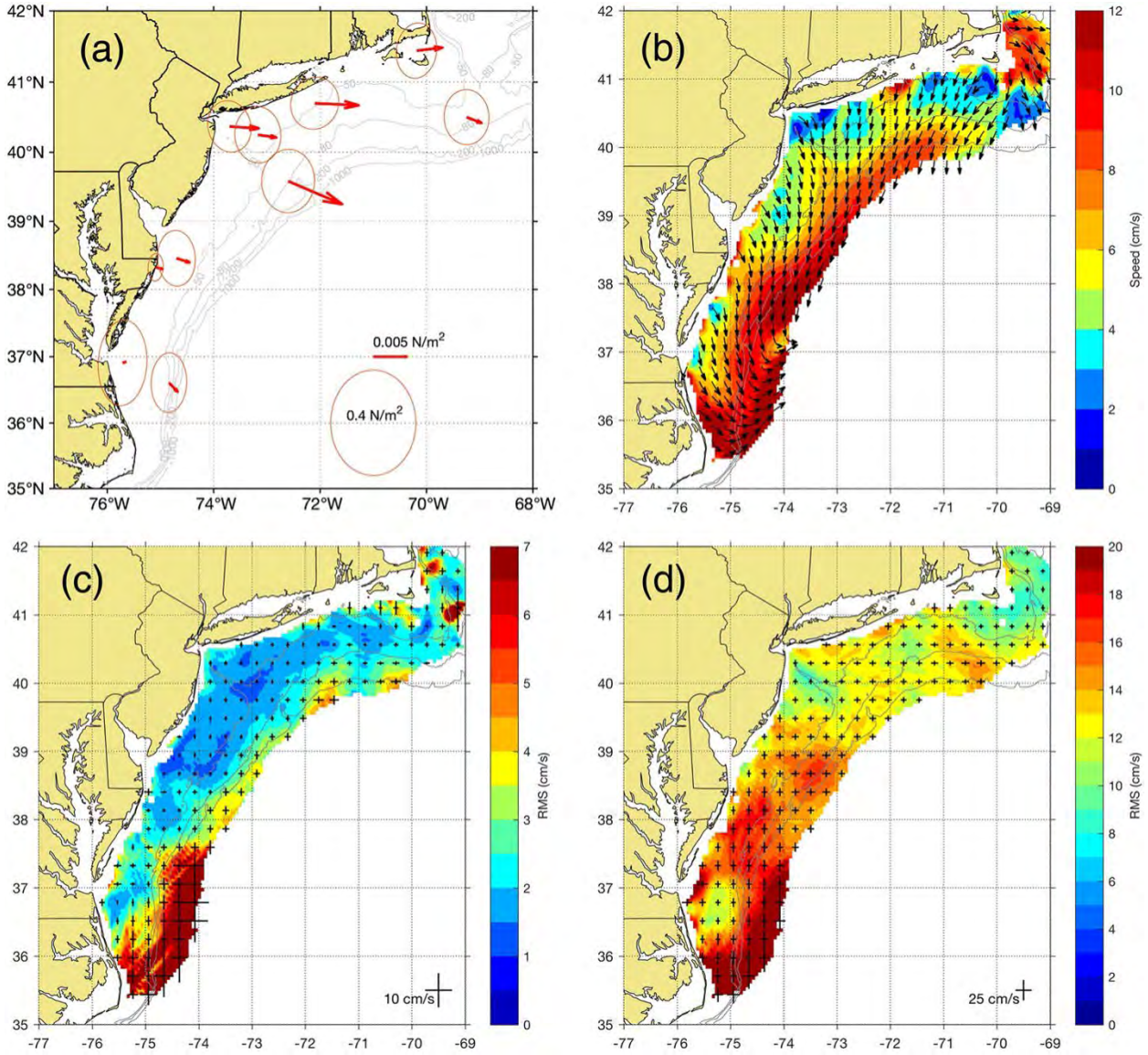

Figure 3-2 – From Roarty et al. (2020). (a) Mean and 95% data ellipse of wind stress (N/m^2) from NDBC stations for 2007–2016. The reference vector of 0.005 and 0.4 N/m^2 variability ellipse is given in the lower right. (b) Mean surface current for the Mid-Atlantic Bight (cm/s) colorbar indicates magnitude and vectors indicate direction toward of surface current. (c) Interannual standard deviation of the surface currents (cm/s). (d) Intra-annual standard deviation of the surface currents (cm/s).

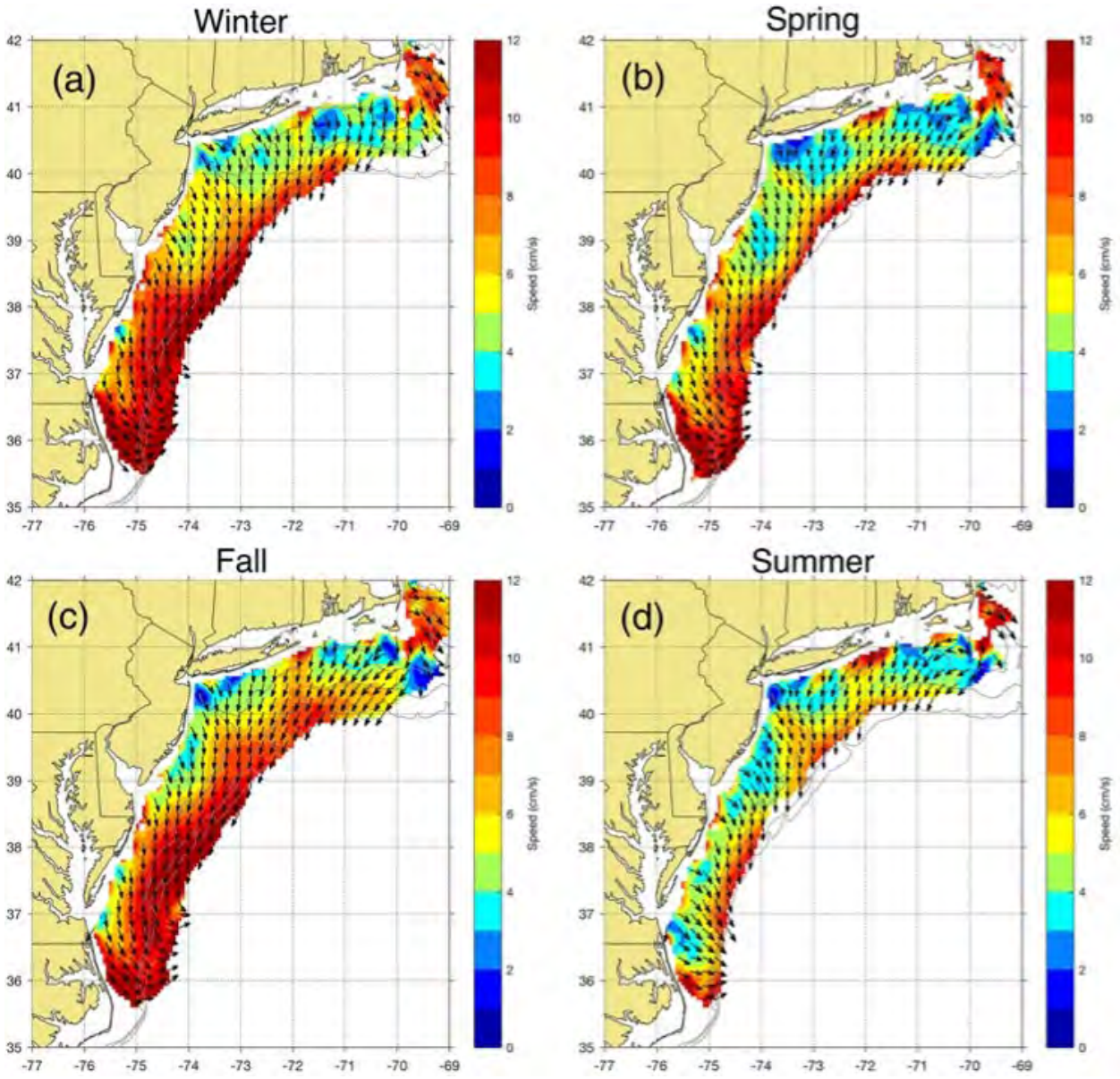

Figure 3-3 – From Roarty et al. (2020). Mean surface currents (2007-2016) broken down by season (a) winter, December–February; (b) spring, March–May; (c) fall, September– November; and (d) summer, June–August. indicates magnitude (cm/s) and vectors indicate direction-toward for surface current.

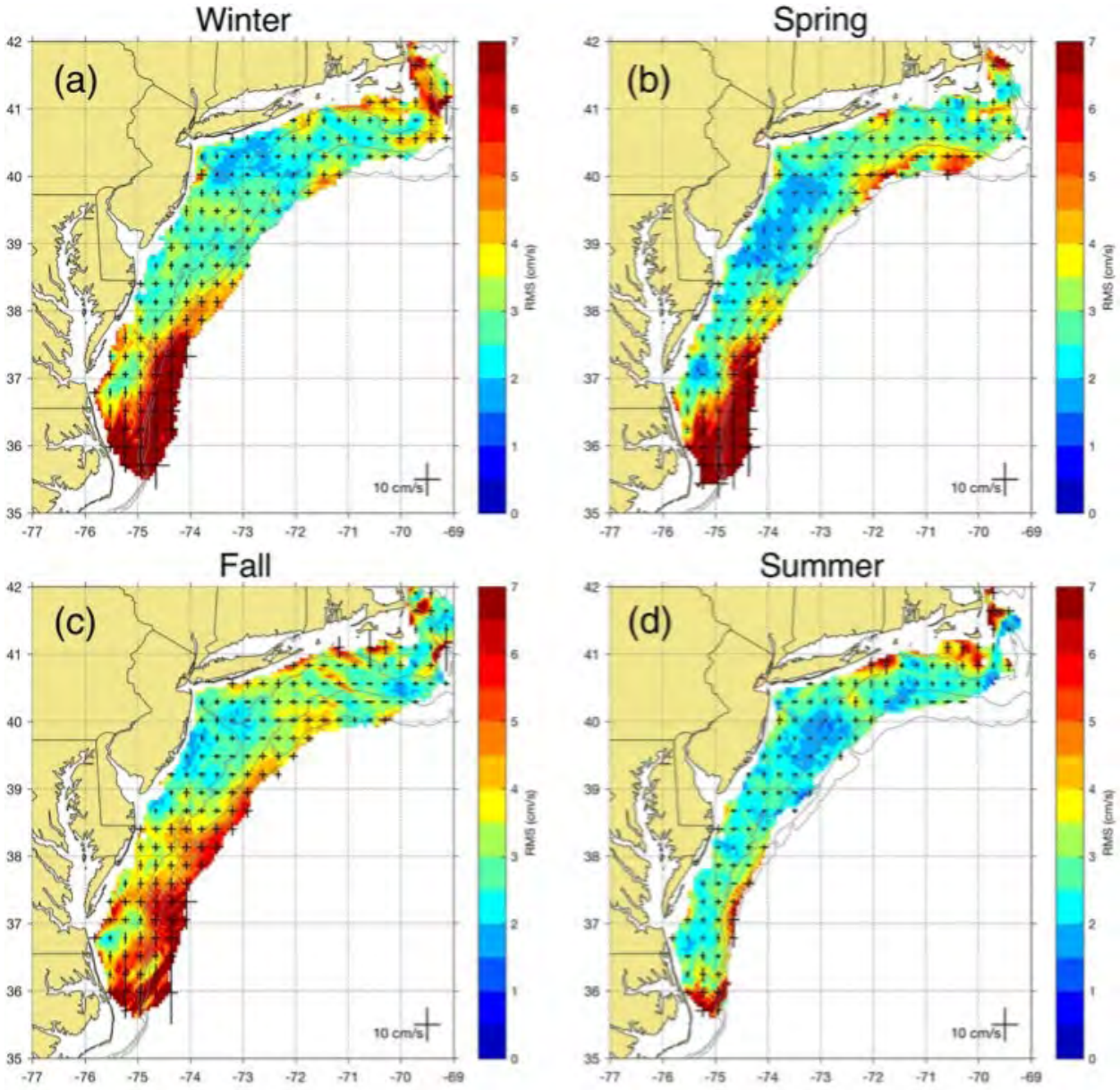

Figure 3-4 – From Roarty et al. (2020). Intraseasonal standard deviation of the surface current (cm/s) in the Mid-Atlantic from (a) winter, December–February; (b) spring, March–May; (c) fall, September–November; and (d) summer, June–August. One standard deviation marks in the east/west and north/south directions are shown for every fifth grid point (30-km spacing) with a reference scale of 25 cm/s in the lower right.

3.3. Subsurface Currents

As part of the **P**rocess driving **E**xchange **a**t **C**ape **H**atteras (PEACH) project, located in the Mid-Atlantic Bight and Southern Atlantic Bight, 10 moored upward looking ADCPs were deployed along the shelf and shelf-break (Haines et al., 2022; Seim et al., 2022). Of these, four ADCPs (A1, A2 A3, and B1) were located within the proposed bounds for the new Pioneer Array site (Figure 3-5) and along the same ~100 m isobath intended for OOI moorings NO, EA and SO. Moorings A1, A2, and A3 were deployed along the shelf break from April 2017 to November 2018; Mooring B1 was deployed on the shelf from April 2017 to December 2018 (Table 3-1). The ADCP data were hourly averaged and regridded to a uniform depth grid (Table 3-1), and the u- and v-velocity were depth-averaged and de-tided.

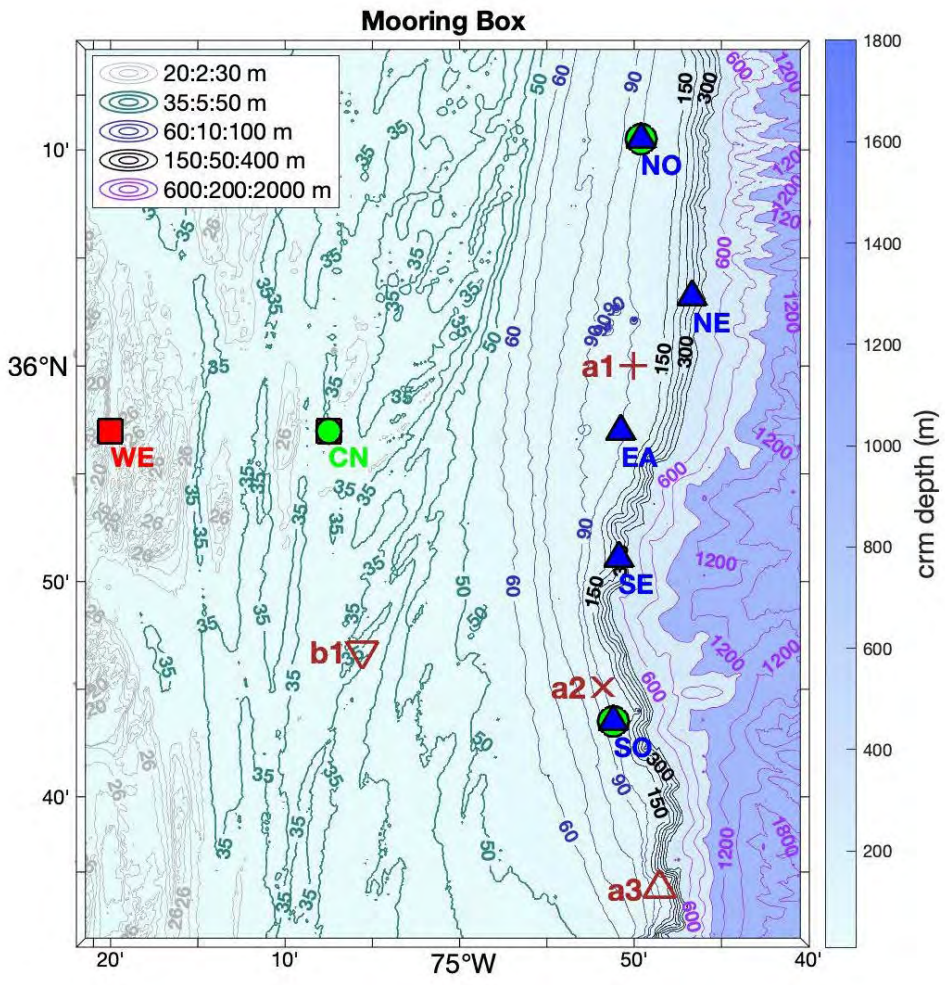

Figure 3-5 – PEACH mooring locations A1, A2, A3, and B1 with the OOI glider (green), and mooring array bounds (red), and shallow (red squares), surface (green circle), and profiler (blue triangles) mooring central locations.

Table 3-1 – PEACH moored ADCP data overview.

Mooring	Dates		Depth	Lon	Lat	Bin size	# of bins	Bin depths
A1 shelf break pod	Apr 18, 2017	Nov 23, 2018	100	-74.834	36.001	4	21	92-12
A2 shelf break pod	Apr 18, 2017	Nov 23, 2018	96	-74.863	35.752	4	20	88-12
A3 shelf break pod	Apr 18, 2017	Nov 19, 2018	97	-74.809	35.595	4	20	92-16
B1 Oregon Inlet bottom frame	Apr 20, 2017	Dec 31, 2018	36	-75.093	35.780	1	29	33-5

The percentage of ADCP current meter data recorded for each of the PEACH moorings are presented in Figure 3-6 as histograms. The histograms are all recorded data for all depth bins, grouped into months. The data return for Moorings A1, A2, and A3 were similar with the lowest return in January (~4%) and the highest returns between May and October (~10%). The data return for Mooring B1 was also lowest in January (~4%) but had fairly consistent data returns from May to December (~10%).

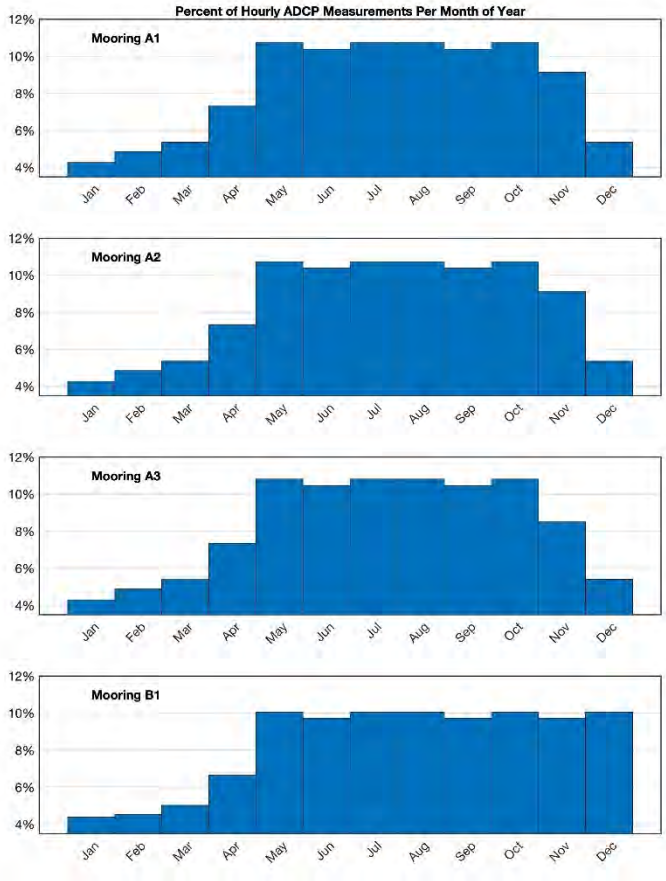

Figure 3-6 – Histograms of the hourly ADCP data from (top to bottom) PEACH moorings A1, A2, A3 and B1, showing percent of hourly current measurements for all depth bins available per month. July had 9.3% of the measurements while February had 7.4% of the measurements.

Evaluation of time-mean currents vs. depth show that the strongest currents were found at Mooring A3, ranging between 4.9 cm s^{-1} to 29.4 cm s^{-1} with the strongest flow at the surface (Figure 3-7). The predominant flow was to the northeast. The time-mean currents at Moorings A1, A2, and B1 were much weaker than at Mooring A3. The flow throughout the water column was uniform, with the highest percentage of flow to the south (Figure 3-7). The minimum, maximum, and mean of the time-mean flow and the predominant direction of flow for each mooring are listed in Table 3-2.

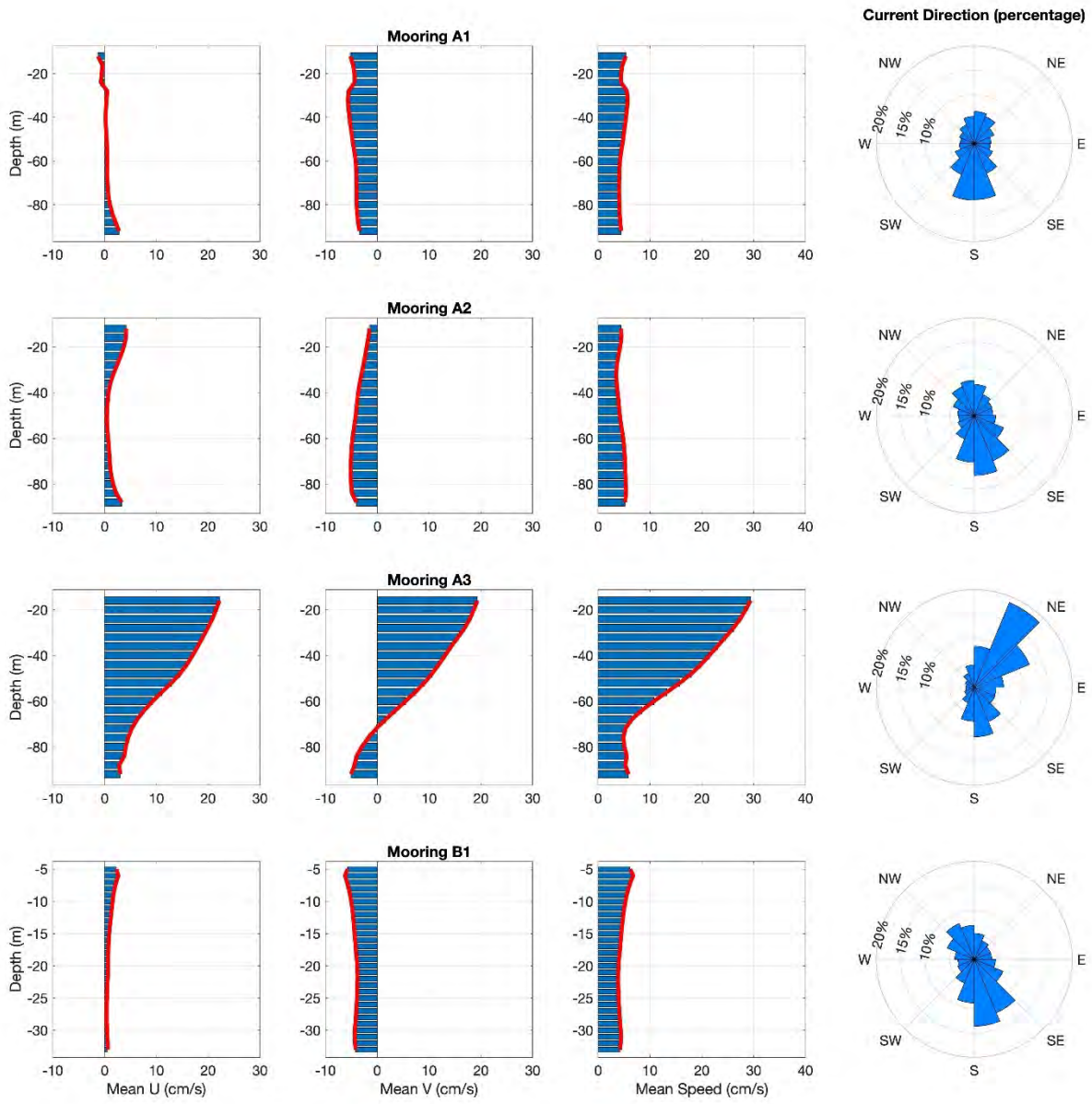

Figure 3-7 – Time-mean u-velocity (column 1), v-velocity (column 2), and speed (column 3). Current direction rose (column 4) for (top to bottom) mooring A1, A2, A3, and B1.

Table 3-2 – Minimum, maximum, and mean of time-mean flows for PEACH moorings and predominant direction.

Mooring	Min Speed (cm/s)	Max Speed (cm/s)	Mean Speed (cm/s)	Predominant direction
A1 shelf break pod	4.0	5.7	4.7	South
A2 shelf break pod	3.5	5.4	4.5	South
A3 shelf break pod	4.9	29.4	15.3	Northeast
B1 Oregon Inlet bottom frame	3.9	6.8	4.6	South

To provide a sense of the possible worst-case currents that might be encountered at a given site, a synthetic maximum current profile was created for moorings A1, A2 and B1 by extracting the maximum at each depth from the full time series (Figure 3-8). This showed surface-intensified currents (within the upper 40 m) of 120 - 135 cm/s and deeper currents (40-90 m depth) at A1 and A2 near 100 cm/s.

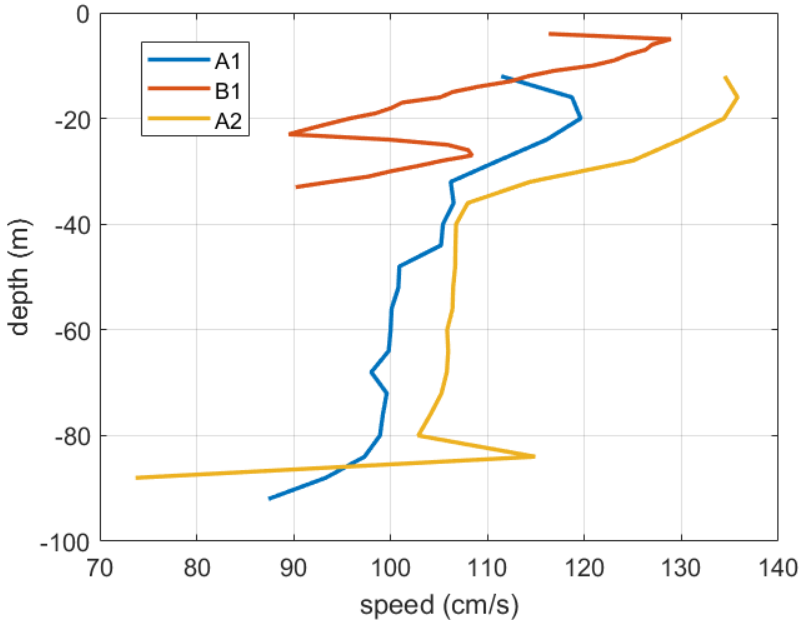

Figure 3-8 – Synthetic vertical current profiles at PEACH moorings A1, A2 and B1 created by selecting the maximum current speed for each depth bin from the full record.

In order to assess vertical current structure and timing for very strong and very weak conditions, two high-current events and two slack-current events were found for each of the four PEACH Moorings (Table 3-3). Features of interest from the high-current events include the following (Figure 3-9 - Figure 3-11):

- Mooring A1, Sep 2017: Surface intensified, southward flow at 100 cm/s, duration 2 days.
- Mooring A2, Mar 2018: Surface to bottom, southward flow at 100 cm/s, duration 3 days.
- Mooring A3, Oct 2017: Surface to bottom, oscillatory, up to 150 cm/s, duration 2.5 days.

Features of interest from the slack current events include (Figure 3-12 and Figure 3-13):

- Mooring A1: Jun 2017: Surface to bottom, <10 cm/s for 2 days, weak tides.
- Mooring A3: Mar 2018 Surface to bottom, <10 cm/s for 2.5 days, weak tides.

Table 3-3 – List high-current and slack-current events for each mooring.

Mooring	Date	Max/Min Speed (cm/s)	Depth of max/min Speed (m)	Comments
High-Current Events				
A1 shelf break	Sep 19, 2017	119.6	20	Hurricane Jose
	Mar 4, 2018	100.9	52	Winter storm Riley
A2 shelf break	Sep 20, 2017	135.8	16	Hurricane Jose
	Mar 4, 2018	111.8	12	Winter storm Riley
A3 shelf break	Dec 21, 2017	149.0	20	
	Sep 7, 2018	170.8	16	Hurricane Florence
B1 Oregon Inlet bottom frame	Aug 30, 2017	128.9	5	
	Oct 12, 2018	119.8	5	
Slack-Current Events				
A1 shelf break	Feb 14, 2018	0.05	40	
	Apr 22, 2018	0.02	56	
A2 shelf break	Aug 12, 2017	0.04	68	
	Jan 19, 2018	0.05	68	
A3 shelf break	Oct 31, 2017	0.09	16	
	Mar 28, 2018	0.09	36	

Figure 3-9 **a)**

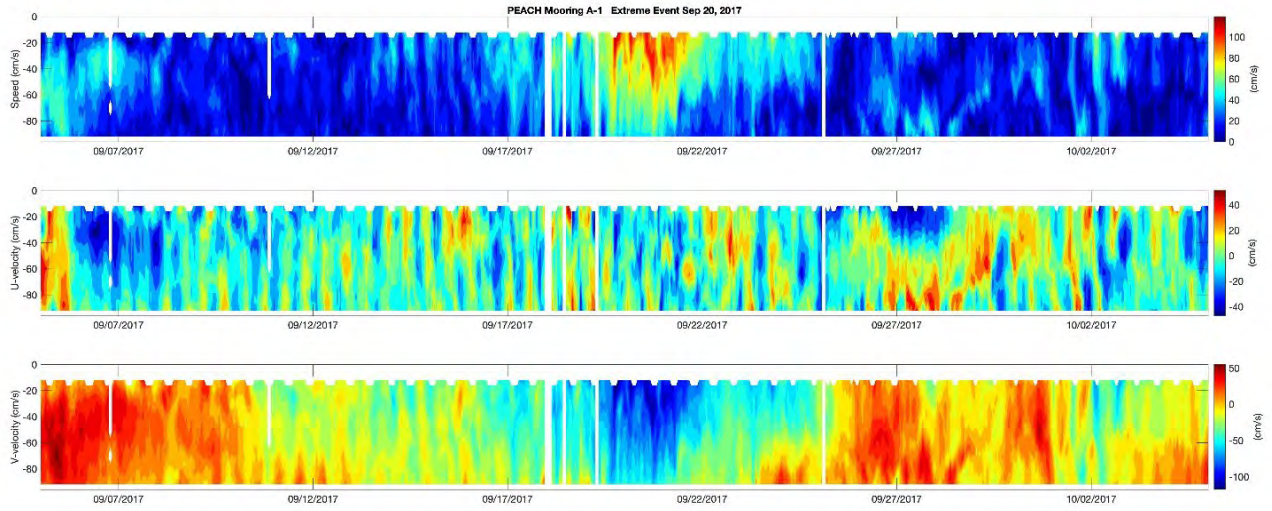

Figure 3-9 **b)**

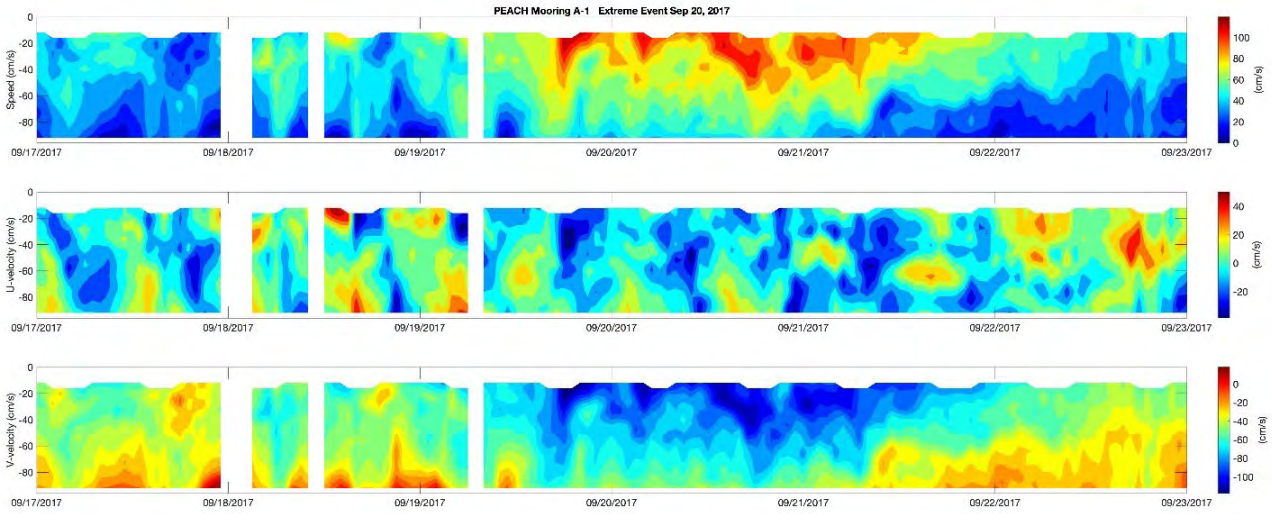

Figure 3-9 – Speed (upper) and east (middle), north (lower) velocities for a) a 30-day period surrounding a high-current event at PEACH mooring A1 during September 2017; and b) a 6-day period surrounding the event.

Figure 3-10 **a)**

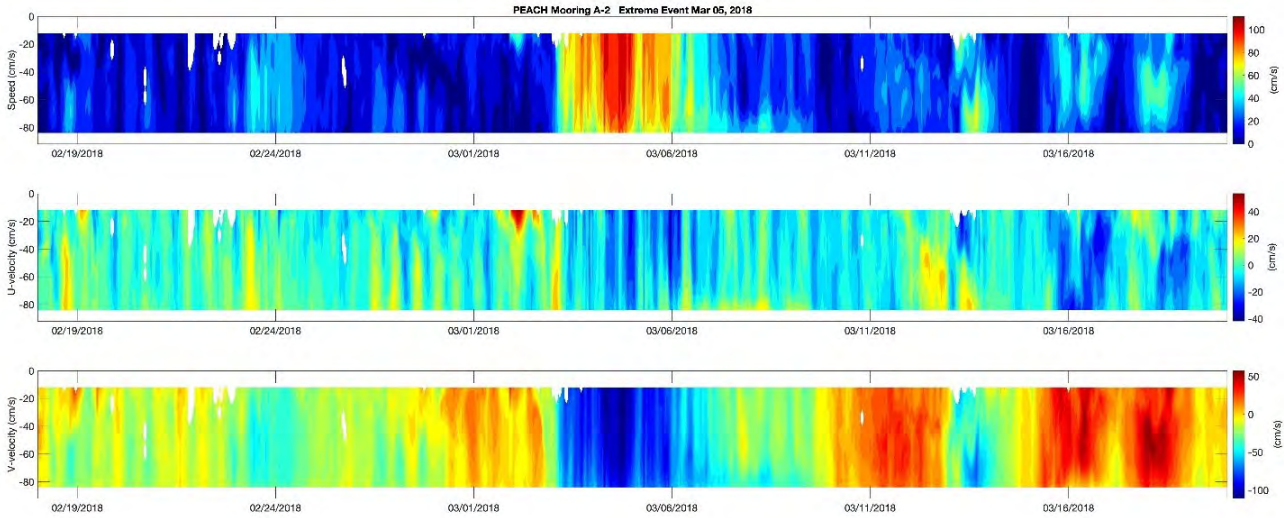

Figure 3-10 **b)**

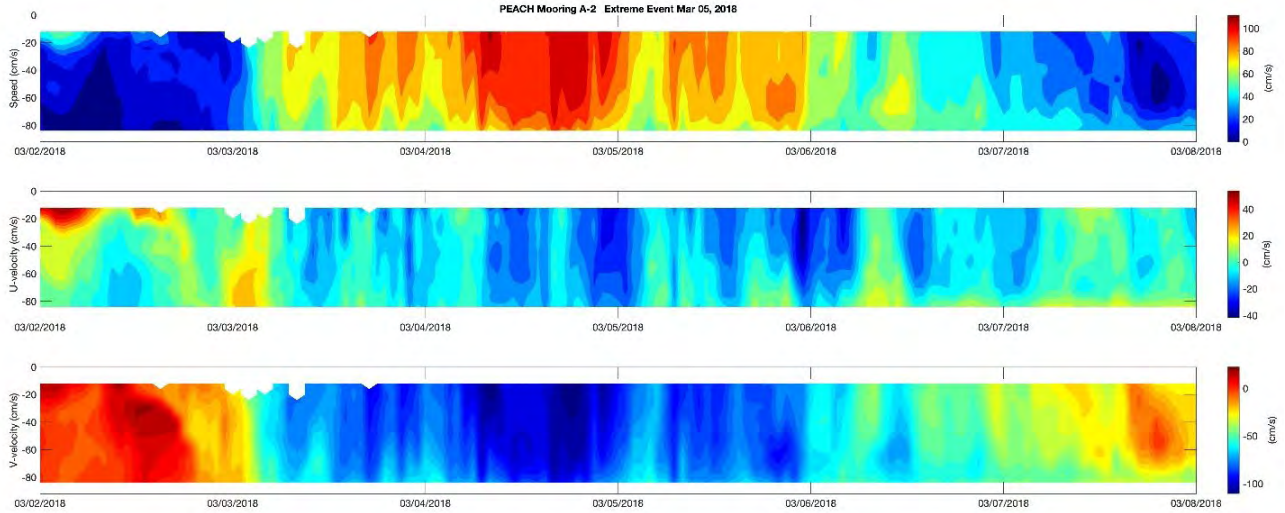

Figure 3-10 – Speed (upper) and east (middle), north (lower) velocities for a) a 30-day period surrounding a high-current event at PEACH mooring A2 during March 2018; and b) a 6-day period surrounding the event.

Figure 3-11 **a)**

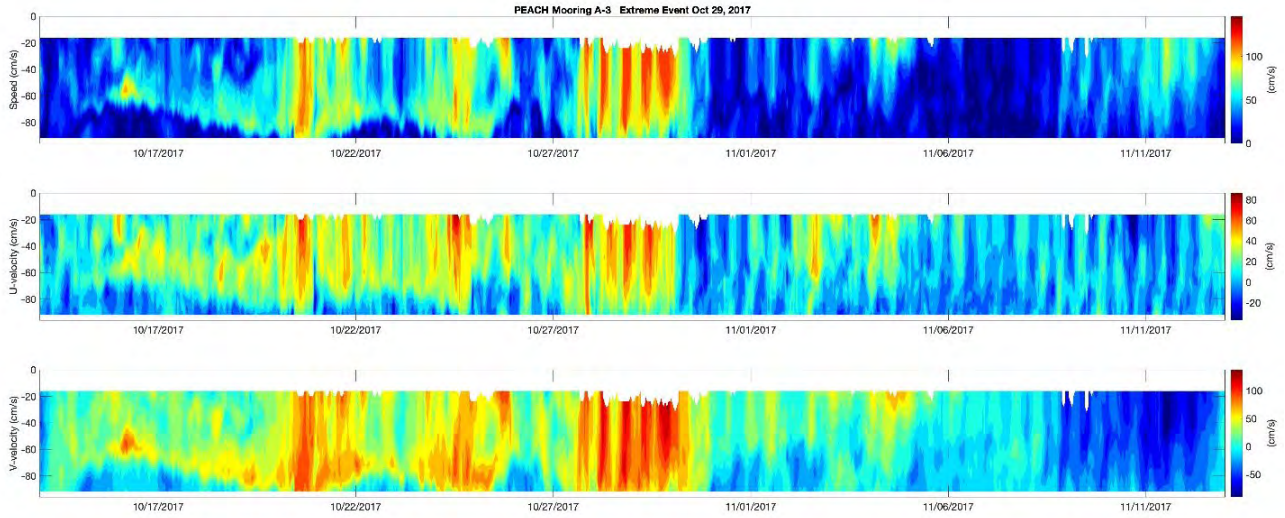

Figure 3-11 **b)**

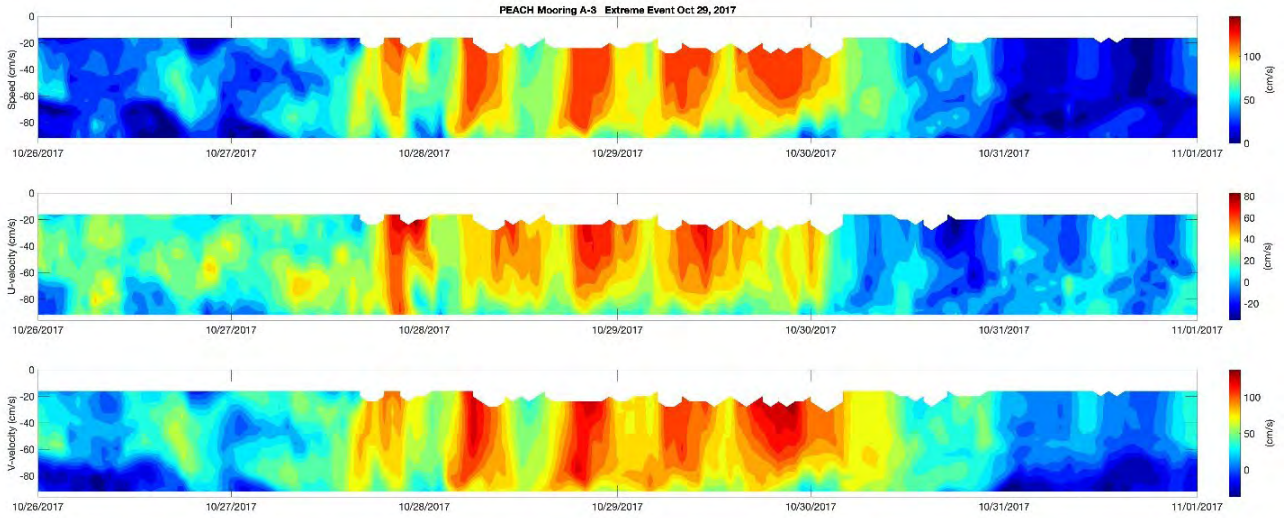

Figure 3-11 – Speed (upper) and east (middle), north (lower) velocities for a) a 30-day period surrounding a high-current event at PEACH mooring A3 during October 2017, and b) a 6-day period surrounding the event.

Figure 3-12 **a)**

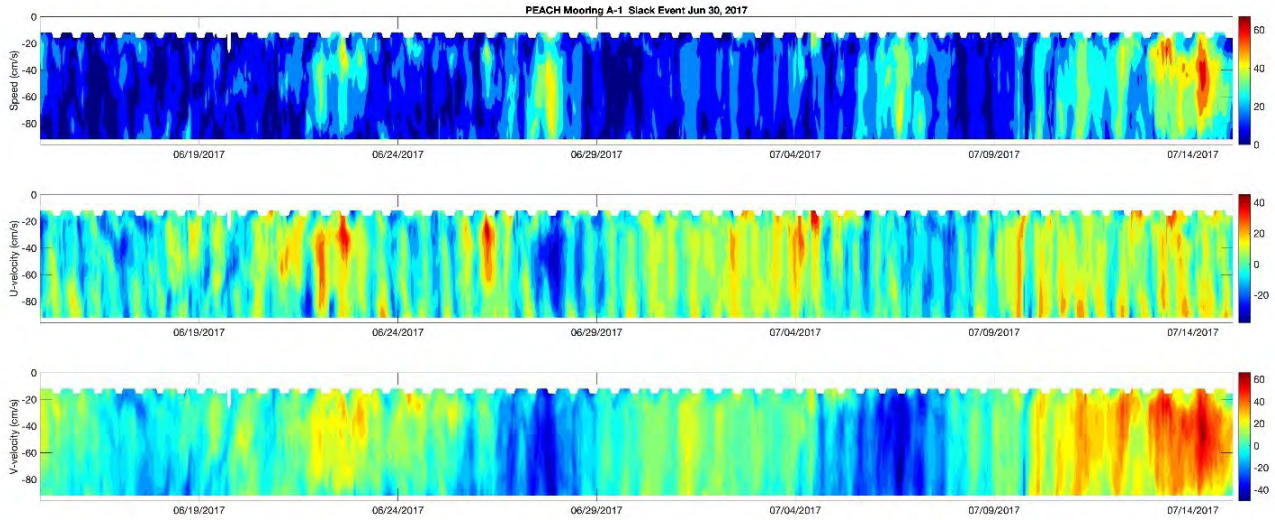

Figure 3-12 **b)**

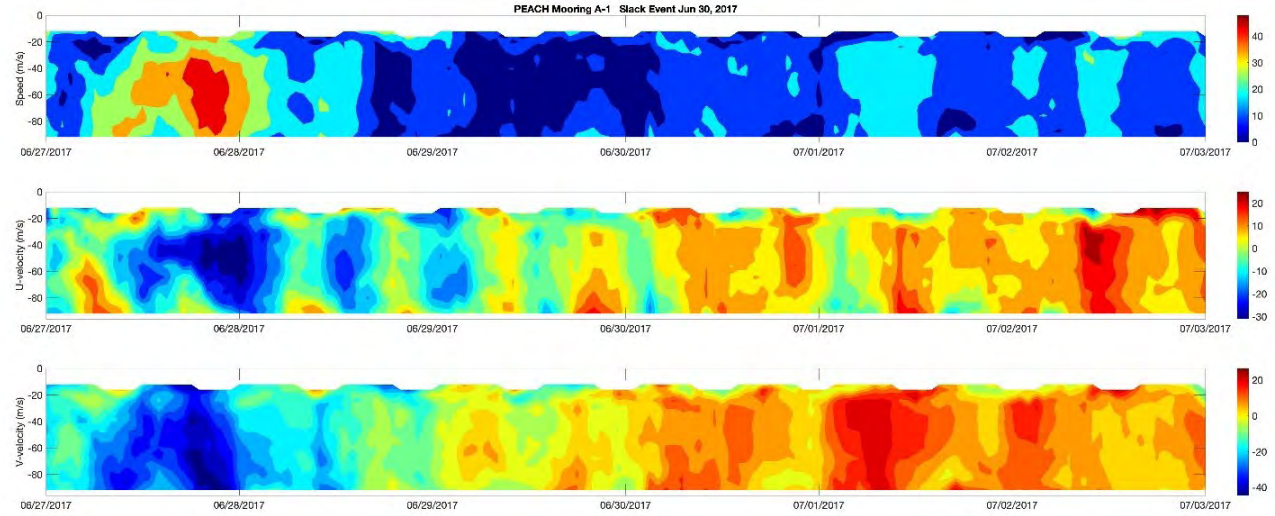

Figure 3-12 – Speed (upper) and east (middle), north (lower) velocities for a) a 30-day period surrounding a slack-current event at PEACH mooring A1 during June 2017; and b) a 6-day period surrounding the event.

Figure 3-13 **a)**

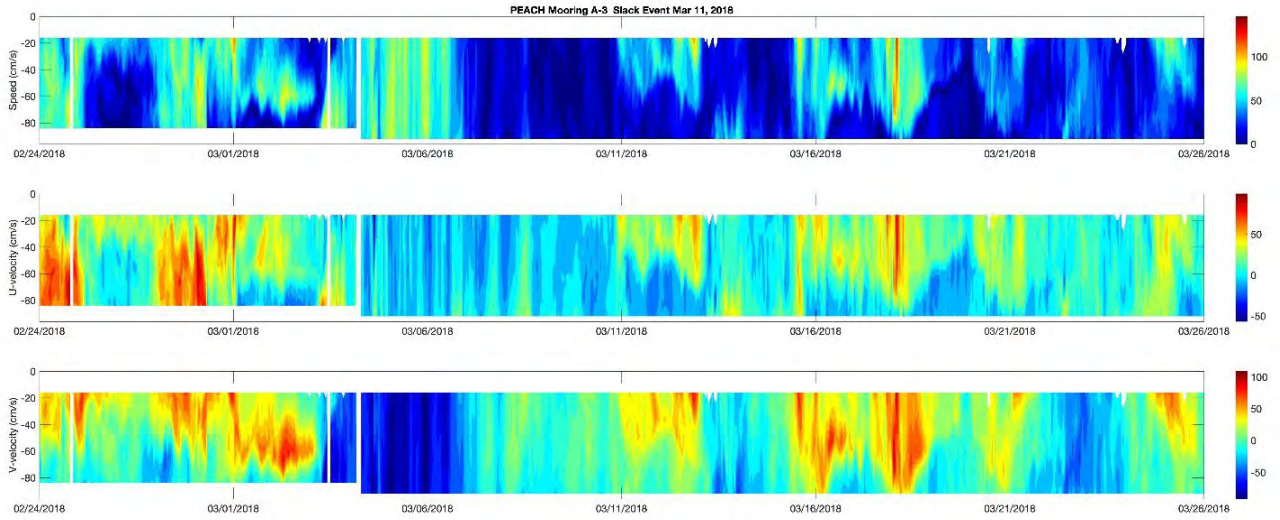

Figure 3-13 **b)**

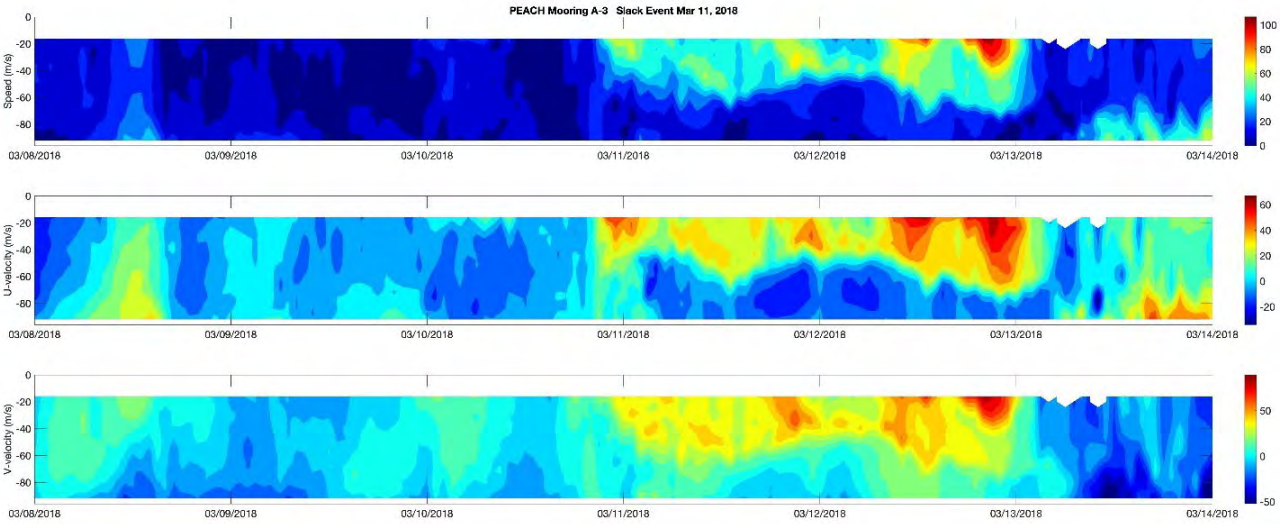

Figure 3-13 – Speed (upper) and east (middle), north (lower) velocities for a) a 30-day period surrounding a slack-current event at PEACH mooring A3 during March 2018; and b) a 6-day period surrounding the event.

3.4. Tides

A field study was conducted in 1994 by Lentz et al. (2001) to determine the barotropic tidal amplitude and phase on the continental shelf region between Chesapeake Bay and Cape Hatteras (Figure 3-14), near the proposed OOI site. Data were collected using eight moored current meters and 18 near-bottom pressure sensors from August 1994 to either October or December 1994. Ten of the pressure gauges were located along a cross-shelf transect, perpendicular to the coast but diagonal to isobaths on outer shelf, between the 5-m and 85-m isobaths (Figure 3-14). The remaining eight pressure gauges were located close to shore, along the 5-m isobath and the 20-m isobath. The eight currents meter moorings deployed by Lentz et al. (2001) were all within 16 km of the coast, at depths of 4 m, 8 m, 14 m, 21 m, and 26 m. In addition, data from three Mineral Management Services (MMS) current meter moorings, deployed August 1992-February 1994 were used as part of the analysis. These were positioned along the mid-shelf (22 m, 35 m, and 60 m), along an east-west line at 36 deg 15'N (Berger et al., 1994).

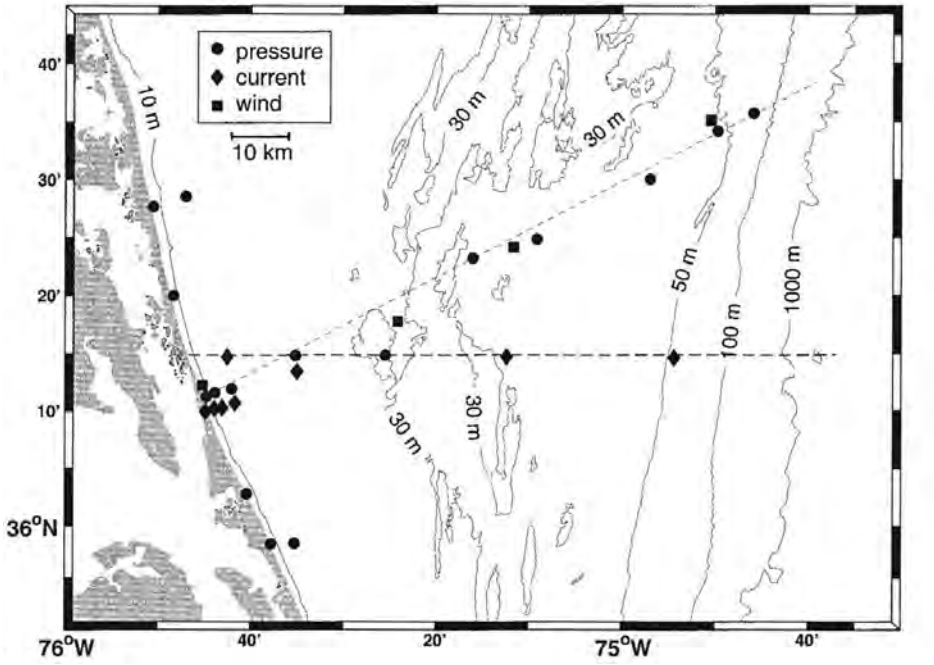

Figure 3-14 – Locations of eight current meter moorings and 18 near-bottom pressure sensors from 1994 field study. (Adapted from Lentz et al., 2001, their figure 2a)

Lentz et al. determined that the largest semidiurnal tidal constituents were M_2, N_2, and S_2 and largest diurnal tidal constituents were K_1/P_1 and O1 (Table 3-4). The semidiurnal tide amplitude and phase increased poleward along coast and decreased by about 10% from the coast to the shelf break. The diurnal K1/P1 tide exhibited constant sea level amplitude across shelf, and an increase in phase with distance offshore. O1 had a small amplitude increase from coast to shelf break and approximately constant phase across shelf. Maximum amplitude was found at mid-shelf to outer shelf with M_2 (10 cm s^{-1}). Amplitudes for all other constituents were small, > 3 cm s^{-1}. Cross-shelf currents were small near coast, increased toward mid-shelf, and approximately constant over mid and outer shelf. Along shelf currents are nonzero near coast, increasing about twice the coast current over mid and outer shelf. (Figure 3-15).

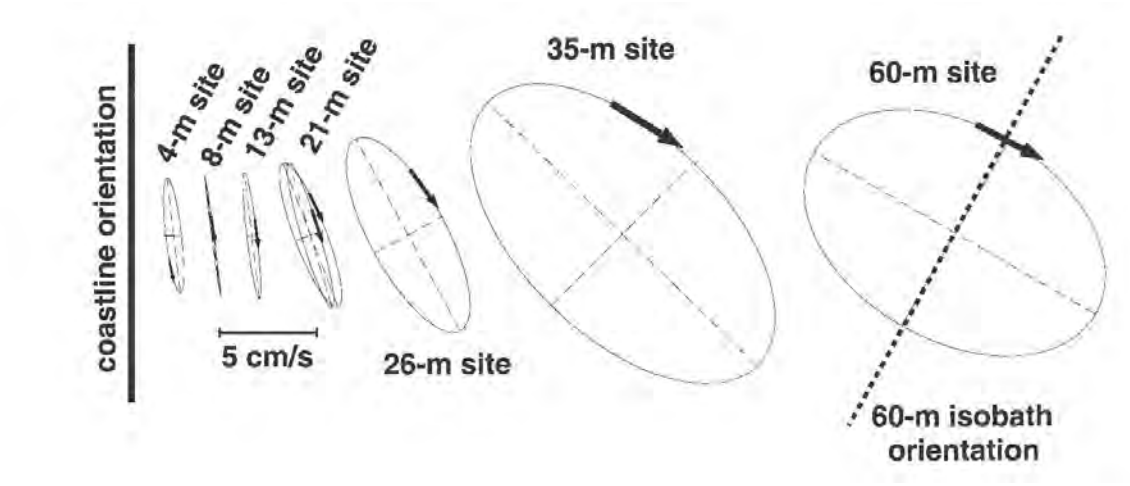

Figure 3-15 – Tidal ellipses showing magnitude and direction of tidal currents for the current meters. Rotation direction indicated by arrows (clockwise) and relative phase indicated by position of arrow. (Adapted from Lentz et al., 2001, their figure 7).

Table 3-4 –Tidal constituents from Lentz et al. (2001)

Constituent	Sea level amplitude at the coast	Type	Depth averaged tidal currents
M_2	47 cm	Semidiurnal	10 cm/s
N_2	11 cm	Semidiurnal	> 3 cm/s
S_2	10 cm	Semidiurnal	> 3 cm/s
K_1/P_1	7 cm	Diurnal	> 3 cm/s
O_1	5 cm	Diurnal	> 3 cm/s

Brunner and Lwiza (2020) examined 12 years of High-frequency radar (HFR) collected by the Mid-Atlantic Regional Association Coastal Ocean Observing System (MARACOOS) project to calculate the mean seasonal and annual tidal amplitude and phase of the dominant M_2 constituent, using classical harmonic analysis. The inherent uncertainty of HFR raw data has been estimated to be 5 cm s^{-1}, but the uncertainty for tidal amplitudes is only 1-4 cm s^{-1}.

Calculating the semi-major, semi-minor axes, phase, and orientation showed mean flow equatorward in the MAB of about 5-10 cm s^{-1}. The flow, driven by an alongshore pressure gradient, increased in strength in the offshore direction, towards the shelfbreak frontal jet. This general circulation pattern agreed with the HFR mean flow results (Figure 3-16).

Tidal ellipses for the HFR data tidal fit showed that the M_2 constituent are oriented roughly perpendicular to coast with ϕ ~120-140° within the majority of the study area (Figure 3-17). The exception is south of Cape Hatteras, where the Gulf Stream disrupts this pattern resulting in scattered orientation for all constituents. The other semidiurnal constituents (N_2 and S_2) tidal ellipse patterns are similar to the M_2 (Figure 3-17). The semi-major axis current amplitudes for all tidal constituents increases with distance from the coast. The maximum is about mid-shelf, then the current amplitudes decrease again towards the shelf break. The dominant tidal energy is in the semidiurnal M_2 constituent, with the maximum semi-major amplitude found at mid-shelf (~10 cm s^{-1}). The maximum semi-major amplitude at mid-shelf for the remaining constituents was of 2-4 cm s^{-1}. The mean seasonal fits and the mean annual fit of the M_2 semi-major axis and phase all appear very similar (Figure 3-18). The seasonal differences in

amplitude are apparent when subtracting the annual amplitude from the seasonal amplitude, with a difference of -1 to 1 cm s^{-1} over the majority of the MAB shelf ranges.

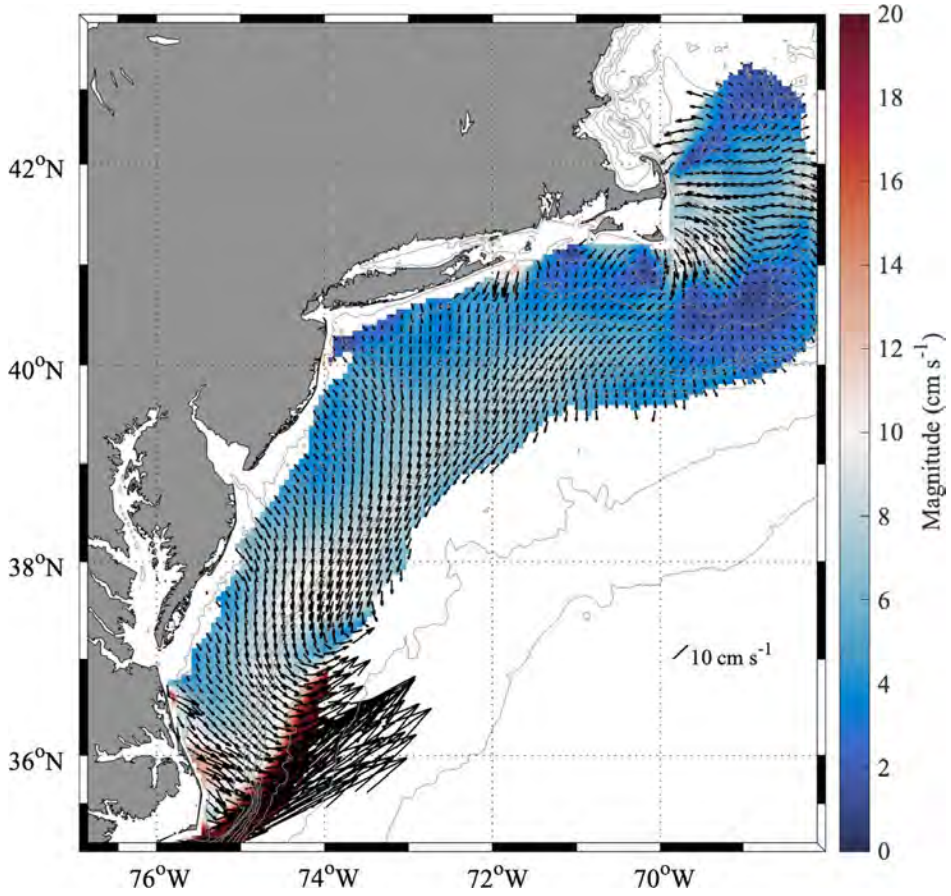

Figure 3-16 – Long-term mean surface velocities (black arrows) and magnitude. (Adapted from Brunner and Lwiza, 2020, their figure 2).

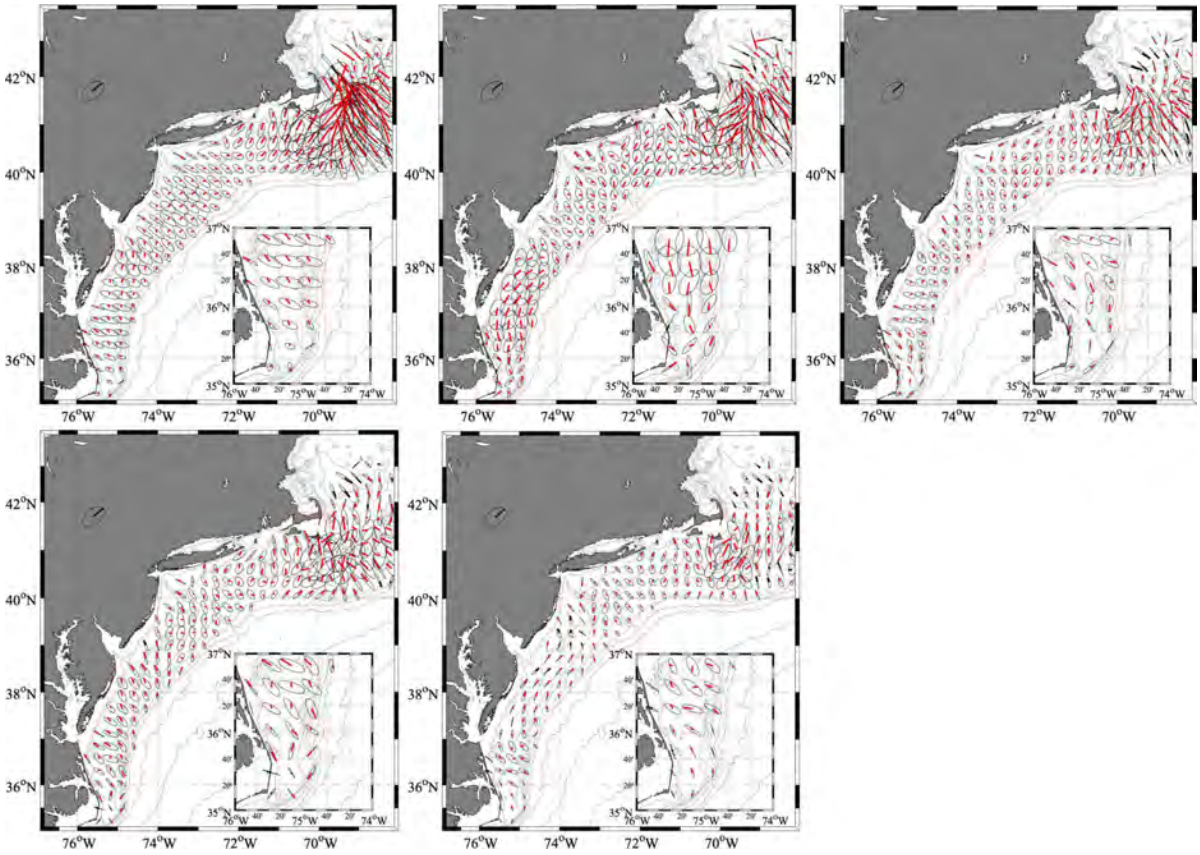

Figure 3-17 – Mean tidal ellipses for (a) M_2, (b) N_2, c(c) S_2, (d) K_1, and O_1 tidal currents. (Adapted from Brunner and Lwiza, 2020, their figure 4).

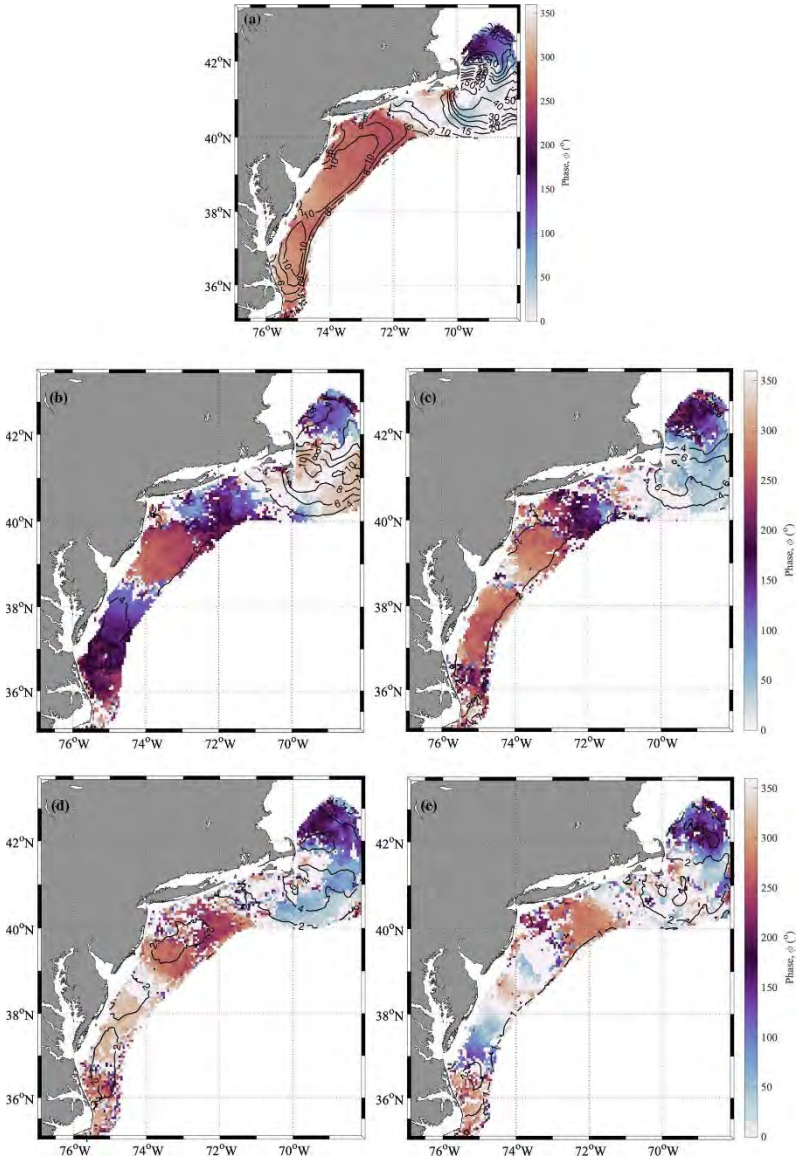

Figure 3-18 – Mean fit of semi-major axis tidal currents (black contours) and phase (color contours) for (a) M_2, (b) N_2, c(c) S_2, (d) K_1, and O_1. (Adapted from Brunner and Lwiza, 2020, their figure 5).

The pressure record from PEACH moorings A1, A2, A3, and B1, shows the maximum tidal range to be approximately 1.5 meters.

3.5. Seasonal stratification - PEACH

In addition to ADCPs, the PEACH moorings also included CTDs: one at the bottom of Moorings A1, A2, and A3 (100 m, 96 m, 97 m respectively) and three on Mooring B1 (4 m, 16 m, and 36 m). The processed CTD data were hourly averaged. Sea surface temperatures from the Copernicus Climate Change Service (C3S) were downloaded and values nearest to each mooring were extrapolated. A 24-hourly running mean of the CTD temperature data were plotted with the extrapolated sea surface temperature values for each mooring (Figure 3-19 and Figure 3-20).

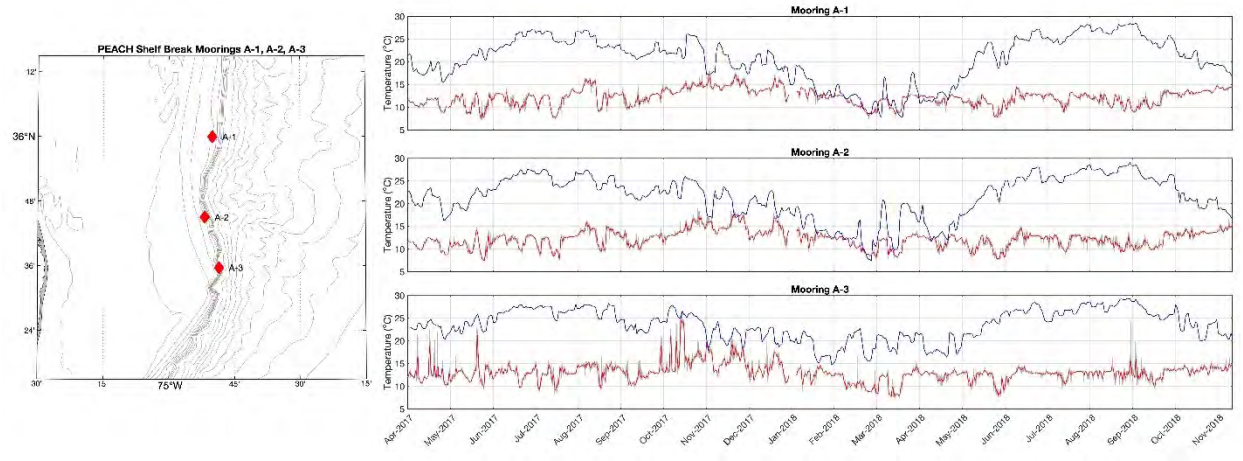

Figure 3-19 – Location map (left) and temperature (right) for moorings A1, A2, and A3. Hourly sea surface temperature from Copernicus Climate Change Service (blue), and hourly (gray) and 24-hour running mean (red) near bottom temperature from mooring A1 (top), Mooring A2 (middle), and Mooring A3 (bottom).

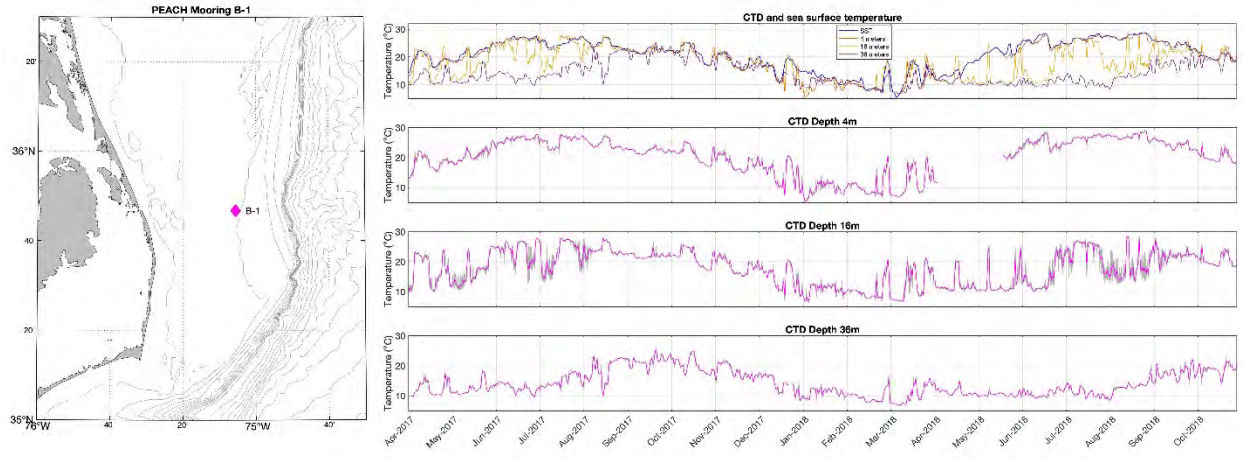

Figure 3-20 – Location map (left) and temperature (right) for mooring B1. Hourly sea surface temperature from Copernicus Climate Change Service (blue), and 24-hour running mean at 4 m (orange), 16 m (yellow) and 36 m (purple; upper panel). Hourly (gray) and 24-hour running mean temperature at 4, 16 and 36 m (second through fourth panels).

Mean, minimum, and maximum of the sea surface temperature and hourly CTD temperature are listed in Table 3-5. The sea surface temperatures at Moorings A1 and A2 display a strong seasonal cycle while the bottom CTD temperature remains consistent. The difference in the surface and bottom summer temperatures is approximately 10°C, while the difference in surface and bottom winter temperatures is within approximately 1°C. The sea surface temperatures at Mooring A3 are warmer than those at the other mooring sites throughout the year with winter temperatures staying above ~15°C. The CTD temperatures at mooring A3 are also noisier with episodes of warm water reaching ~29°C.

At Mooring B1, sea surface temperatures and the 4-meter CTD temperature have discernable seasonal cycles. The 36-meter CTD has a smaller annual range with warmer temperatures occurring in October 2017 and 2018. The temperature signal in the mid-water column is extremely noisy during the summer, which is likely due to instrumentation error. Haines et al. (2022) note that the primary cause of offsets in PEACH CTD salinity values was bubbles or

debris being sucked into the conductivity sensors. in winter, sea surface and all CTD temperatures at Mooring B1 are within approximately 1.5°C of each other.

Table 3-5 – Mean, minimum, and maximum values for sea surface temperatures and hourly CTD temperatures at Moorings A1, A2, A3, and B1.

Mooring		Range (°C)	Min (°C)	Max (°C)	Mean (°C)
A1	SST	20.8	7.8	28.6	20.2
	CTD	9.6	7.6	17.2	12.1
A2	SST	21.7	7.4	29.1	20.9
	CTD	10.3	7.4	17.9	12.2
A3	SST	14.6	14.8	29.3	23.3
	CTD	16.7	7.9	24.6	13.0
B1	SST	23.4	5.4	28.8	20.0
	4 m CTD	23.7	5.3	29.0	20.3
	16 m CTD	22.2	6.3	28.5	17.8
	36 m CTD	19.7	6.6	26.3	14.1

The CTD salinity data from Moorings A1, A2, and A3 all exhibit similar signals, with Mooring A2 slightly fresher than Mooring A1 and Mooring A3 fresher than both Moorings A1 and A2 during 2017 only (Figure 3-21). At Mooring B1 (Figure 3-22), the 4-meter CTD and 16-meter CTD data are extremely noisy, especially in the spring and summer months. Salinity at the 36-meter CTD is less erratic, ranging between (~32-36 psu). A 7-day running mean was used to smooth the data (Figure 3-22). From the 7-day running mean, a 30-day cycle was apparent with stronger differences in summer than in winter. Mean, minimum, and maximum values of hourly CTD salinity for all moorings are listed in Table 3-6.

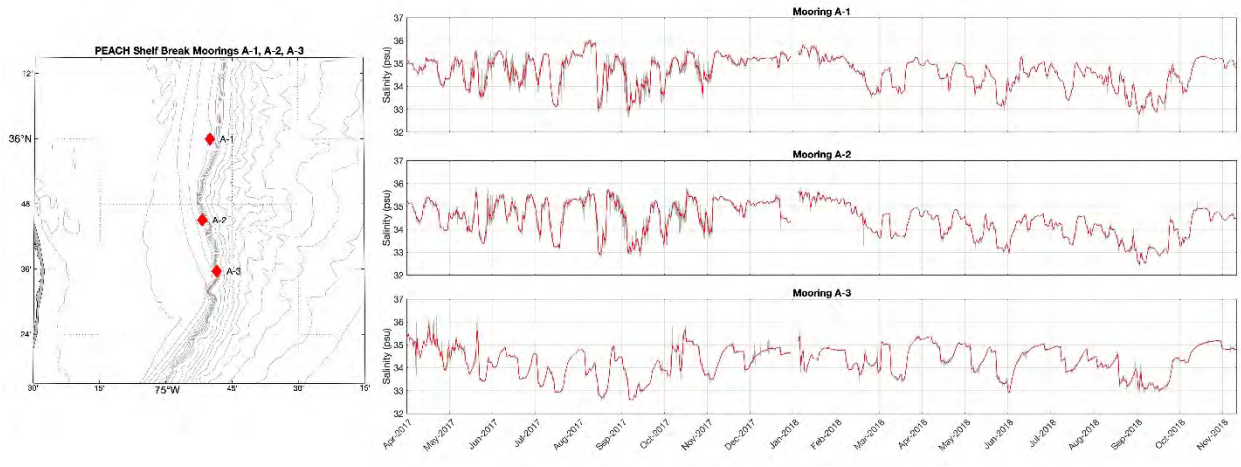

Figure 3-21 – Location map (left) and salinity (right) for moorings A1, A2, and A3. Hourly (gray) and 24-hour running mean (red) near bottom salinity from mooring A1 (upper), Mooring A2 (middle), and Mooring A3 (lower).

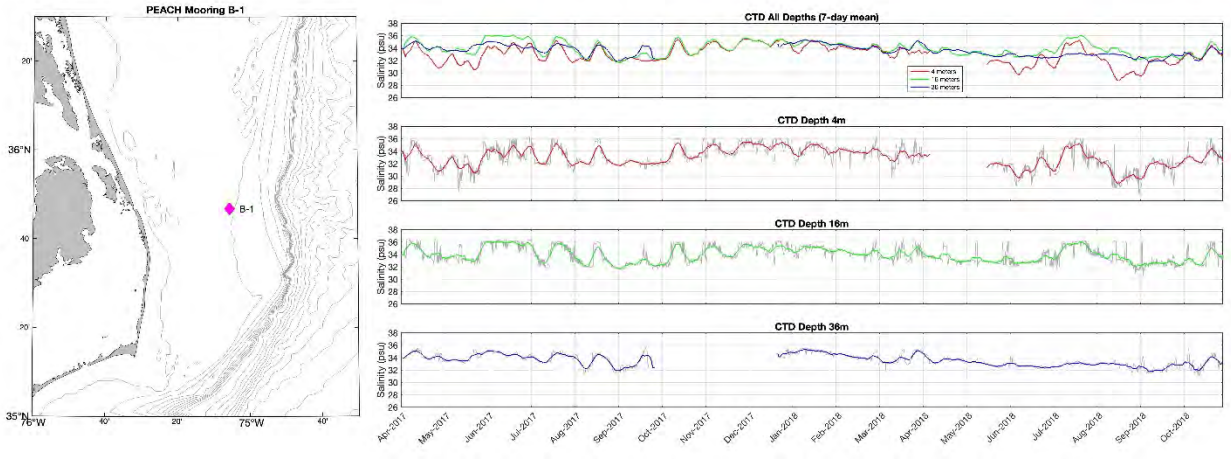

Figure 3-22 – Location map (left) and salinity (right) for mooring B1. Seven-day running mean salinity at 4 m (orange), 16 m (yellow) and 36 m (purple; upper panel). Hourly (gray) and 7-day running mean salinity at 4, 16 and 36 m (second through fourth panels).

Table 3-6 – Mean, minimum, and maximum values for hourly CTD salinity at Moorings A1, A2, A3, and B1.

Mooring	Range (psu)	Min (psu)	Max (psu)	Mean (psu)
A1	3.9	32.1	36.0	34.6
A2	3.4	32.4	35.8	34.4
A3	3.8	32.6	36.4	34.3
B1 4 m	9.4	26.9	36.3	33.0
B1 16 m	6.1	30.5	36.5	34.0
B1 36 m	5.1	30.8	36.0	33.6

3.6. Seasonal Stratification - World Ocean Database

To further explore the seasonal differences in temperature and salinity, CTD data were extracted from the World Ocean Database using instrument, variable, and location selection criteria. Only stations for which both temperature and salinity data were available were downloaded. Using Ocean Data View (ODV) (Schlitzer, Reiner, 2021) these observations were subsequently divided into three regions defined as **Shelf**: 75.33°W to 75.00°W (75° 20' to 75° 00'), **Slope**: 75.00°W to 74.70°W (75° 00' to 74° 42'), and **Offshore**: 74.70°W to 74.00°W (74° 42' to 74° 00'), all with latitudinal limits describing the glider box 35.5°N to 37.25°N. The observations in each of these geographical regions were also divided into seasons defined as winter (December-February), spring (March-May), summer (June-August) and fall (September-November). The next subsections describe the resulting geographical and temporal distributions of the temperature and salinity observations and provide some basic statistics on the WOD data available.

Shelf Region (Figure 3-23 through Figure 3-27, Table 3-7)

In the shelf region, the mean depths are ~15.5±9 m regardless of season, while the mean temperature ranges from 9.1±2.8°C in winter to 20.7±3.8°C in fall. The spring mean temperature is similar to winter, while the summer mean is similar to fall. The extrema in the Tables include outliers. Therefore, without further statistical analysis, the expected ranges are best illustrated by the ranges of the Figure 3.6.1-3 axes. According to Figure 3-23 the minimum/maximum shelf region temperatures are ~4°C/30°C. This same figure suggests that temperatures are coldest in the January through March time frame (upper left panels). Warming begins in mid-April (note there are no data in early April) and continues through the fall with the highest temperatures and lightest densities occurring in July and mid-September. Note there are no December observations.

Winter Shelf (Figure 3-24): Winter sampling is sparse (3658 data points). There are no December observations and no observations in early January or late February (upper left panels). That said, there is no obvious pattern to the depth range sampled during the winters where there are observations (upper right panel). With slightly cooler temperatures in the later part of the record, densities are also greater in the late winter (upper left panels). There is a tendency for waters to be warmer and more saline on the offshore side, particularly south of 36.5°N (i.e., in the Mooring Box). There is an inshore fresh region to the south of 35.75°N just of barrier islands.

Spring Shelf (Figure 3-25): There are nearly twice as many spring observations compared to Winter or Summer (6783 data points). That said they are concentrated in March and late May with very few profiles between and the April/early May profiles tend to be shallower than the others (upper left panels). The coolest waters are the deepest and occur earlier in the years (upper right and center panels, respectively). The coldest and densest waters are seen before April and by May the waters appear to be more stratified with warmer lighter waters lying above the cooler denser waters (upper left panels). With slightly cooler temperatures in the later part of the record, densities are also greater in the late winter (upper left panels). As in winter, there is a tendency for waters to be warmer and more saline on the offshore side, again particularly south of 36.5°N (i.e., in the Mooring Box), but also further. Also as in winter, there is an inshore fresh region, but in spring it reaches to the north of 36°N.

Summer Shelf (Figure 3-26): There are more shallow observations in summer months than in any other season (2375 data points). June is well covered as is later July through August, but there is a gap in July (upper left panels). The coolest waters are the deepest and occur earlier in the years (upper right and center panels, respectively). As in the spring, the coolest but not the densest waters are seen earlier in the season and stratification strengthens throughout the summer (upper left panels). The densest waters occur deep in this shallow water column in early August, and it appears that salinification is contributing to the summer densification (upper center panel). There is a north-south gradient in surface salinities, with the largest values occurring to the south of 36°N (lower center panel) and there is an apparent surface cool patch just to the north of 36.5°N. This could be the result of the scatter sampling and relatively low number of observations.

Fall Shelf (Figure 3-27): There are 5660 shelf observations in the fall months and the only obvious gap occurs around the second week of October (upper left panels). The warmest waters in the entire shelf record are seen in September and it appears that stratification begins to weaken by late September/early October. Along with the weakening stratification, the spread in salinities and temperatures is reduced later in the season. Returning to the pattern seen earlier in the year, surface waters are freshest and warmest south of 36°N.

Table 3-7 – Shelf CTD statistics.
Overall (upper panel) and seasonal (successive panels) statistics for the MAB Shelf defined between 35.5-37.25°N and 73.3-75.0°W, Based on all available World Ocean Database. Statistics, including the mean, standard deviation, standard error, number of observations, and the minimum and maximum values for Conservative Temperature (°C), Absolute Salinity (g kg^{-1}), and depth (m). Mean, Stand. Dev., Stand. Err. and Count do not include outliers, but the extrema do include outliers (see caption of Figure 3-23 for definition). The table was created using ODV (right-click on T/S plot – summary statistics.

Shelf

		Mean	Stand.Dev.	Stand.Err.	Count	Minimum	Maximum
Conservative Temperature (	:	14.204	6.456	0.0474	18544	3.830	29.333
Absolute Salinity SA [g/kg]	:	33.3850	1.1898	0.00874	18544	22.6738	36.7863
Depth [m]	:	15.5	9.0	0.07	18544	1.0	44.7

Shelf Winter: December – February (cf. Figure 3-24).

		Mean	Stand.Dev.	Stand.Err.	Count	Minimum	Maximum
Conservative Temperature (	:	9.144	2.789	0.0461	3658	3.830	19.700
Absolute Salinity SA [g/kg]	:	33.8050	1.1013	0.01821	3658	24.0424	36.5371
Depth [m]	:	15.2	9.0	0.15	3658	1.0	43.7

Shelf Spring: March – May (cf. Figure 3-25).

		Mean	Stand.Dev.	Stand.Err.	Count	Minimum	Maximum
Conservative Temperature (	:	10.092	3.741	0.0454	6783	4.547	22.496
Absolute Salinity SA [g/kg]	:	33.5643	1.1450	0.01390	6783	22.6738	36.4728
Depth [m]	:	15.5	9.0	0.11	6783	1.0	44.7

Shelf Summer: June – August (cf. Figure 3-26).

		Mean	Stand.Dev.	Stand.Err.	Count	Minimum	Maximum
Conservative Temperature (	:	18.154	5.712	0.1172	2375	8.375	28.354
Absolute Salinity SA [g/kg]	:	33.3954	1.3808	0.02833	2375	27.3158	36.7863
Depth [m]	:	15.7	9.1	0.19	2375	1.0	42.7

Shelf Fall: September – November (cf. Figure 3-27).

		Mean	Stand.Dev.	Stand.Err.	Count	Minimum	Maximum
Conservative Temperature (	:	20.720	3.842	0.0511	5660	9.639	29.333
Absolute Salinity SA [g/kg]	:	32.9073	1.0388	0.01381	5660	28.6611	36.5854
Depth [m]	:	15.6	9.0	0.12	5660	1.0	42.7

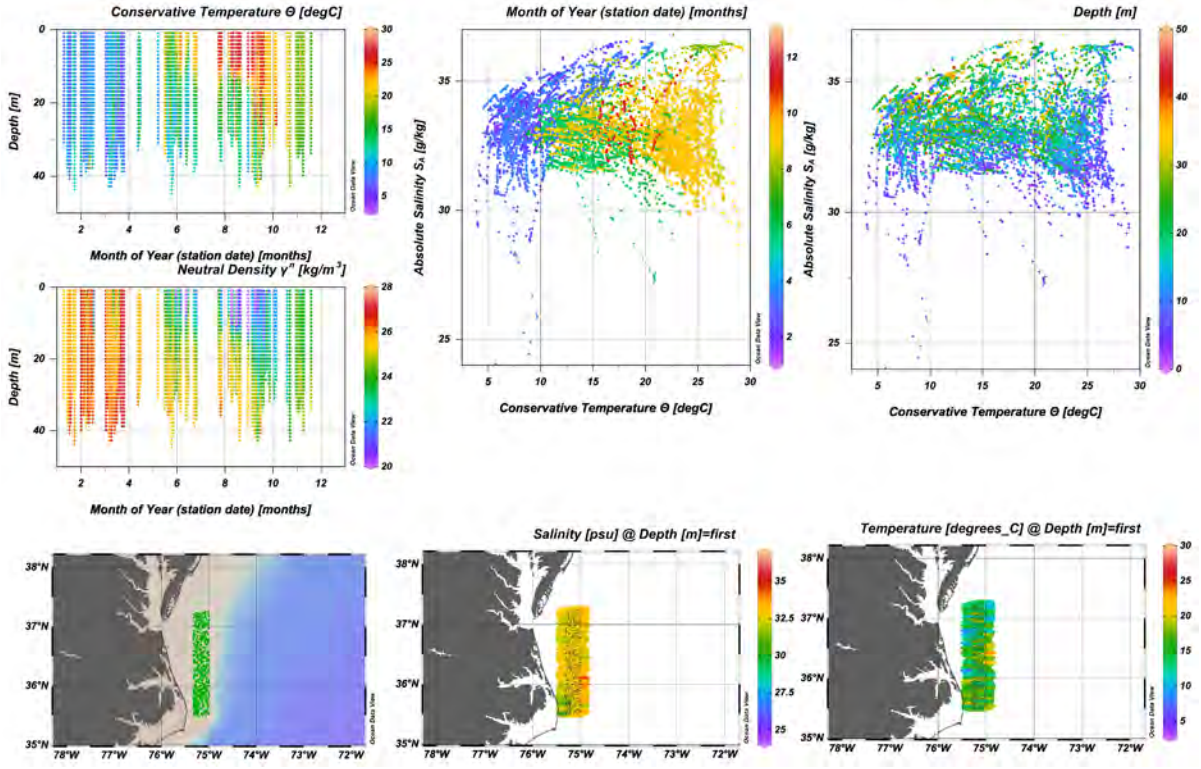

Figure 3-23 –Shelf CTD data for the MAB Shelf defined between 35.5-37.25°N (~latitudinal range of the glider box) and 75.33—75.0°W based on all available World Ocean Database:

upper left profiles of month of the year vs. depth (m) with color shading indicating Conservative Temperature (CT,°C), and just below, the same with color shading representing Neutral Density (γ^n, kg m^{-3}); upper center T/S diagram (CT/SA) color-coded by month of the year; upper right the same color-coded by depth; lower left maps of station locations; lower center a weighted-average gridded field of SA; lower right the same for CT. Note, there is some extrapolation at the edges. The figure was created using an ODV six-window layout. Outliers, defined as data values deviating from the mean of the field of values by more than 1.5 times the standard deviation, have been removed.

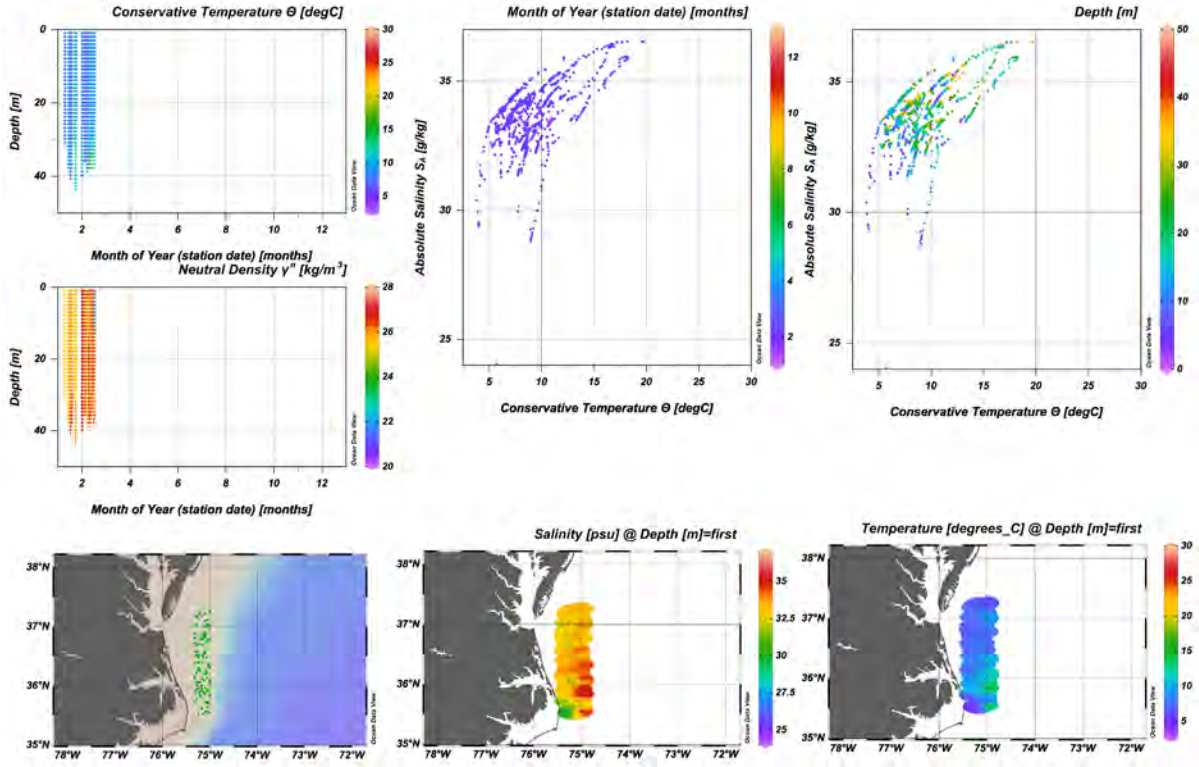

Figure 3-24 – Same as Figure 3-23, but just the winter months (December-February).

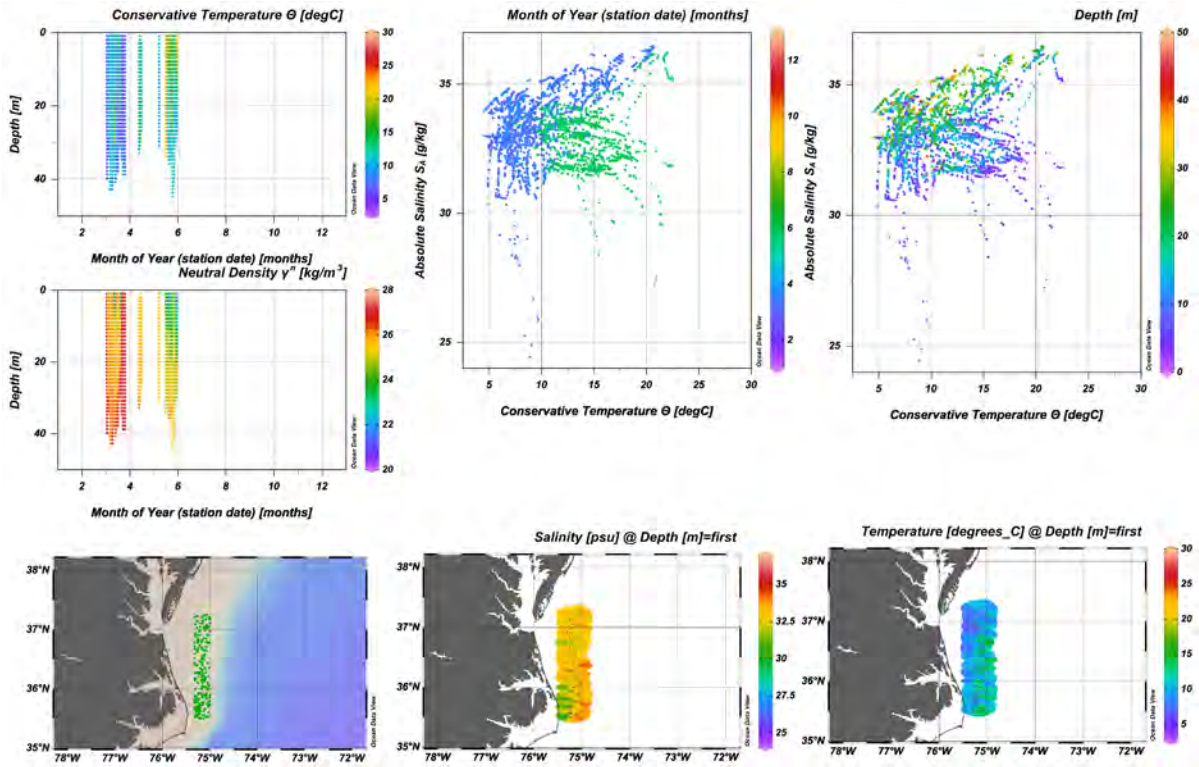

Figure 3-25 – Same as Figure 3-23, but just the spring months (March-May).

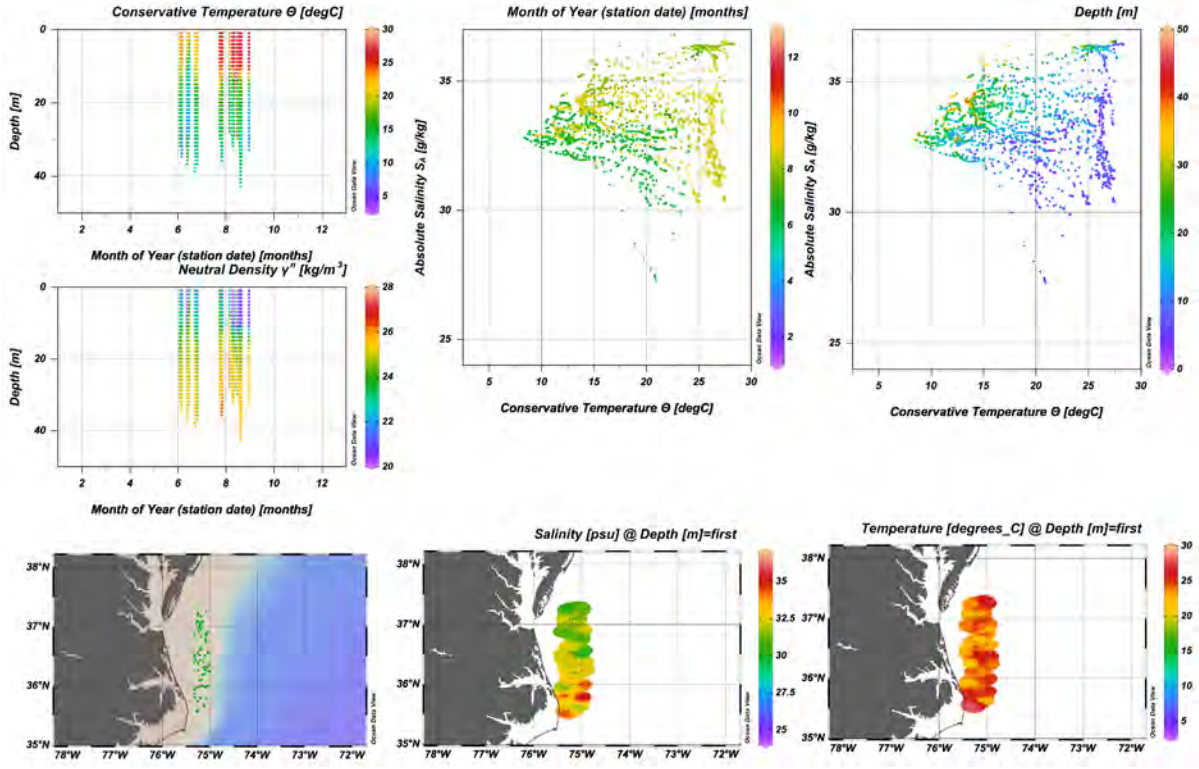

Figure 3-26 – Same as Figure 3-23, but just the summer months (June-August).

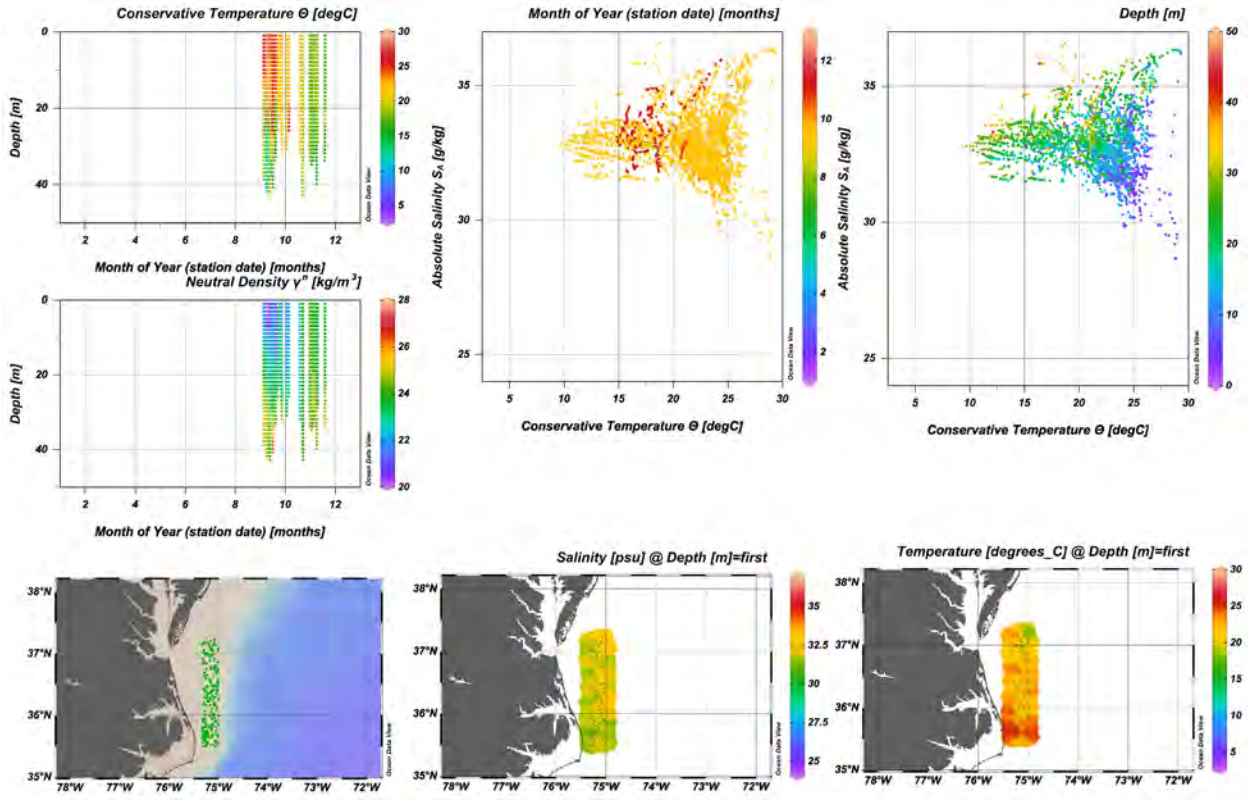

Figure 3-27 – Same as Figure 3-23, but just the fall months (September-November).

Slope Region (Figure 3-28 through Figure 3-32, Table 3-8)

In the slope region Figure 3-28, the mean depths of the observed data are similar, ranging from 91 - 103 m in the different seasons and having large variability are not significantly different from the overall mean of the data record (96±111 m). Mean temperature ranges from 11.5±2.9°C in spring to 15.1±5.3°C in fall. As on the shelf, the spring mean temperature is similar to winter, but here the average summer temperature is equally distant from the spring and fall values. The magnitude of the variability (σ_{CT} = 5.8°C) is more similar to that seen in the fall. While the extrema in Table 3-8 (3.8°C < T < 29.8°C, 28.06 g kg^{-1}< SA <41.19 g kg^{-1}) includes outliers, the figure axes suggest that it is only the maximum salinity which is likely an outlier. The largest salinities are ~38 g kg^{-1}. Full water column 0-50 m, coldest temperatures and densest waters are seen January through May, while below about 30 m, the lowest temperatures are seen from January through August (upper left panels). As on the shelf the warmest and lightest waters appear in the fall. Cool saline waters are seen early in early in the year (center top, blue shading), and the freshest waters are most prevalent in May-June. Note, as on the shelf, there are no December observations.

Winter Slope (Figure 3-29): On the slope, Winter sampling is less sparse than on the shelf (~20,000 data points) - half what is measured in the spring and fall, but more than measurements than in the summer. There are no December observations and no observations in early January or late February (upper left panels). There is no obvious pattern to the depth range sampled during the winters where there are observations (upper right panel). As on the shelf, densities are greatest late in the winter, but not necessarily when the waters are coldest, suggesting the effect of greater salinities. There is a patch of higher winter salinities between 36-36.5°N - it is possible there is fresh water input to the south and north. This slope pattern is consistent with the fresh winter shelf region to the south of 35.75°N (Figure 3-24), but different from the tendency for waters to be warmer and more saline on the offshore side of the shelf.

Spring Slope (Figure 3-30): There are nearly two/three times as many spring observations (~38,000) compared to winter/summer. As on the shelf, these data are concentrated in March and mid-later May with fewer profiles between and the April/early May profiles. Like the shelf, spring observations on the slope tend to be in shallower waters in March and deeper in May (upper right and center panels). In May, the coolest waters are the deepest, but in March the water column is less stratified. (upper left panels). With slightly cooler temperatures in the early part of the record, densities are also greater in the early spring (upper left panels). Temperatures are generally lower to north of ~36.75°N, but salinities are quite patchy (lower right panels). There are fresher waters offshore of the various freshwater sources, but there are also some extremely low values (purple) which one should probably question without further investigation and it appears the contouring has perhaps smeared a few questionable data points.

Summer Slope (Figure 3-31): In spite of the lower number of observations (~13,000), there is good spatial and temporal spread in the slope summer data. The only gap is later June to early July (upper left panels). Summer slope waters are stratified. The coolest waters are the deepest and unlike on the shelf (where they occur earlier in the year), on the slope cool temperatures are seen throughout the summer period (upper right and center panels, respectively). The coolest, most saline, and densest waters are seen at depth, particularly below ~20-25 m (upper left panels, upper right panel). As on the shelf, there is a north-south gradient in surface salinities, with the largest values occurring to the south of 36°N (lower center panel) and an apparent surface cool patch just to the north of 36.5°N. While this could be real, we again note that this could be the result of the scatter sampling and relatively low number of observations, or a single cruise with uncalibrated salinities that ran from spring into summer. Further investigation would be required to better understand this pattern.

Fall Slope (Figure 3-32): There are ~36,000 slope observations in the fall months with more scattered sampling later in the season than earlier, but no obvious temporal gaps (upper left

panels). Loss of stratification is seen throughout September. The deepest records are the most saline and coldest (upper right panels). Along with the weakening stratification, as on the shelf the spread in salinities and temperatures is reduced later in the season. As on the shelf, where there is a fall pattern of surface waters being warmest south of 36°N, but unlike the shelf pattern, here the most saline waters are also found in the south.

Table 3-8 – Slope CTD statistics. Overall (upper panel) and seasonal (successive panels) statistics for the MAB Slope defined between 35.5-37.25°N and 75.0—74.7°W. Data description same as for Table 3-7.

Slope

	Mean	Stand.Dev.	Stand.Err.	Count	Minimum	Maximum
Conservative Temperature (:	13.046	4.536	0.0138	107601	3.841	29.802
Absolute Salinity SA [g/kg] :	34.8125	1.1052	0.00337	107601	28.0643	41.1907
Depth [m] :	96.4	111.2	0.34	107601	0.3	1427.9

Slope Winter: December – February (cf. Figure 3-29).

	Mean	Stand.Dev.	Stand.Err.	Count	Minimum	Maximum
Conservative Temperature (:	11.975	2.793	0.0198	19818	5.198	21.248
Absolute Salinity SA [g/kg] :	35.1487	0.8945	0.00635	19818	32.0721	36.7391
Depth [m] :	91.1	89.8	0.64	19818	1.0	495.7

Slope Spring: March – May (cf. Figure 3-30).

	Mean	Stand.Dev.	Stand.Err.	Count	Minimum	Maximum
Conservative Temperature (:	11.469	2.847	0.0146	38186	3.841	23.488
Absolute Salinity SA [g/kg] :	34.9829	0.8161	0.00418	38186	29.5090	41.1907
Depth [m] :	95.3	110.0	0.56	38186	1.0	1427.9

Slope Summer: June – August (cf. Figure 3-31).

	Mean	Stand.Dev.	Stand.Err.	Count	Minimum	Maximum
Conservative Temperature (:	13.530	5.842	0.0511	13071	4.380	29.328
Absolute Salinity SA [g/kg] :	34.1942	1.4597	0.01277	13071	28.0643	36.6195
Depth [m] :	102.8	147.9	1.29	13071	1.0	874.7

Slope Fall: September – November (cf. Figure 3-32).

	Mean	Stand.Dev.	Stand.Err.	Count	Minimum	Maximum
Conservative Temperature (:	15.101	5.308	0.0278	36526	3.924	29.802
Absolute Salinity SA [g/kg] :	34.6733	1.2073	0.00632	36526	29.9330	36.7140
Depth [m] :	98.1	107.3	0.56	36526	0.3	1208.2

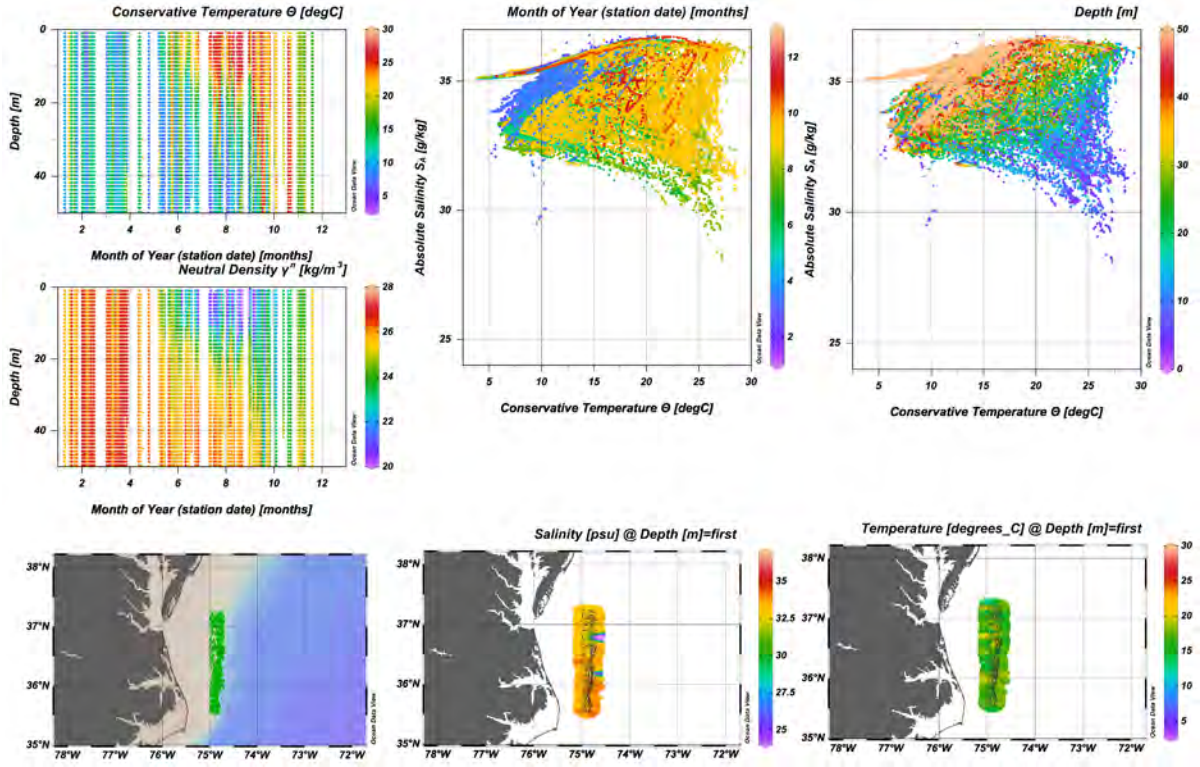

Figure 3-28 – Same as Figure 3-23, but for the slope region defined between 75.0–74.7° W

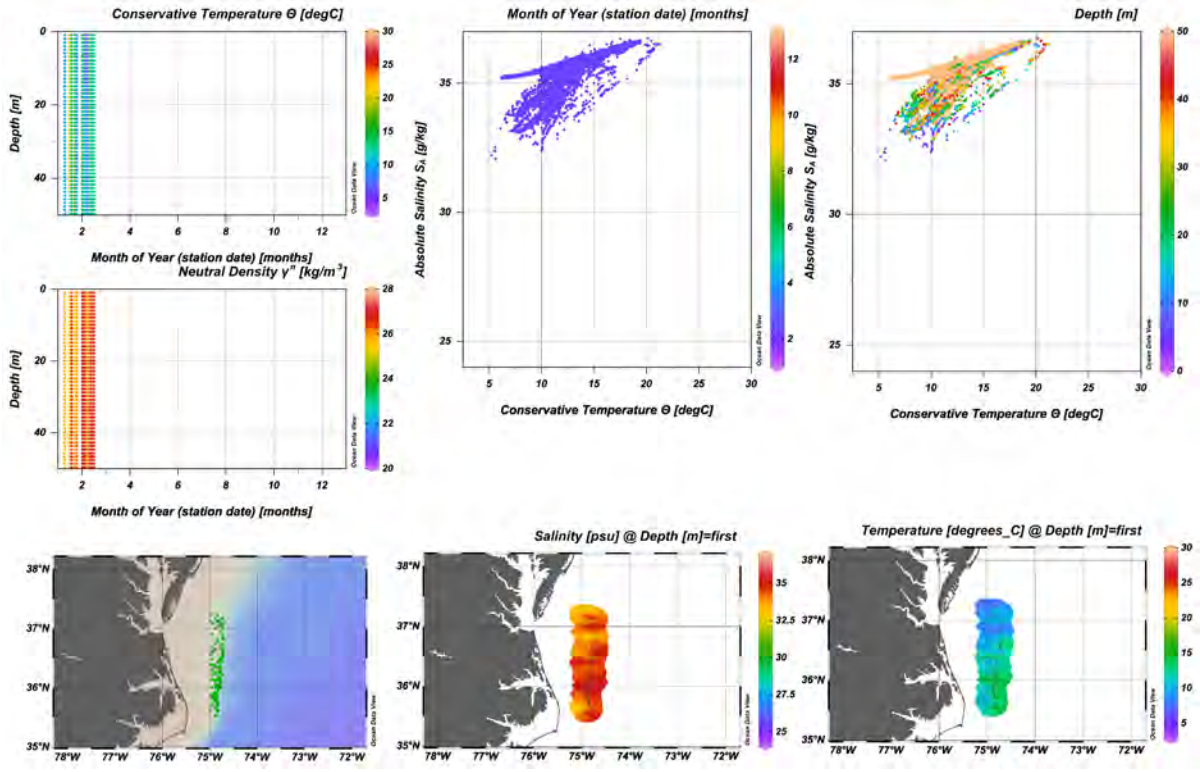

Figure 3-29 – Same as Figure 3-28, but just the winter months (December-February).

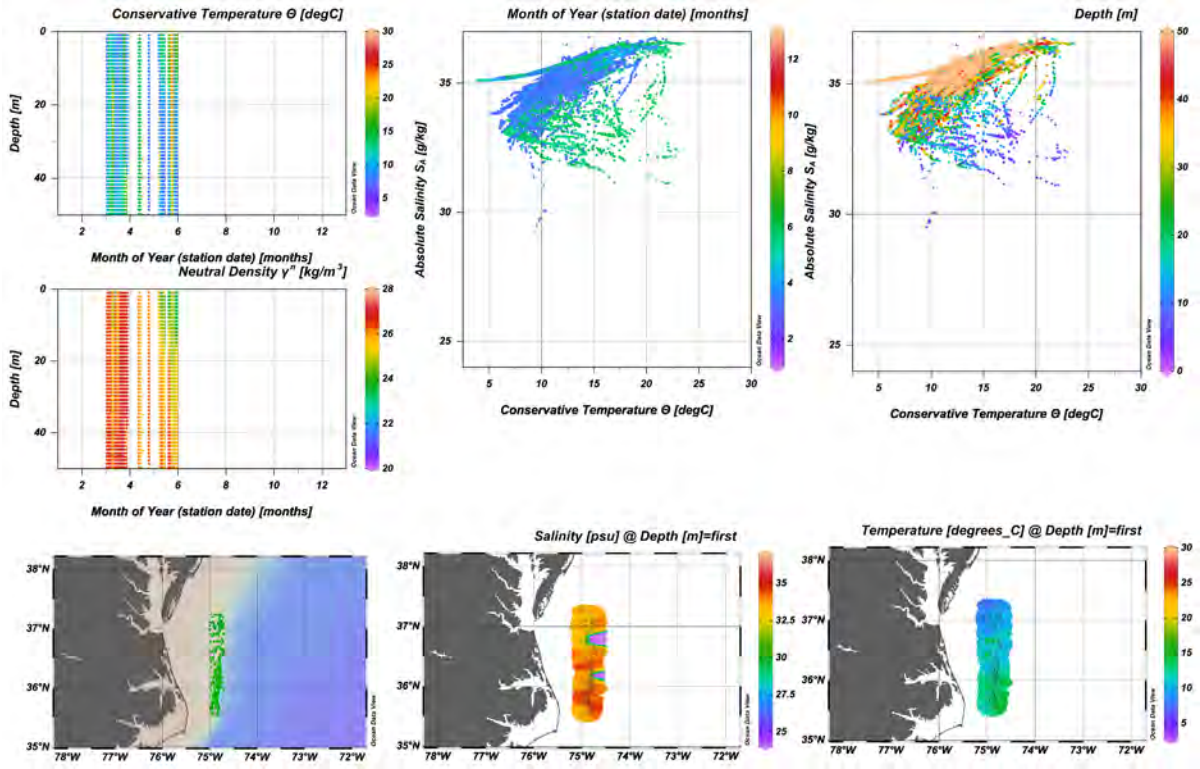

Figure 3-30 – Same as Figure 3-28, but just the spring months (March-May).

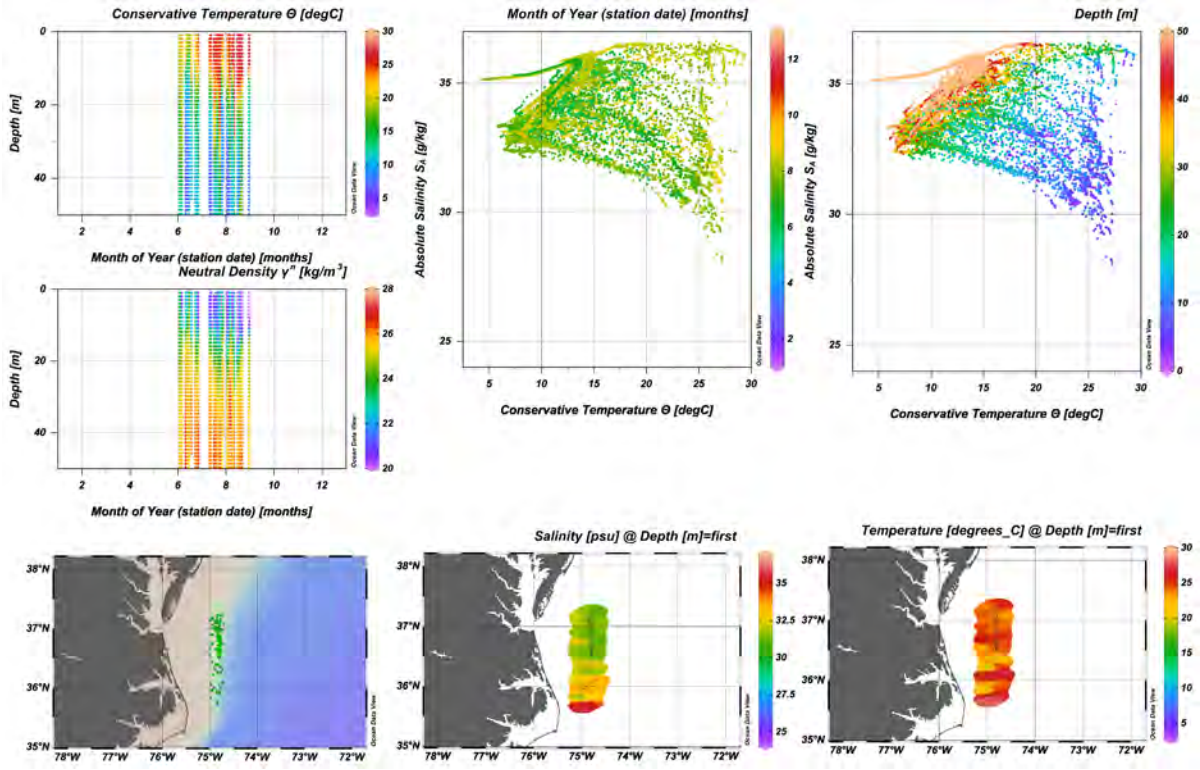

Figure 3-31 – Same as Figure 3-28, but just the summer months (June-August).

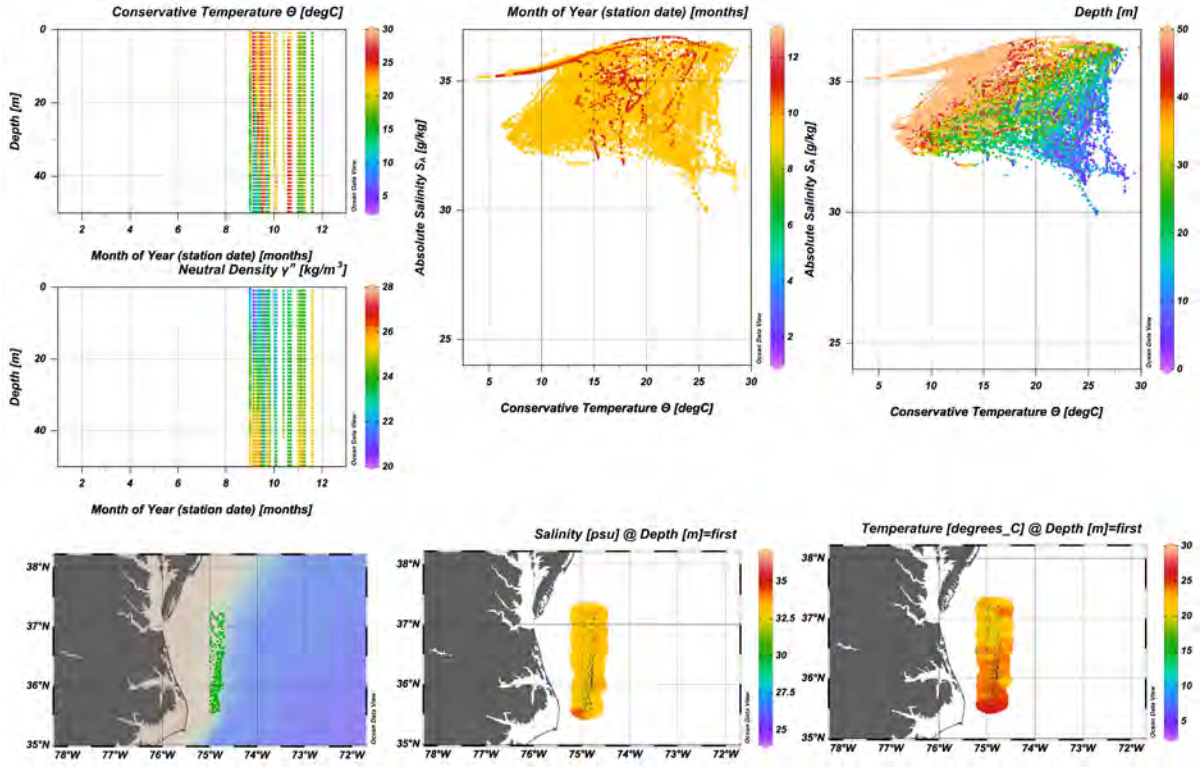

Figure 3-32 – Same as Figure 3-28, but just the fall months (September-November).

Offshore Region (Figure 3-33 through Figure 3-37, Table 3-9)

The offshore dataset includes almost 121,000 records with winter, spring, summer and fall containing 20%, 30%, 39% and 11% of the observations, respectively. In the offshore region, the mean depths of the observed data range from 122±102 m in the fall to 759±702 m in the summer creating a shallow/deep bias between these two seasons in particular, but also including the winter which has only one profile reaching below ~1000 m (upper left panels). This "deeper" profile happens to be the only December profile in the entire shelf/slope/offshore data collection. There is also a geographic bias, with most of the observations in the northwest corner of the region (lower right panels). The latter creates a diagonal surface pattern of cool-fresh to warm-saline from northwest to southeast (lower right panels). As the deepest waters are also the most saline, there is tail in the T/S diagrams (upper right panels) that is also seen on the slope (Figure 3-28 through Figure 3-32)

Offshore (Figure 3-33), ranges from 2.4°C to ~29°C, with the lowest values in the summer because they are deepest. Mean water column temperature is similar in the winter, spring and summer (8.5°C to 9.4°C), but is greater in the fall (~14.3) because these profiles are the shallowest. As in both the shelf and slope regions, average salinity is similar in the winter and spring (35.23 to 35.24±0.46 g kg^{-1}). Summer salinities are higher (35.42 g kg^{-1}) and fall lower (35.18 g kg^{-1}), but neither significantly so. The range is likely due to the different depth ranges in the two seasons. Regardless of the sampling biases, as would be expected, throughout the year in the offshore region there is stratification with a tendency for the greatest densities to occur in the late winter and early spring (upper left panels).

Winter Offshore (Figure 3-34): There are approximately the same number of offshore winter samples as on the slope (21,000) - here less than what is observed for in the spring and summer, but more than that measured in the fall. As previously mentioned, here we have the only December observations in the entire dataset, a single profile reaching to about 1200 m.

January sampling is particularly shallow (all < 1000 m) and with samples to 2000 m February provides the deepest sampling during the season (upper left panels). Stratification is apparent in all winter months, with the warmest surface temperatures in December and the clearest and deepest mixed layer (based on a likely color-biased visual inspection of the temperature and density gradients, upper left panels) later in the season. Above and below 50 m there is clear distinction between water masses in the T/S diagrams (upper right panels) suggesting an average mixed layer depth at around 200 m, though the temperature-density/depth plots (upper left panels) would suggest that the mixed layers could reach deeper. Further analysis is required. The cold/saline T/S tail is again apparent and is associated with the deeper samples. The one December profile produces its own high salinity/high temperature. With most samples congregated in the northwest corner, the geographic picture is difficult to unravel, but there appear to be lower surface salinities and temperatures to the north (lower center and right panels). There are distinctly different high salinity and temperatures to the south, particularly offshore. These are possibly associated with Gulf Stream intrusions or they could be single values whose quality should be considered in light of a larger (further offshore) region of WOD data. In either case, they are different from the shelf/slope patterns which both suggested fresher winter waters to the south of 35.75°N (Figure 3-24 and Figure 3-29).

Spring Offshore (Figure 3-35): There are more than 35,000 spring observations. There is a reasonable spread temporally with no obvious gaps. Again, the data locations are biased to the northwest corner of the region and while there are a good number of profiles reaching below 1000 m throughout the season, the mean depth is only about 350 m and none of the profiles are as deep as those obtained during the winter and summer. Therefore, one ought to assume a shallow bias for the spring observations. That said, the distinction between shallower and deeper values is again apparent in the T/S diagrams (upper right panels) with the visual (color) distinction noted at about 200 m. As in winter, the cold/saline tail is associated with deeper waters and is apparent throughout the season, and the T/S diagrams fill out in the direction of warm and fresh in the late spring. The upper tail of temperatures warmer than 15°C that was seen only in the December profile during the winter is also apparent throughout the spring, but especially in May. As in the winter, there are fresh colder waters to the north (lower right panels) with the same caveats as mentioned in the previous subsection. To the north of 36.5°N there is once again the tendency for waters further offshore to be warmer and more saline.

Summer Offshore (Figure 3-36): Unlike on the shelf and slope there are more summer data offshore than in any other season (~47,000 data points). The overall coverage depth-wise is decent with the deeper profiles available than in the other seasons (upper left panels). That said, the deep profiles are intermingled with much shallower sampling, particularly early in the summer and July to early August where there is a single deep profile. Very warm (> 25°C) light surface waters are scattered through the middle of the season (mid-June to mid-August). Warmer (> 26.5°C, visually red, upper left panel) waters reach below 500 m. This might be particularly so later in the season, but the sampling depth bias may be playing into this interpretation. The T/S diagrams (upper right panels) again show the cold/saline/deep tail and the area of warmer fresher upper waters is filled out compared to the spring. The warm/saline (upper right hand) edge of the T/S pattern is provided by the August data (upper center panel).

There is good spatial and temporal spread in the slope summer data. The only gap is later June to early July (upper left panels). Summer slope waters are stratified. The coolest waters are the deepest and unlike on the shelf (where they occur earlier in the year), on the slope cool temperatures are seen throughout the summer period (upper right and center panels, respectively). The coolest, most saline, and densest waters are seen at depth, particularly below ~20-25 m (upper left panels, upper right panel). As on the shelf, there is a north-south gradient in surface salinities, with the largest values occurring to the south of 36°N (lower center panel) and an apparent surface cool patch just to the north of 36.5°N. While this could be real, we again note that this could be the result of the scatter sampling and relatively low

number of observations, or a single cruise with uncalibrated salinities that ran from spring into summer. Further investigation would be required to better understand this pattern.

Fall Offshore (Figure 3-37): There are ~13,500 fall offshore observations - far fewer than in any other season. As in the other seasons, the data are concentrated in the northwest corner. Contributing to the lack of fall observations is the fact that all the profiles are shallower than 500 m, and the ones that go this deep occur later in the season with most of the profiles concentrated in September (upper left panels). The saline/cold tail in the T/S diagrams is represented by late October/November observations, but so are some of the warmer (15-20°C)/fresher (<34 g kg^{-1}) values (upper center panel). The former are deep (closer 500 m) while the latter are shallower (closer to 100 m) and form the southernmost blob in the surface contour plots (lower right panels). The fresher, colder central blob in the surface contour plots represents early September data, while the elongated shape to north depicting somewhat warmer values is strongly influenced by the northwest concentration of data and span the entire season. There is no obvious on/offshore gradient, but there is some suggestion of higher temperatures along the eastern edge of the region of concentrated sampling. These higher values come from multiple cruises in multiple years, so although appearing somewhat unnatural are perhaps real (i.e. have a physical cause).

Table 3-9 – Offshore CTD statistics. Overall (upper panel) and seasonal (successive panels) statistics for the MAB Offshore region defined between 35.5–37.25°N and 74.7–74.0°W. Data description same as for Table 3-7.

Offshore

		Mean	Stand.Dev.	Stand.Err.	Count	Minimum	Maximum
Conservative Temperature (	:	9.777	5.703	0.0164	120748	2.372	29.362
Absolute Salinity SA [g/kg]	:	35.3073	0.6034	0.00174	120748	23.6586	39.1850
Depth [m]	:	527.8	596.3	1.72	120748	0.1	2815.9

Offshore Winter: December – February (cf. Figure 3-34).

		Mean	Stand.Dev.	Stand.Err.	Count	Minimum	Maximum
Conservative Temperature (	:	8.525	3.828	0.0264	21000	3.484	24.447
Absolute Salinity SA [g/kg]	:	35.2404	0.4611	0.00318	21000	33.0820	36.6828
Depth [m]	:	502.3	500.1	3.45	21000	1.0	1976.8

Offshore Spring: March – May (cf. Figure 3-35).

		Mean	Stand.Dev.	Stand.Err.	Count	Minimum	Maximum
Conservative Temperature (	:	9.258	3.625	0.0193	35457	3.612	24.182
Absolute Salinity SA [g/kg]	:	35.2331	0.4698	0.00250	35457	23.6586	36.7090
Depth [m]	:	346.9	358.1	1.90	35457	1.0	1595.9

Offshore Summer: June – August (cf. Figure 3-36).

		Mean	Stand.Dev.	Stand.Err.	Count	Minimum	Maximum
Conservative Temperature (	:	9.401	6.907	0.0319	46873	2.372	28.884
Absolute Salinity SA [g/kg]	:	35.4187	0.5935	0.00274	46873	23.8545	36.9953
Depth [m]	:	758.5	701.6	3.24	46873	1.0	2799.4

Offshore Fall: September – November (cf. Figure 3-37)

		Mean	Stand.Dev.	Stand.Err.	Count	Minimum	Maximum
Conservative Temperature (	:	14.283	4.702	0.0405	13502	5.739	28.881
Absolute Salinity SA [g/kg]	:	35.1777	0.9164	0.00789	13502	31.6673	36.7351
Depth [m]	:	122.2	102.1	0.88	13502	1.0	500.7

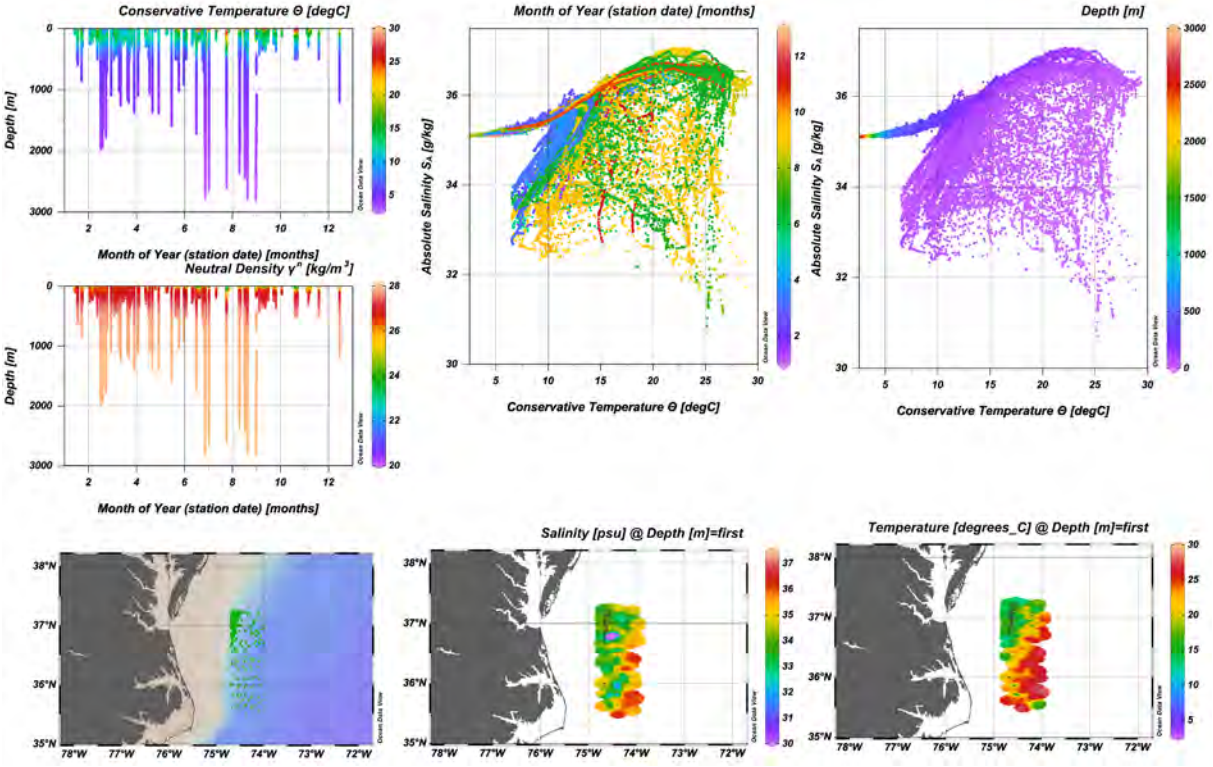

Figure 3-33 – Same as Figure 3-23, but for the offshore region defined between 74.7–74° W

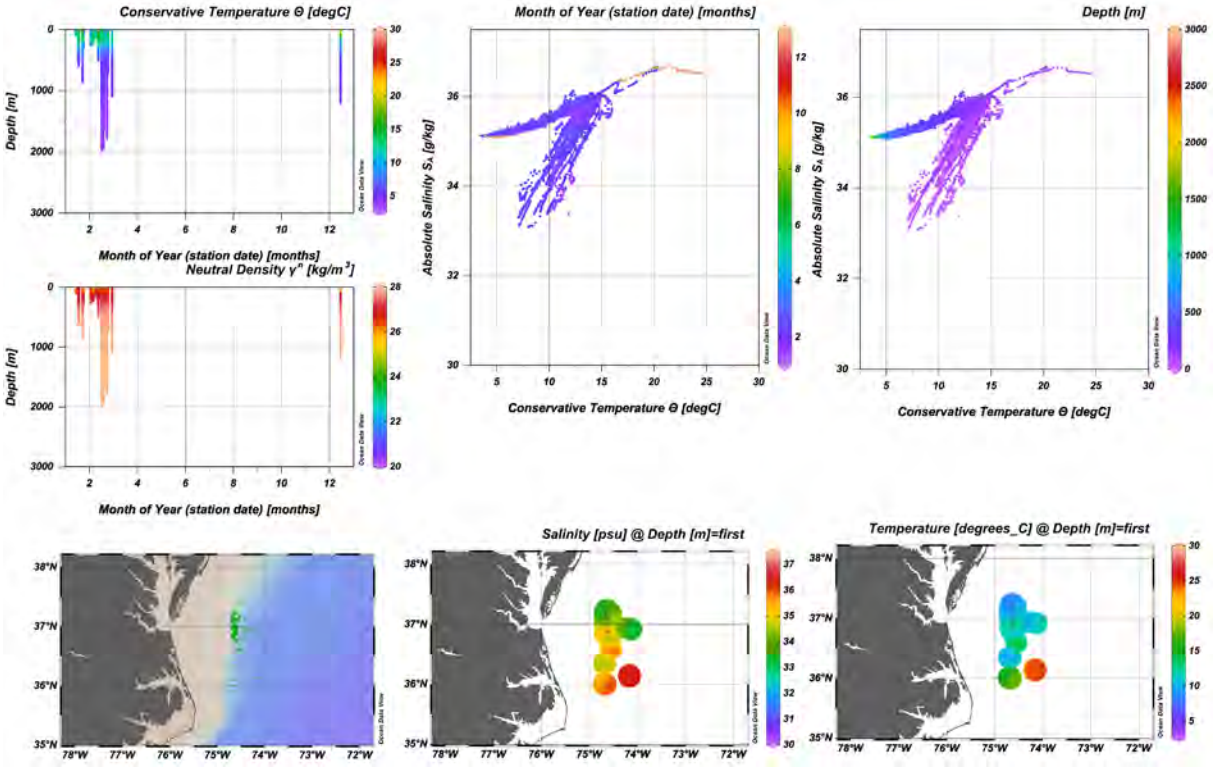

Figure 3-34 – Same as Figure 3-33, but just the winter months (December-February).

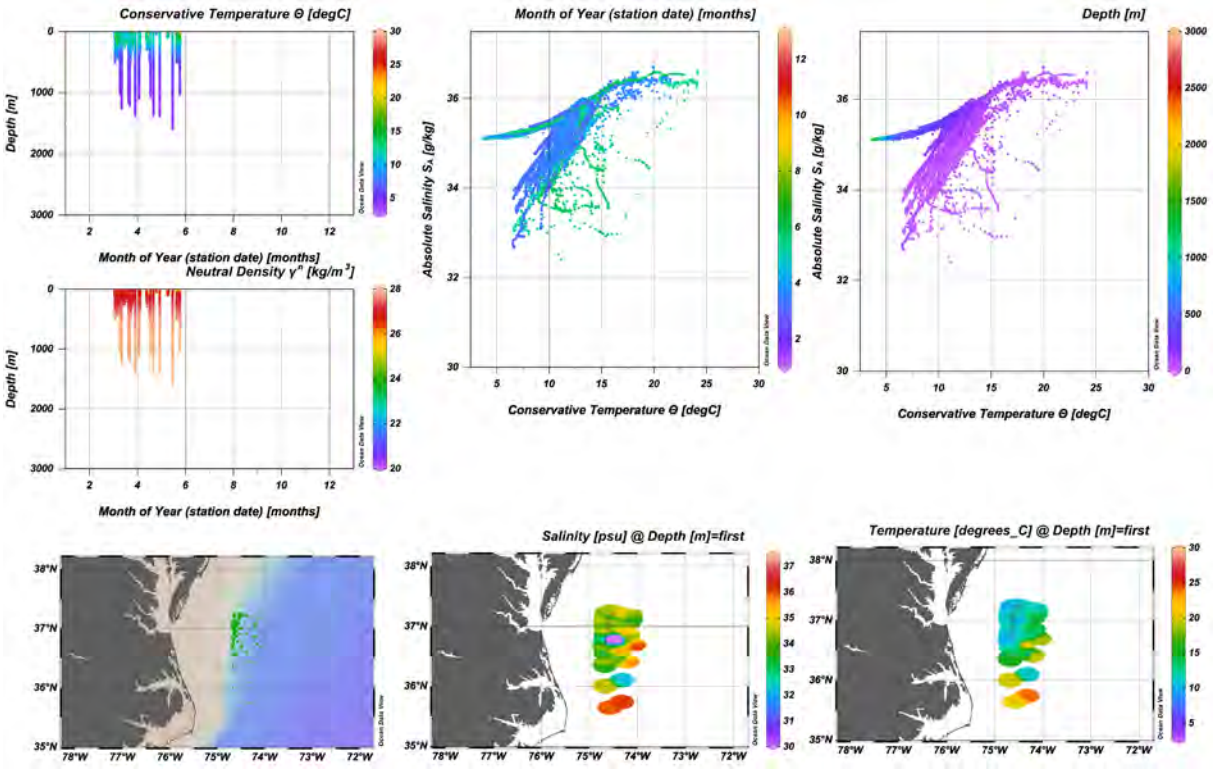

Figure 3-35 – Same as Figure 3-33, but just the spring months (March-May).

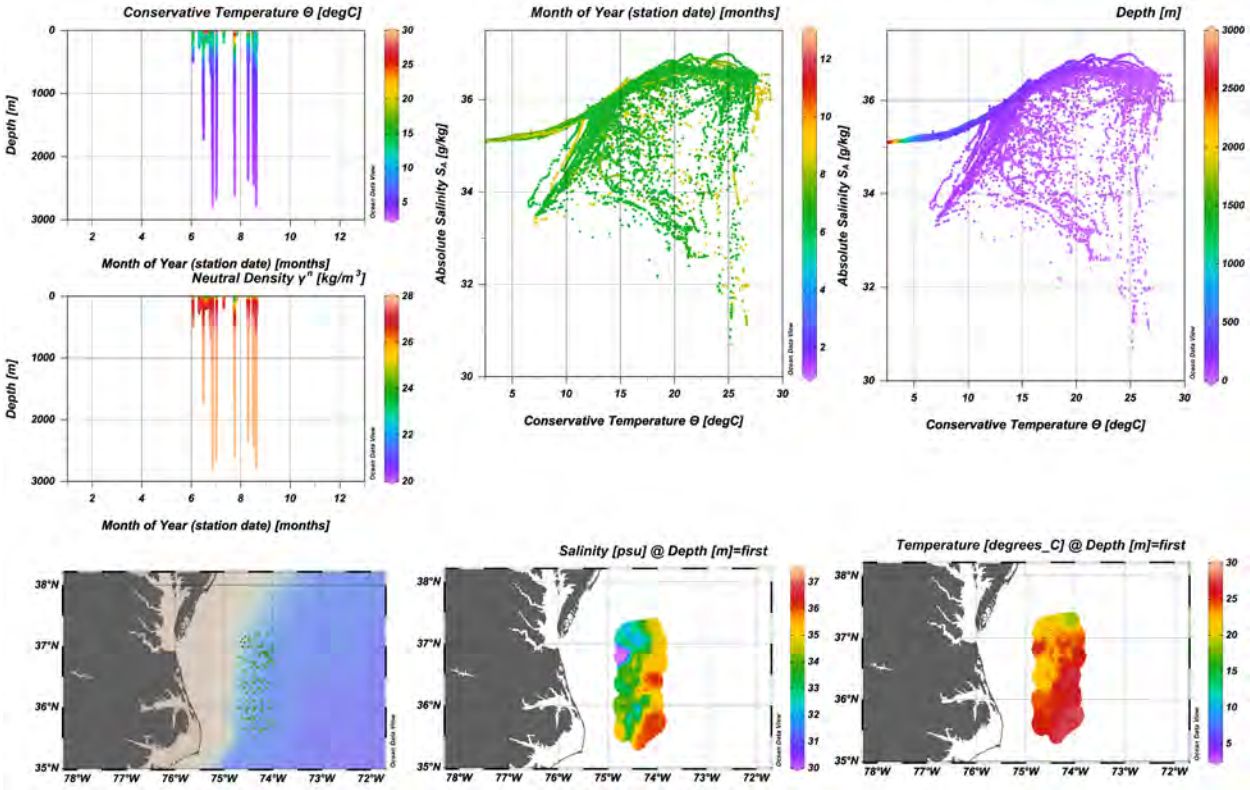

Figure 3-36 – Same as Figure 3-33, but just the summer months (June-August).

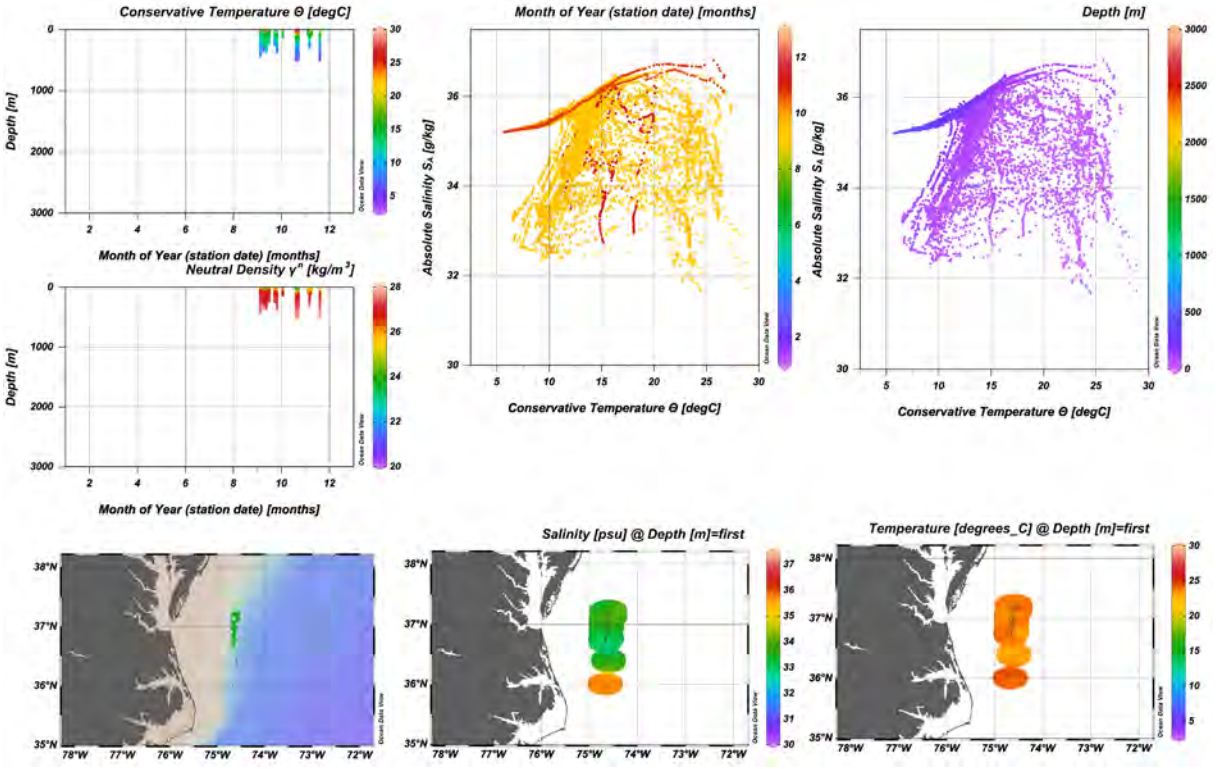

Figure 3-37 – Same as Figure 3-33, but just the fall months (September-November).

WOD Spatial Sampling Assessment

With 247,929 CTD observations in the defined shelf-slope-offshore regions, there are approximately 5-6 times fewer CTD data points on the shallow shelf(~18.5K, Table 3-7) compared to the deeper slope (~108K, Table 3-8) and offshore regions (~121K, Table 3-9). The WOD CTD dataset includes observations from 1982 to 2021, however, the 1980's data are sparse with records in 1982, and more regular sampling not beginning until 1987. With just a few early years with deeper records, until about 2010, most of the data are limited to the upper ~200 m (Figure 3-38). The offshore plots in particular should be interpreted with caution as there are seasonal biases in the depth range of the profiles and the majority of profiles are confined to the northwest corner of the region (see location maps in Figure 3-33 though Figure 3-37). Most of the offshore profiles deeper than 600 m are located to the north and/or west of the mooring box. There are 4 exceptions which might be useful references when considering bottom water conditions for the NE and SE moorings (Figure 3-39).

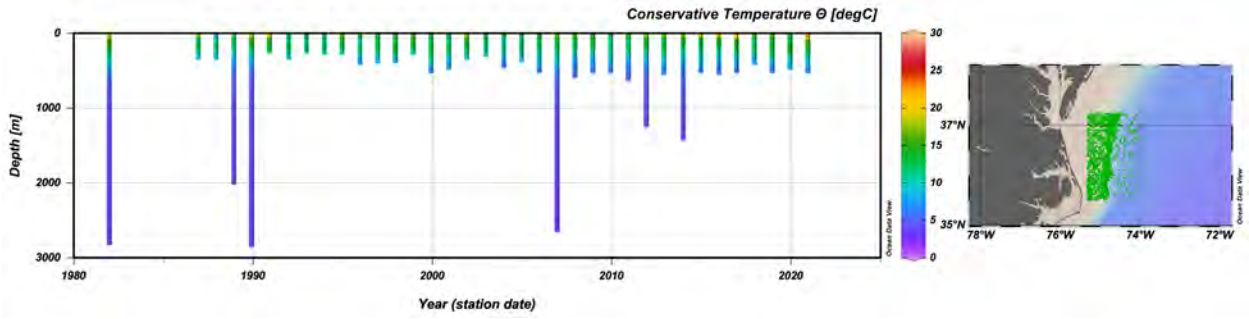

Figure 3-38 – CTD depth range and temperature by year (left) based on all available World Ocean Database CTD data for the SMAB shelf defined between 35.5-37.25°N and 75.33—75.0°W. Color shading indicates the overall average Conservative Temperature (CT °C) for the individual year. CTD location map (right). Software credit as in Figure 3-23.

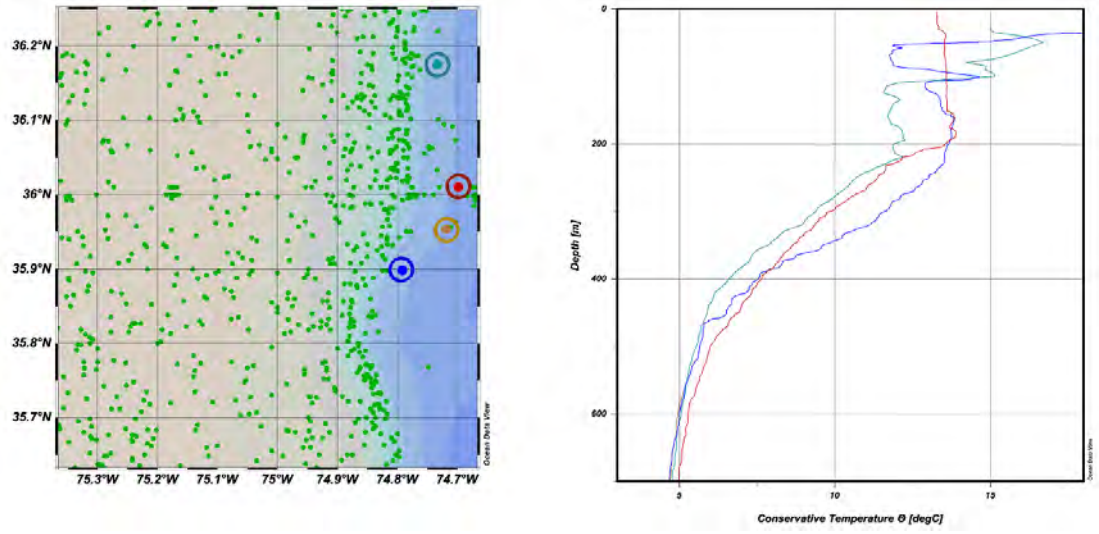

Figure 3-39 – CTD profiles near 600 m depth within the Mooring Box. Based on all available World Ocean Database CTD data within the mooring box. Right panel - Conservative Temperature (CT, °C)/Depth (m) profiles from the four stations in the Mooring Box with observations that reach 600 m (see Figure 3.6.4). These are: 1) WOD Station ID 10416495 from 04/24/1989 at 74.733°W, 36.175°N (teal dot); 2) WOD Station 11554728 from 09/01/1990 with partial profile crossing 600 m at 74.733°W, 36.175°N (orange dot); 3) WOD Station 11190264 from 07/23/2007 at 74.791°W, 35.898°N (blue dot); and 4) WOD Station 15808283 from 02/15/2012 at 74.698°W, 36.01°N (red dot). Left panel - map of the data points with the locations of profiles color coded to match the right panel. Software credit as in Figure 3-23.

Comparing WOD to PEACH

Comparing the WOD-based slope findings (1982-2022, mean depth ~96 m, Table 3-8) to the PEACH mooring A1, A2 and A3 results (April 2017-November 2018, mean CTD depth ~96, Table 3-5 and Table 3-6) we begin with the caveats: a) while for a general comparison it should not matter, be aware that the WOD values are TEOS-10 variables (CT and SA) (McDougall and Barker, 2011), while the PEACH variables are ITS-90 and Practical Salinity; b) the mooring data represent a little more than 1.5 years of data at single locations, while the WOD data represent a broader region and 4 decades of observations; and c) the mooring data have smaller temporal gaps than the WOD data and while not having obvious seasonal biases in gaps, they include two instances of April-November data and one instance of December-March data.

Full range of the bottom PEACH CTD sensors and SSTs from the Copernicus Climate Change Service, 7.4°C to 29.3°C. The WOD slope region data set includes a much lower minimum, 3.8°C and a similar maximum, 29.8°C. The colder WOD minimum is likely because WOD represents more winters than PEACH. The similarity in maxima is hard to judge without knowing details of what went into the Copernicus SST values. It may be that summer maximum temperatures are generally more consistent though that seems unlikely given climate change. It is more likely that the more recent summers (including 2017 and 2018) have been warmer and therefore better represent the maximum. This explanation would also provide a reason for the comparatively warm SST 14.8°C minimum at A3, which is not significantly different from the WOD mean slope temperature (13.1±4.5°C). The mean depth of all the WOD slope values that go into the temperature is approximately the same as the depth of PEACH A1 to A3 bottom CTDs. The PEACH 20-month mean temperatures range between 12.1°C and 13.0°C, which suggests that near the bottom this 2017-2018 record is representative of the longer-term mean.

In salinity, because the WOD tables include outliers, it is a little hard to judge ranges, but the maximum salinity seen in the full-record slope T/S diagrams (Figure 3-28, upper right panels) is 36.6 g kg^{-1}. This compares well with PEACH A1-A3 maximum salinity of 36.4. The minimum salinity seen in the WOD slope data is 28.06 g kg^{-1}. This is quite a bit less than the 32.1 minimum in PEACH. It seems unlikely that minimum salinities have become this more saline over time. Again, looking at the WOD T/S diagrams, it is apparent the minimum S is represented by a single profile. That said, there are multiple profiles in multiples in multiple locations that indicate minimum salinity of order 29 g kg^{-1}. This suggests that the four decades of WOD data saw more fresh events than the year and half of PEACH, i.e. the 2017-2018 time frame is not completely representative of possible extrema in salinity. That said, the mean salinity WOD slope salinity is 34.8±1.1 g kg^{-1}, which is consistent with the PEACH A1-A3 mean bottom salinity range of 34.3 to 34.6.

4.0 Surface Conditions

4.1. Wind speed and direction statistics

Mean hourly wind speed and direction data along with maximum hourly wind gusts were downloaded from NDBC Historical Standard Meteorological Data files for buoy stations 41062 and 44014 (Figure 4-1, Table 4-1). Although the record was discontinuous, data for Station 44014 spanned Oct 1, 1990, to Oct 31, 2021, (Figure 4-2). Notable gaps include Nov to Dec 1993; Jan 1995; Nov 1997 to Mar 1998; Mar 1999; Oct 2003; Jan to Feb 2006; April to May 2006; Apr 2010 to Mar 2011; Mar to May 2012; Oct 2012 to Dec 2013; Mar to Apr 2020. The available wind record for Station 41062, approximately 100 km to the south, had only 19 months of continuous data and was not used for analysis in this report.

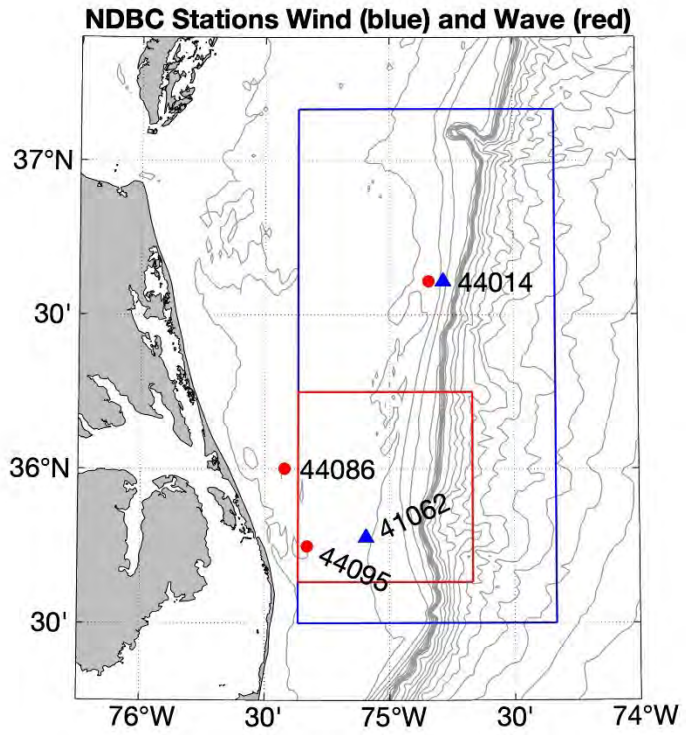

Figure 4-1 – NDBC buoy locations providing historical wind data (two blue triangles) and historical wave data (three red dots) shown with the glider bounds (blue) and mooring bounds (red). Bathymetric contours are every 20 m to 200 m and every 250 m from 250 to 3000 m.

Table 4-1 – NDBC Buoy station information for wind data. Only Buoy 44014 was used in this report, as Buoy 41062 had only 19 months of continuous data available.

NDBC Buoy	Name	Location	Height	Years
41062	Hatteras Bay (B1)	35.778 -75.095	3.5 m	2014, 2017-2018
44014	Virginia Beach offshore	36.609 -74.842	3.2 m	1990-2012, 2014-2021

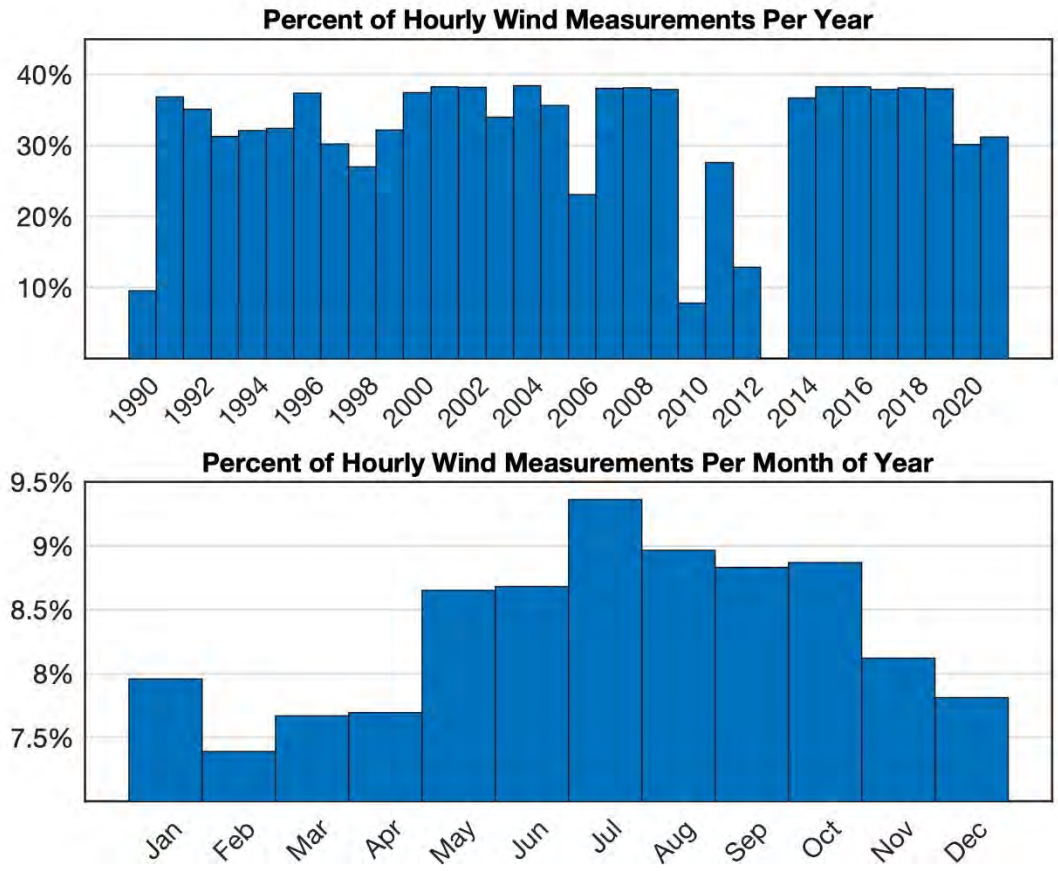

Figure 4-2 – Histogram of the hourly NDBC wind data for Buoy 44014. Top panel - percent of hourly wind measurements available for each year. Bottom panel - percent of hourly wind measurements available per month for all years. No data were available for 2013. Month with the maximum/minimum measurements was July/February, with 9.3%/7.4%.

NDBC wind speed (m s^{-1}) and wind direction are measured as eight-minute averages. These data are then hourly averaged and provided to the public via the website. Wind gust values are taken as peak 5 to 8 second gust speed (m s^{-1}) measured during the same eight-minute time period as the wind speed, and then also averaged hourly. The one exception is for the 2021 data which are available at 10-minute intervals and not averaged hourly. For consistency, in this report, the 2021 data are averaged hourly before use.

To show the highest occurrence of winds speeds for all hourly wind speeds, the data were binned into 1 m s^{-1} bins for wind speeds between 0 to 17 m s^{-1} and wind speeds greater than 18 m s^{-1} were grouped together into one bin (Figure 4-3). Hourly wind speeds in the 5 m s^{-1} bin were the most common (12%). The cumulative occurrence for wind speeds less than or equal to 10 m/s was approximately 79%. Wind speeds greater than or equal to 18 m/s occurred less than 1% of the time.

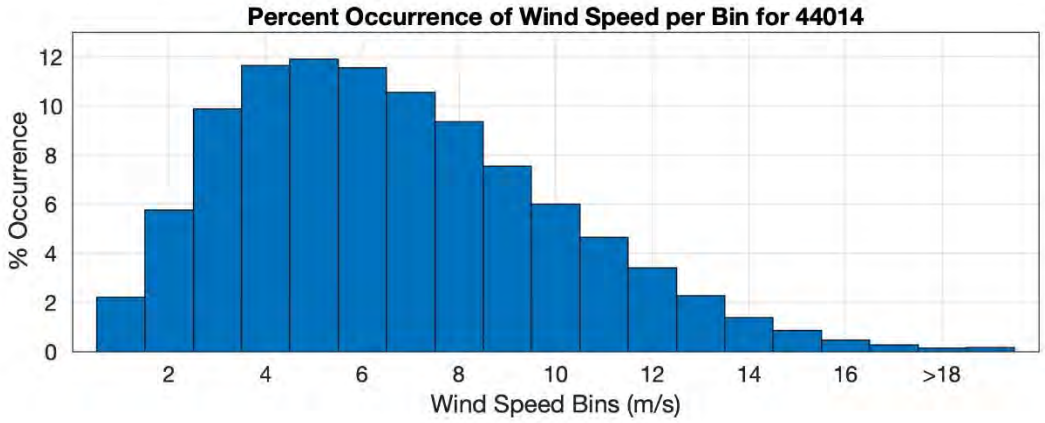

Figure 4-3 – Hourly wind speed data from Station 44014 showing the distribution of wind speeds for all data. The wind speeds were binned into 1 m s^{-1} bins between 0 to 17 m s^{-1}. All wind speeds greater than 18 m $s^{-1}$are binned together.

The hourly wind speed data was averaged daily for all available data at Station 44014 to identify trends in the data (Figure 4-4 and Figure 4-5). The wind speed has an annual trend with faster wind speeds in the winter and slower wind speeds in the summer. Binning the wind speed data by month of year and calculating the mean speed for each bin, January has the fastest wind speeds (~7.8 m s^{-1}), while the slowest wind speeds occur in June (~4.5 m s^{-1}) over the 31-year data record of hourly wind (Figure 4-6); September has the highest maximum wind speed (~28 m s^{-1}), while the June has the lowest maximum wind speed (~17 m s^{-1}) (Figure 4-6).

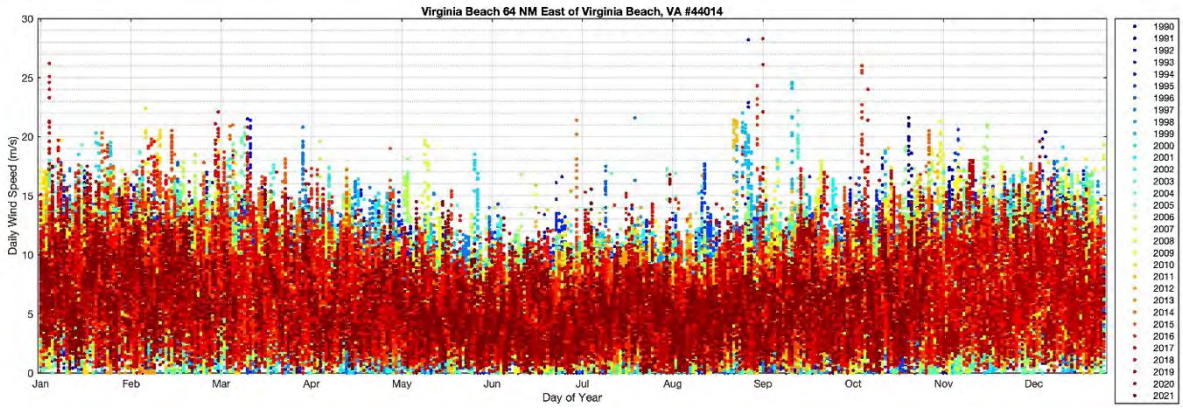

Figure 4-4 – Hourly wind speed data averaged daily versus day of year for Station 44014. Legend shows color for each year.

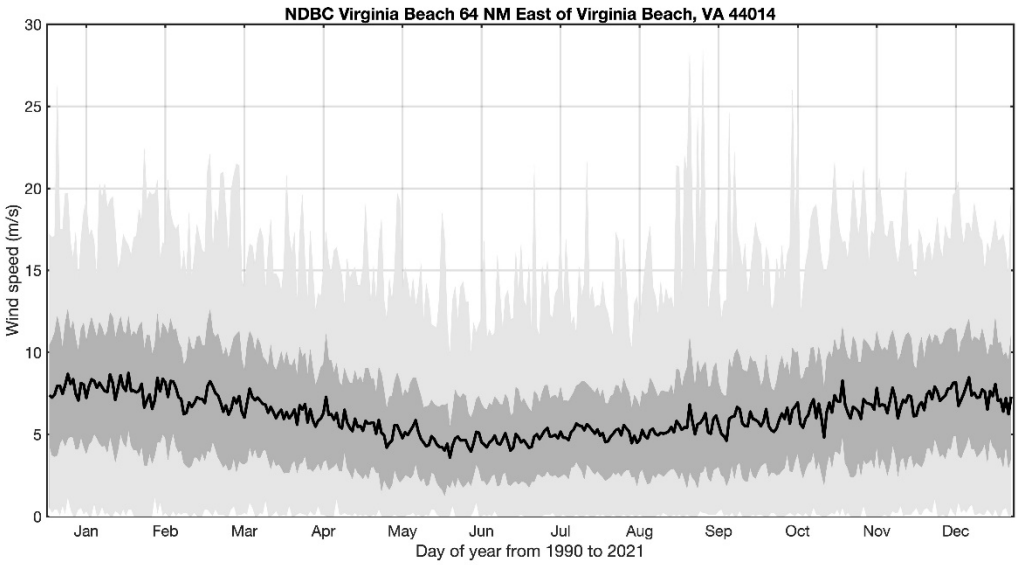

Figure 4-5 – Mean of hourly wind speed versus day of year (thick black line), minimum and maximum hourly wind speed versus day of year (dark shaded area), and standard deviation of hourly wind speed versus day of year (light shaded area) for Station 44014.

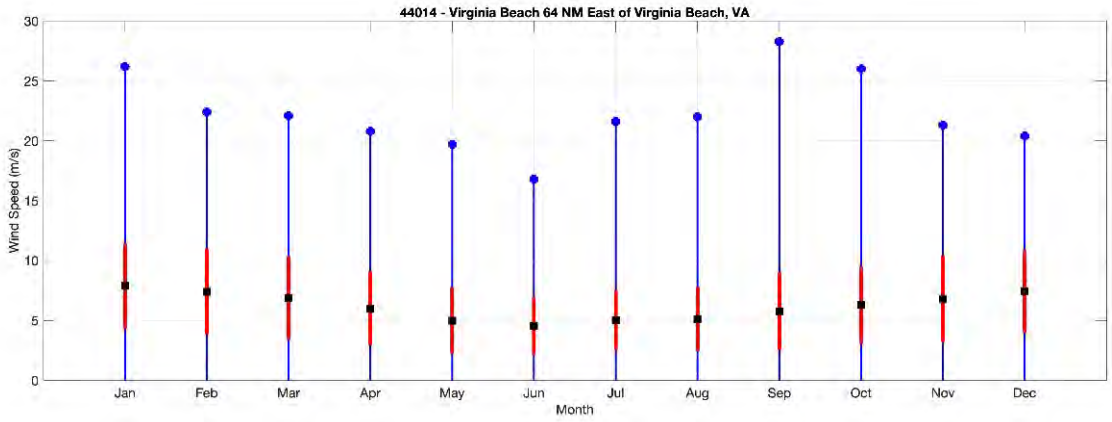

Figure 4-6 – Stem plot showing monthly statistics of hourly-average wind speed. Monthly mean (black square), maximum (blue circle), and standard deviation (red line) plotted year over year for Station 44014.

Percent occurrences of wind from different directions are presented in Figure 4-7. The data were divided into 16 equal compass segments of 22.5 deg. The predominant annual wind direction is SSW (~40%). The predominant spring and summer wind direction is also SSW (~27% and ~35% respectively). The winter wind direction is mostly SW to NNW with the strongest wind direction NNW (~12%). Most of the fall wind direction tends to be between NW and NE with the strongest direction being NNE (~11%) (Figure 4-8). Wind direction is further divided into months and shows that July has the strongest winds in the SSW direction (~20%) (Figure 4-9).

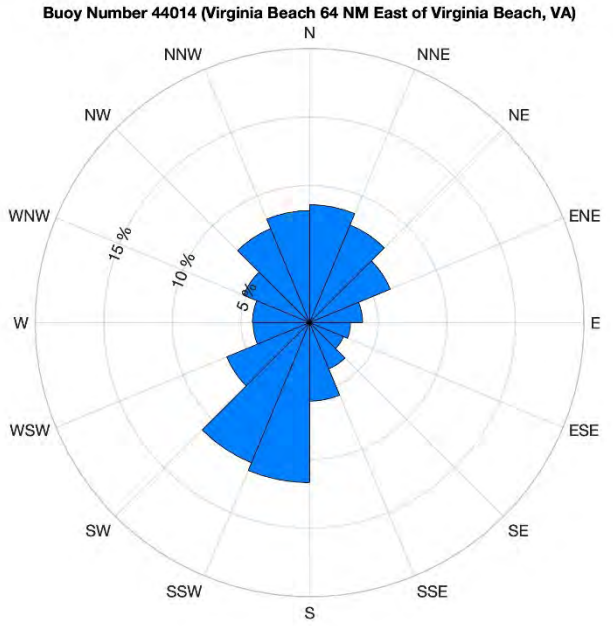

Figure 4-7 – Percent occurrence of wind direction for Station 44014.

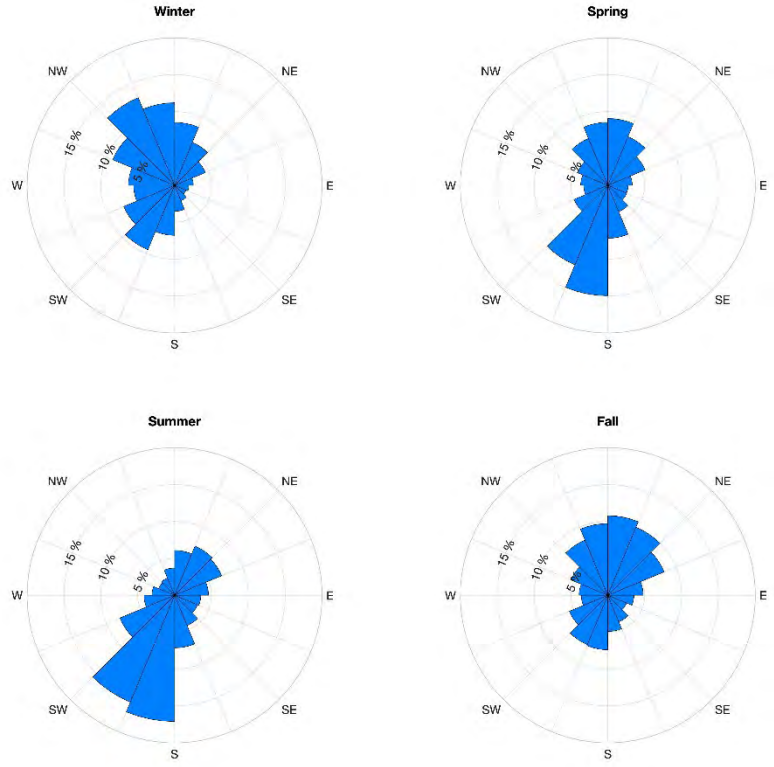

Figure 4-8 – Percent occurrence of wind direction for Station 44014 divided into seasons.

Figure 4-9 – Percent occurrence of wind direction for Station 44014 by month.

The weaker summer winds coming from the southwest are due to the Bermuda High, a semi-permanent, high-pressure system that migrates between the East Coast of North America (near Bermuda) in the summer and near the Azores in the winter and spring. The strong variable winds in the fall and winter are due to tropical storms, hurricanes, extratropical winter storms, and cold air outbreaks.

4.2. Wave statistics

Three NDBC buoys (Figure 4-1) providing historical, hourly wave data records measuring significant wave height, peak wave direction, peak wave period, and average wave period were downloaded from National Data Buoy Center and/or the Coastal Data Information Progrm. Table 4-2 lists the names, locations, depth, and years of available data.

Table 4-2 – NDBC Buoy information for wave data used in this report.

NDBC Buoy	Name	Location	Depth	Years
44014	Virginia Beach offshore	36.609 -74.842	47 m	1990-2022
44086	Nags Head, NC	36.001 -75.421	21 m	2018-2022
44095	Oregon Inlet, NC	35.750 -75.330	18 m	2012-2022

The number of days of available wave data downloaded from NDBC for Buoy 44014 is shown in Figure 4-10. No data was available for 2013 and fewer than 90 days were available in 1990. The bottom panel of Figure 4-10 shows the percent of hourly wave measurements available per month for all years. The highest percentage of measurements were in July (9.2%) while the lowest percentage of measurements were in February (7.7%).

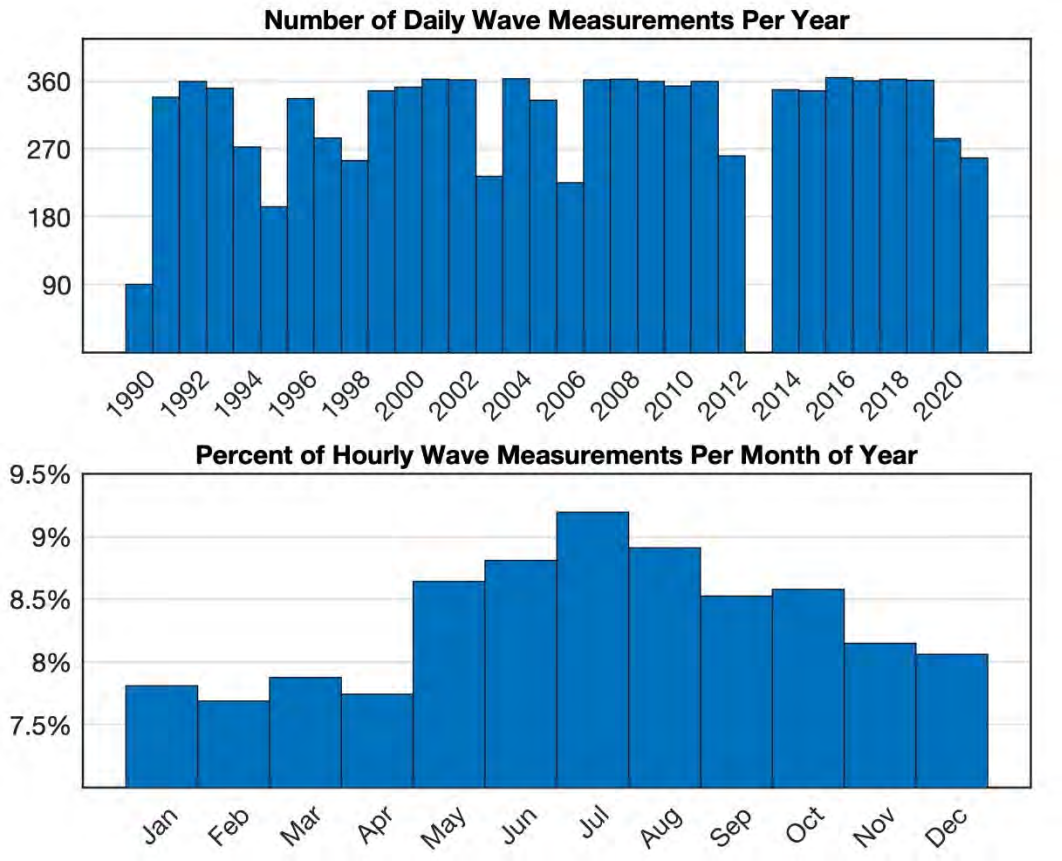

Figure 4-10 –Histogram of the available wave data downloaded from NDBC for Buoy 44014. Top panel shows the number of daily wave measurements available for each year. Bottom panel shows percent of hourly wave measurements available per month for all years. No data was available for 2013. The highest percentage of measurements were in July (9.2%) while the lowest percentage of measurements were in February (7.7%).

To show the highest occurrence of significant wave heights for all hourly wave data, the data were binned into 0.5 m bins between 0 to 4.0 m, and all significant wave heights greater than 4.5 m grouped together into one bin (Figure 4-11). The most common significant wave height was 1.0 m (33%). The cumulative occurrence for wave heights less than or equal to 3 m was approximately 93%. Wave heights greater than or equal to 4.5 occurred less than 2% of the time.

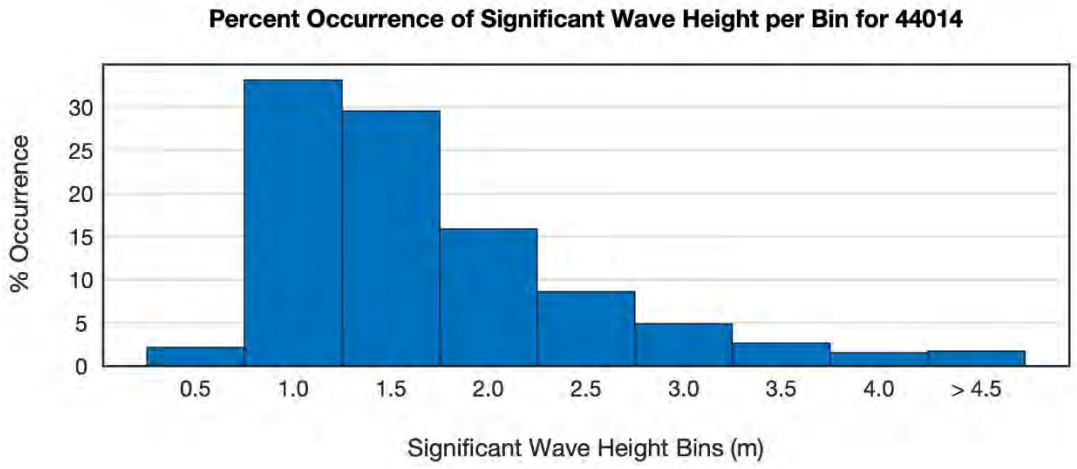

Figure 4-11 – Hourly significant wave height data from Station 44014 showing the distribution of significant wave heights for all data. The significant wave heights were binned into 0.5 m bins between 0 to 4.0 m, and all significant wave heights greater than 4.5 m were binned together.

Significant wave height (meters) is calculated by taking the mean of the one-third highest wave heights in a 20-minute sampling period. These data are hourly averaged and provided to the public on the NDBC website. The dominant wave period (seconds) the hourly maximum wave energy. The average wave period (seconds) is the mean of all waves in a 20-minute period, and then averaged hourly. The one exception is for the 2021 data which was available at 10-minute intervals and not averaged hourly. For consistency, the 2021 data was averaged hourly before any of the observations provided in this report were made.

Figure 4-12, Figure 4-13 and Figure 4-14 are day-of-year (x-axis) plotted with daily mean of hourly significant wave height (black line), daily minimum and maximum of hourly significant wave height (m) (light gray), and daily +/- standard deviation or hourly significant wave height (dark gray) (y-axis). Years are stacked on top of each other. Note the absence of data in March for Buoy 44086 which is evident in the standard deviation calculations over this time period. All figures are plotted with the same y-axis for direct comparison.

The Figure 4-15, Figure 4-16, and Figure 4-17 are the day-of-year (x-axis) plotted with daily average of the hourly significant wave height (m) values for that day (y-axis). Years are plotted on top of each other with the color bar denoting the year.

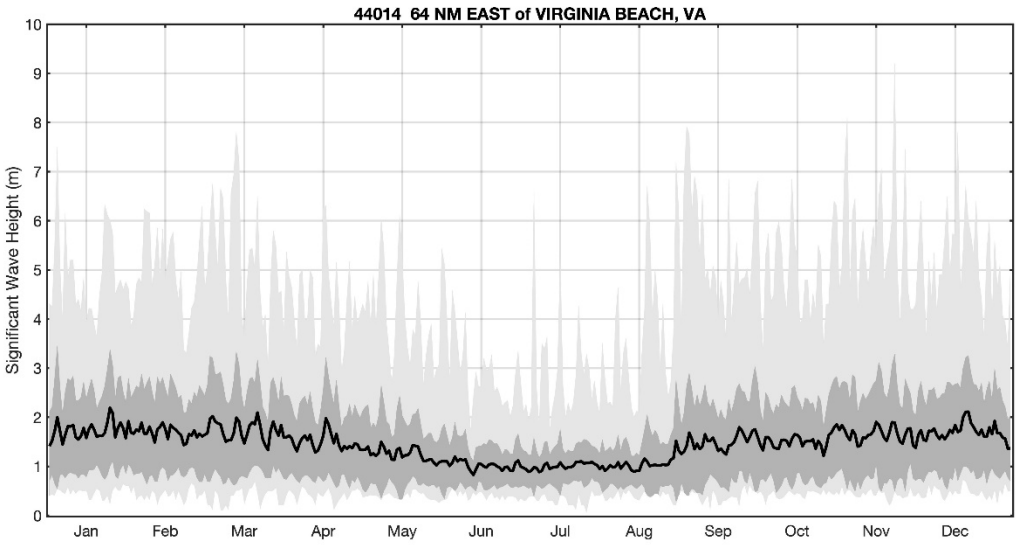

Figure 4-12 – Daily mean of hourly significant wave height versus day of year (thick black line), daily minimum and maximum of hourly significant wave height versus day of year (dark shaded area), and daily standard deviation of hourly significant wave height versus day of year (light shaded area) for Station 44014.

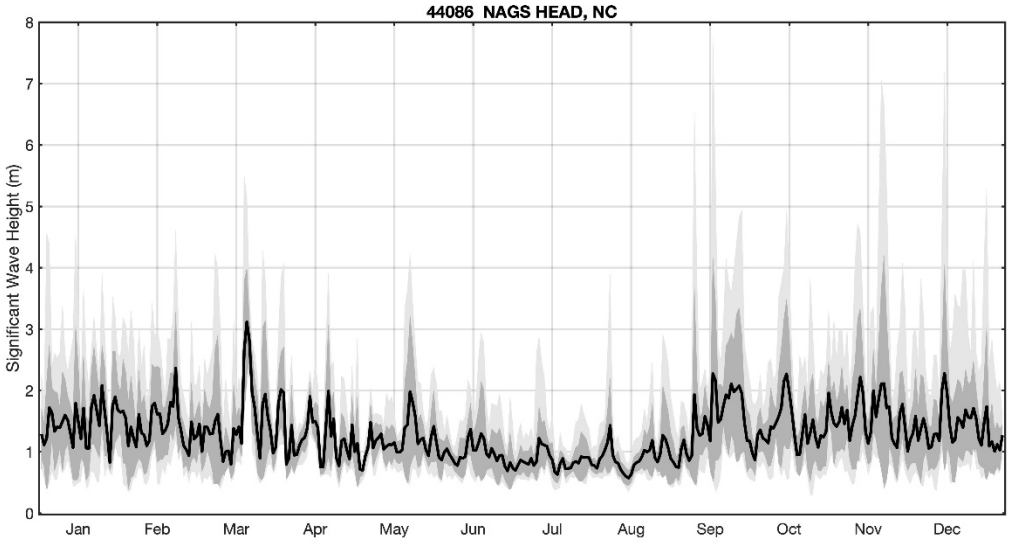

Figure 4-13 – Daily mean of hourly significant wave height versus day of year (thick black line), daily minimum and maximum of hourly significant wave height versus day of year (dark shaded area), and daily standard deviation of hourly significant wave height versus day of year (light shaded area) for Station 44086.

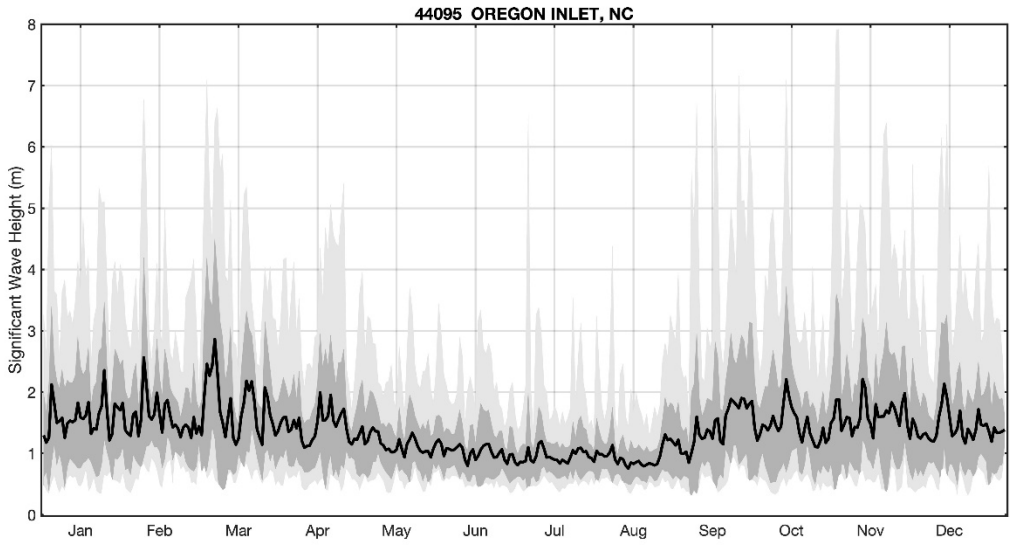

Figure 4-14 – Daily mean of hourly significant wave height versus day of year (thick black line), daily minimum and maximum of hourly significant wave height versus day of year (dark shaded area), and daily standard deviation of hourly significant wave height versus day of year (light shaded area) for Station 44095.

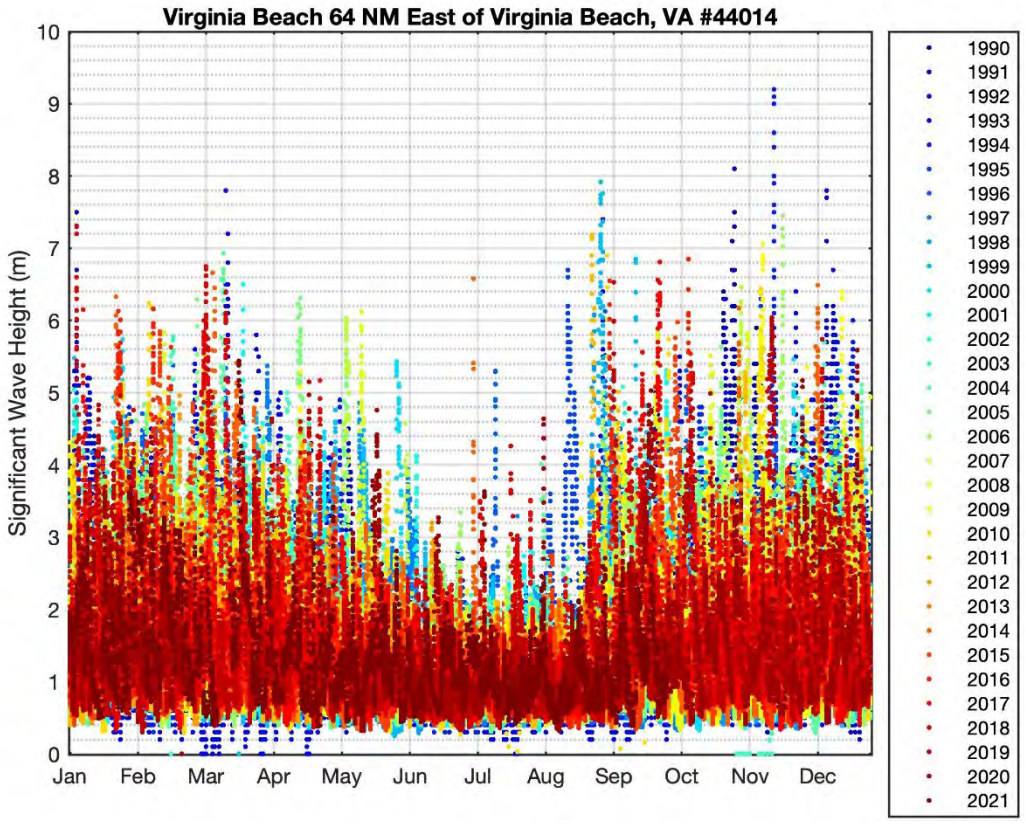

Figure 4-15 – Daily average of the hourly significant wave height (m) values for that day (y-axis) versus day of year for Station 44014. Years are plotted on top of each other with the color bar denoting the year.

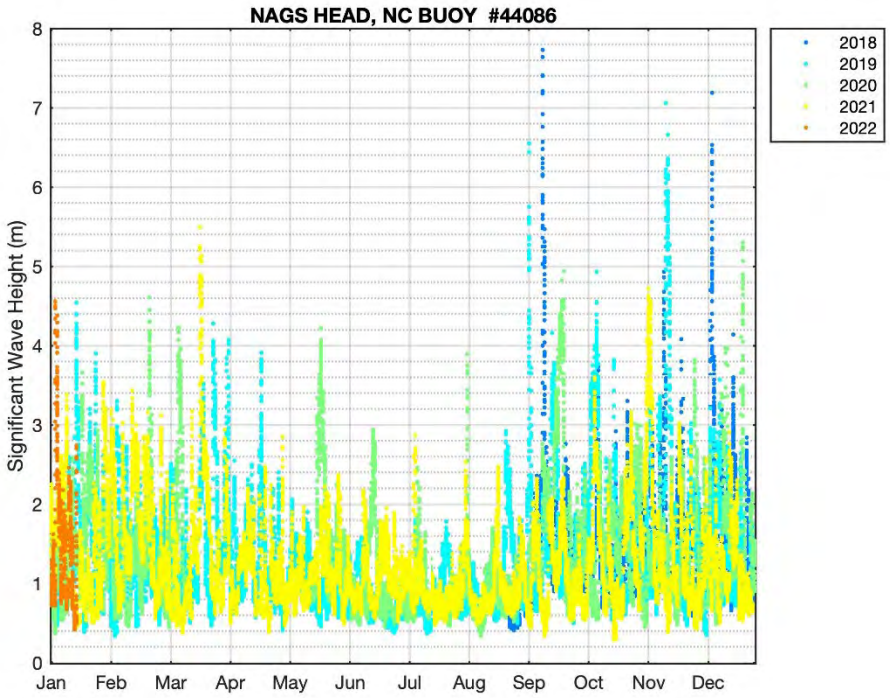

Figure 4-16 – Daily average of the hourly significant wave height (m) values for that day (y-axis) versus day of year for Station 44086. Years are plotted on top of each other with the color bar denoting the year.

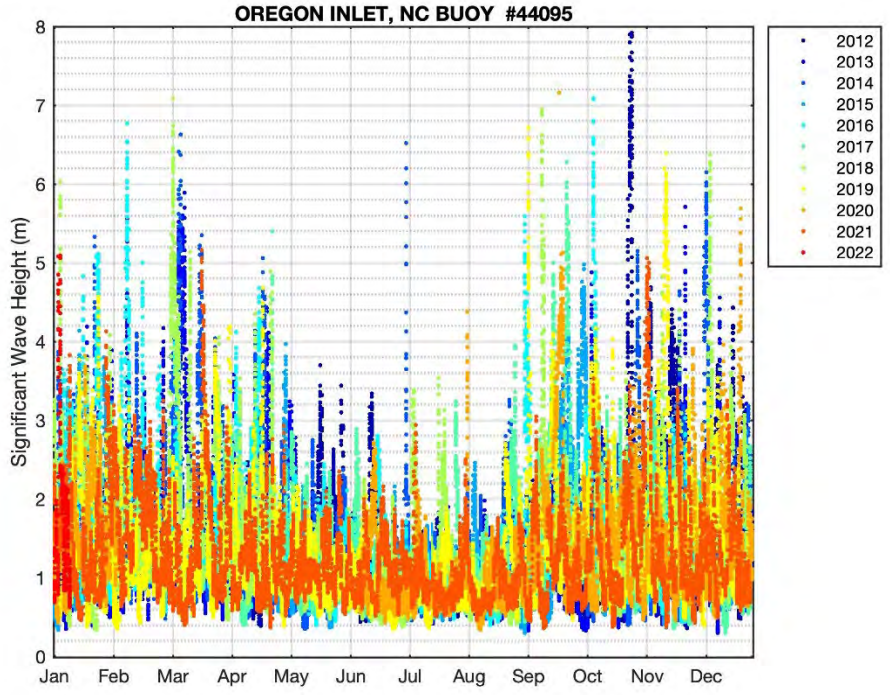

Figure 4-17 – Daily average of the hourly significant wave height (m) values for that day (y-axis) versus day of year for Station 44095. Years are plotted on top of each other with the color bar denoting the year.

Figure 4-18, Figure 4-19, and Figure 4-20 are the percent occurrence of waves from different directions. The data were divided into 16 equal compass segments of 22.5 deg. The dominant wave direction for all three sites was either ENE or E, as expected based on the orientation of the shoreline relative to the Atlantic Ocean.

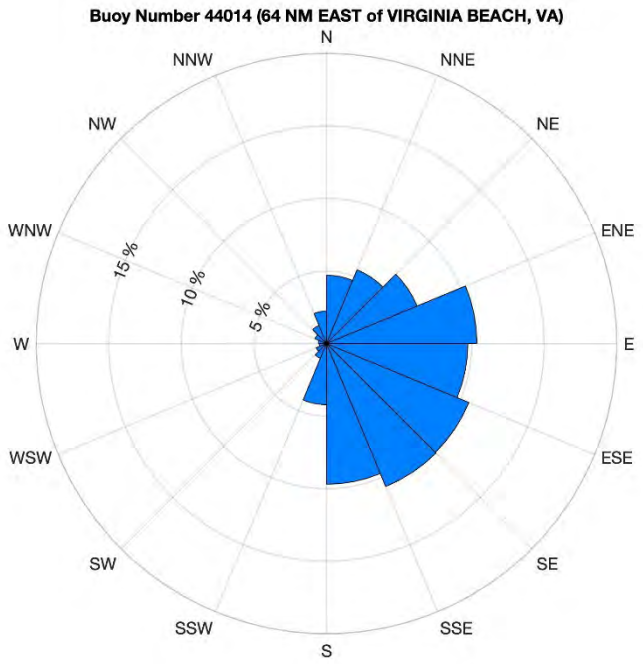

Figure 4-18 – Percent occurrence of wave direction for Station 44014.

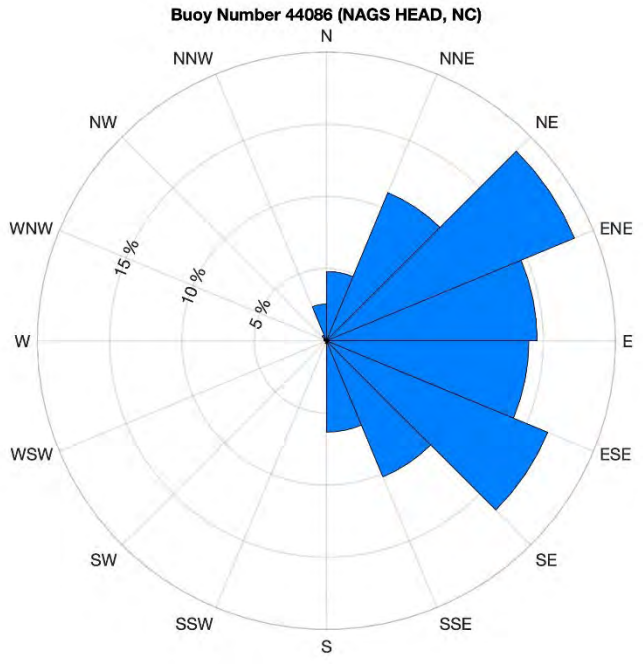

Figure 4-19 – Percent occurrence of wave direction for Station 44086.

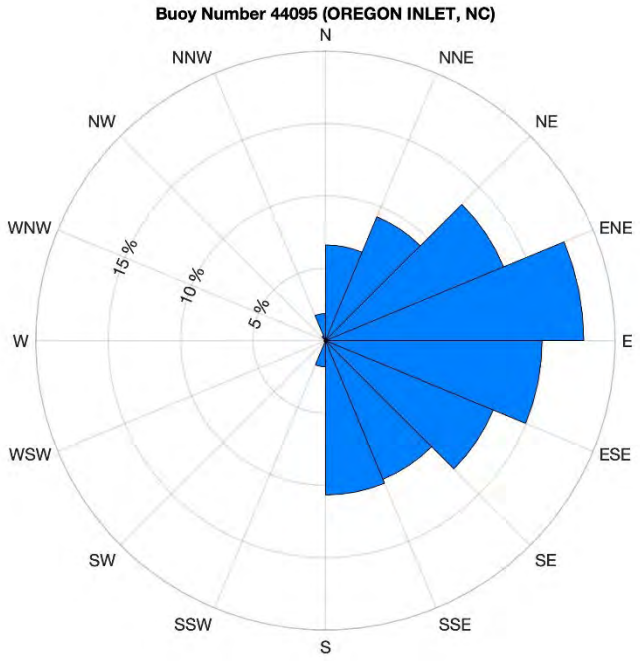

Figure 4-20 – Percent occurrence of wave direction for Station 44095.

Figure 4-21, Figure 4-22, and Figure 4-23 are the monthly maximum of the hourly significant wave height versus the associated wave period. As expected, there is significant variability in wave periods for storm events associated with energetic waves. However, there is generally a trend that indicates that longer period waves are associated with higher significant wave heights. Note the evidence of events that generate long period/ high energy waves from distant storm events as shown by high energy waves with periods greater than 12 seconds.

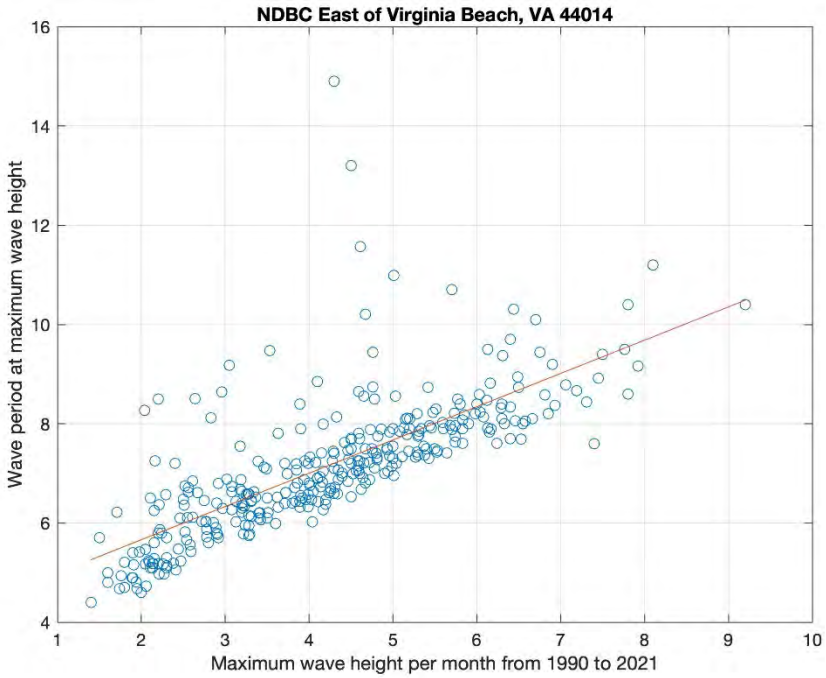

Figure 4-21 – Monthly maximum significant wave height from hourly averaged data plotted against the associated wave period for Station 44010.

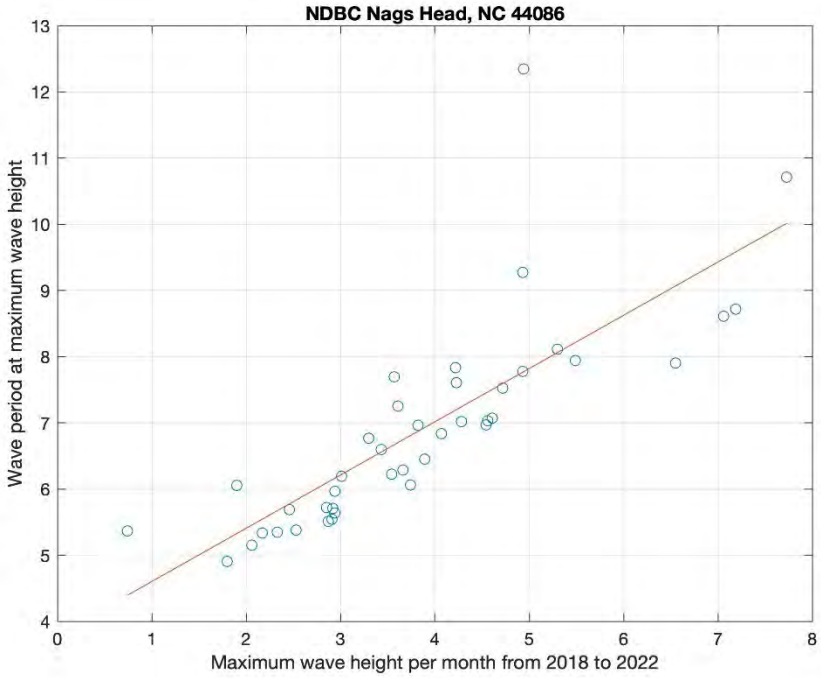

Figure 4-22 – Monthly maximum significant wave height from hourly averaged data plotted against the associated wave period for Station 44086.

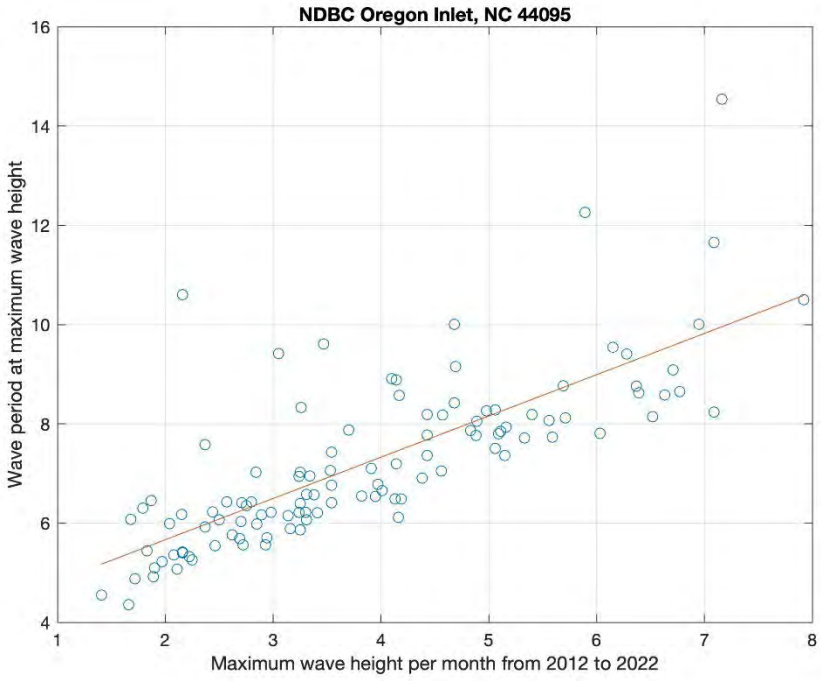

Figure 4-23 – Monthly maximum significant wave height from hourly averaged data plotted against the associated wave period for Station 44095.

The predicted return period for storm wave heights were calculated using the Fisher-Tippett Distribution (also known as the Extreme Value Distribution and the Log-Weibull Distribution), a statistical method for calculating the extreme values of an asymptotic distribution (Coles, 2001). The input data were the hourly significant wave height (m), hourly peak wave period (s), and hourly mean wave period (s) from the NDBC Buoys 44014, 44086, 44095, and the Army Corps of Engineers Wave Information Study hindcast model results for stations 44010 and 63257. Results are presented in Table 4-3. All NDBC Buoy data have similar storm wave characteristics, with a 10-year storm wave height of approximately 7.7 meters. The WIS hindcast model data tends to over predict the storm wave heights with results getting larger as time increases. This is especially true for WIS station 63257, which differs from the NDBC buoys ~4.5-meters in 100-years.

Table 4-3 – Return period (years) for extreme significant wave heights (m) using the Fisher-Tippett Distribution on NDBC buoy data and Wave Information Study hindcast model. Inputs were hourly significant wave height (m), peak wave period (s), and mean wave period (s).

Buoy	Years	1-year	5-year	10-year	25-year	50-year	100-year
44014 (offshore VA)	32	5.6	7.3	7.8	8.5	9.0	9.5
44086 (Nags Head, NC)	5	4.5	7.0	7.7	8.7	9.4	10.2
44095 (Oregon Inlet, NC)	11	5.3	7.1	7.6	8.4	8.9	9.4
WIS 44010	20	4.9	7.6	8.4	9.5	10.2	11.0
WIS 63257	20	5.0	9.3	10.6	12.3	13.5	14.8

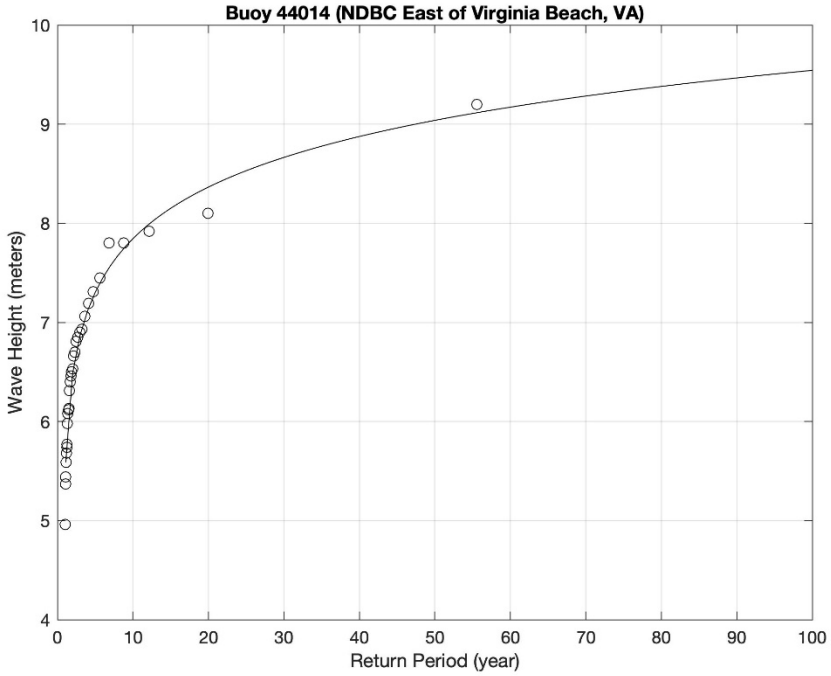

Figure 4-24 – Return period for extreme significant wave heights (m) using monthly average of the hourly significant wave height (m) data for Station 44014, east of Virginia Beach, VA. The black circles are the calculated storm wave heights; the black line is the line fitted to the output.

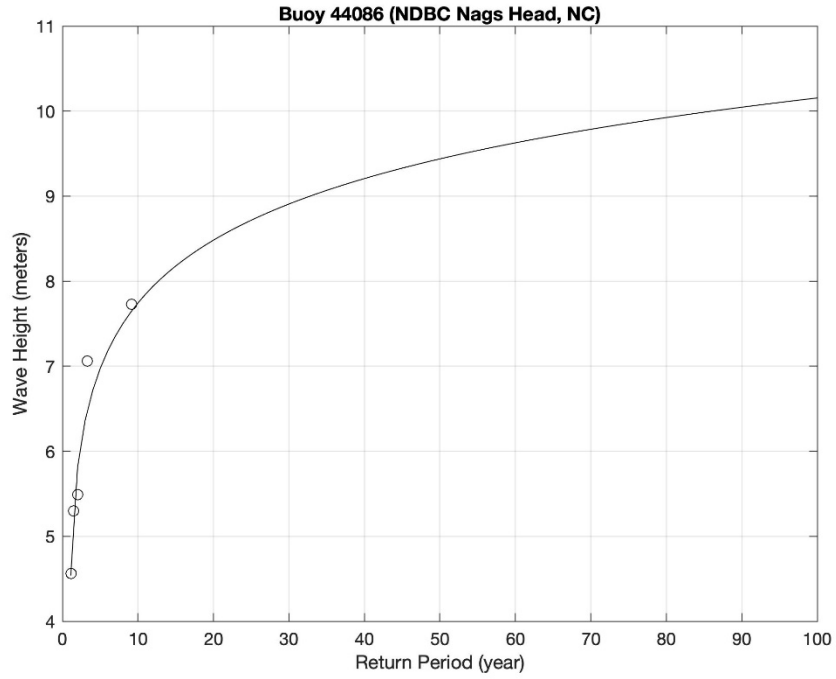

Figure 4-25 – Return period for extreme significant wave heights (m) using monthly average of the hourly significant wave height (m) data for Station 44086, Nags Head, NC. The black circles are the calculated storm wave heights; the black line is the line fitted to the output.

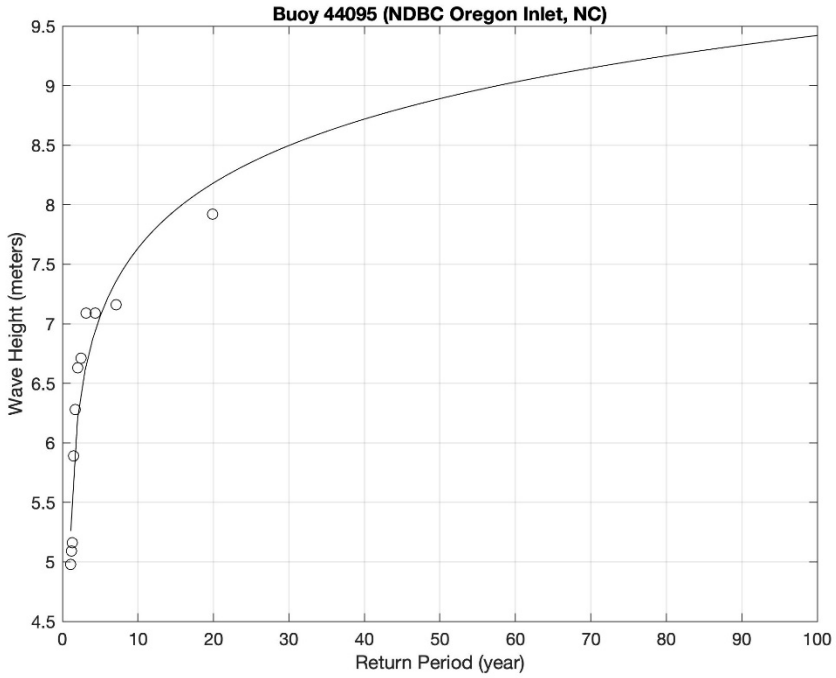

Figure 4-26 – Return period for extreme significant wave heights (m) using monthly average of the hourly significant wave height (m) data for Station 44095, Oregon Inlet, NC. The black circles are the calculated storm wave heights; the black line is the line fitted to the output.

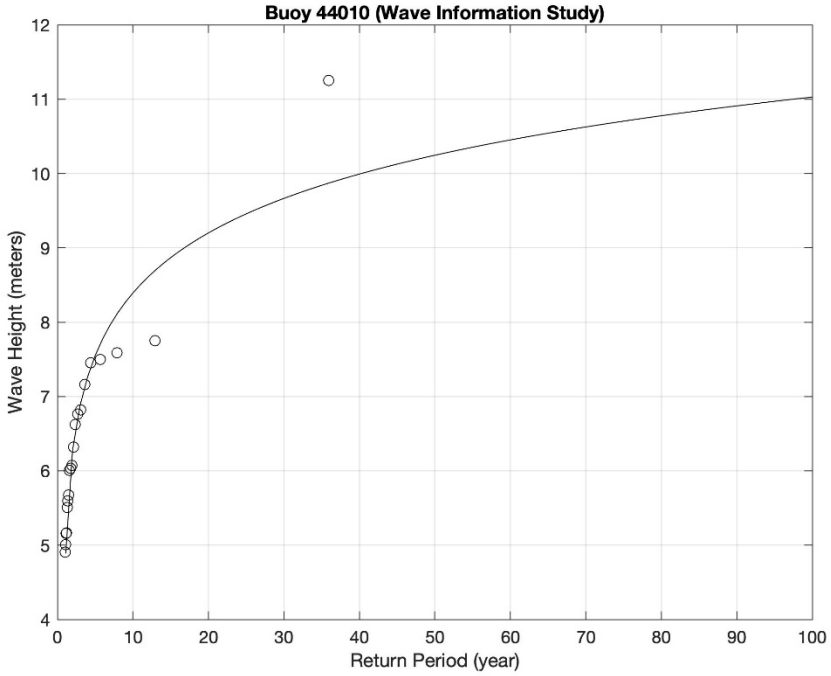

Figure 4-27 – Return period for extreme significant wave heights (m) using monthly average of the hourly significant wave height (m) data for WIS Station 44010. The black circles are the calculated storm wave heights; the black line is the line fitted to the output.

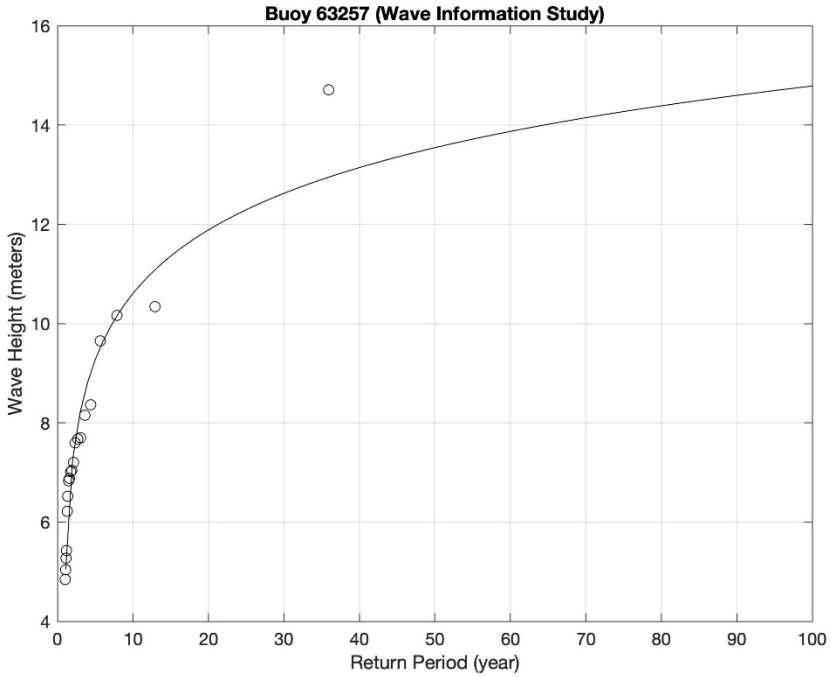

Figure 4-28 – Return period for extreme significant wave heights (m) using monthly average of the hourly significant wave height (m) data for WIS Station 63257. The black circles are the calculated storm wave heights; the black line is the line fitted to the output.

4.3. Major Storm Events

Major storms in the area of interest include tropical storms, hurricanes, major hurricanes, and nor'easters. Tropical storms and hurricanes are warm-core lows that usually occur between June and November and are categorized by the Saffir-Simpson Hurricane Wind Scale (Table 4-4). Storms with a defined circulation pattern and sustained winds greater than 38 mph are given predetermined names by the National Hurricane Center. During hurricane events, wind and waves bring colder saltier waters up from below causing water temperatures to drop and salinity to rise. The increased salinity remains high and does not decrease as quickly as temperature, etc. The rainfall does not make the surface water fresher as one might expect.

Nor'easters are cold-core lows that form along the East Coast of North America and usually occur between October and April. Nor'easters are named after the strongest wind direction blows over the northeast states, including the Mid-Atlantic and New England regions.

Table 4-4 – Saffir-Simpson Hurricane Wind Scale

Storm Type	Category	Sustained Wind Speed (mph)
Tropical Depression	0	<38
Tropical Storm		39-74
Hurricane	1	74-95
	2	96-110
Major Hurricane	3	111-129
	4	130-156
	5	>157

Tropical Storms and Hurricanes

The National Hurricane Center (NHC) has summarized the number of hurricanes and the number of named storms in the Atlantic Ocean for the months of August and September over the past 100 years (Figure 4-29, Figure 4-30, Figure 4-31, Figure 4-32). Cape Hatteras, which sits just to the south of the Glider Box, touches the 35-49 hurricanes contour in both August and September (Figure 4-29, orange contour) while the Mooring Box region lies in the 20-34 hurricane contour for both months (Figure 4-30, green contour). While hard to tell at this scale, it looks as if the Mooring Box does lie wholly or partly within the 50-69 named storms region (Figure 4-31 and Figure 4-32, orange contour).

The National Hurricane Center has also summarized the Return Period (Years) for Hurricanes (Figure 4-33) and for Major Hurricanes (Figure 4-34). The Mooring Box return period for hurricanes lies in the 5-7 year range category (Figure 4-33), while for major hurricanes it lies somewhere in the 16–25-year range category (Figure 4-34).

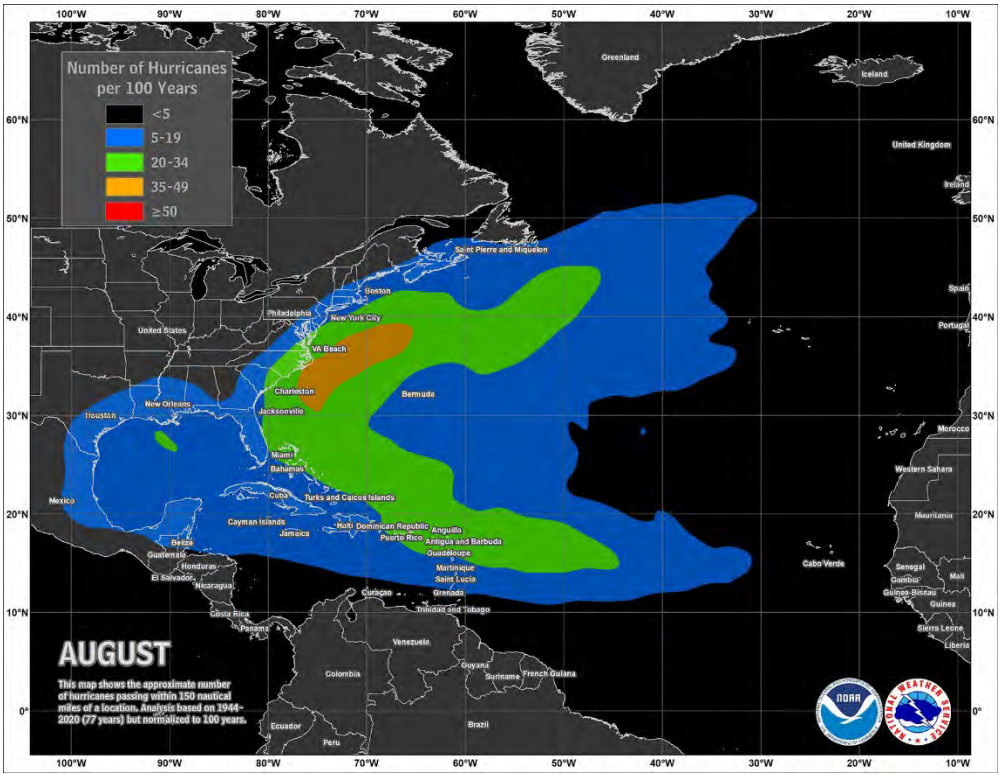

Figure 4-29 – Number of hurricanes per century during August (color shading). Colorbar shown in legend. Based on 77 years of data from 1944-2020 (NHC).

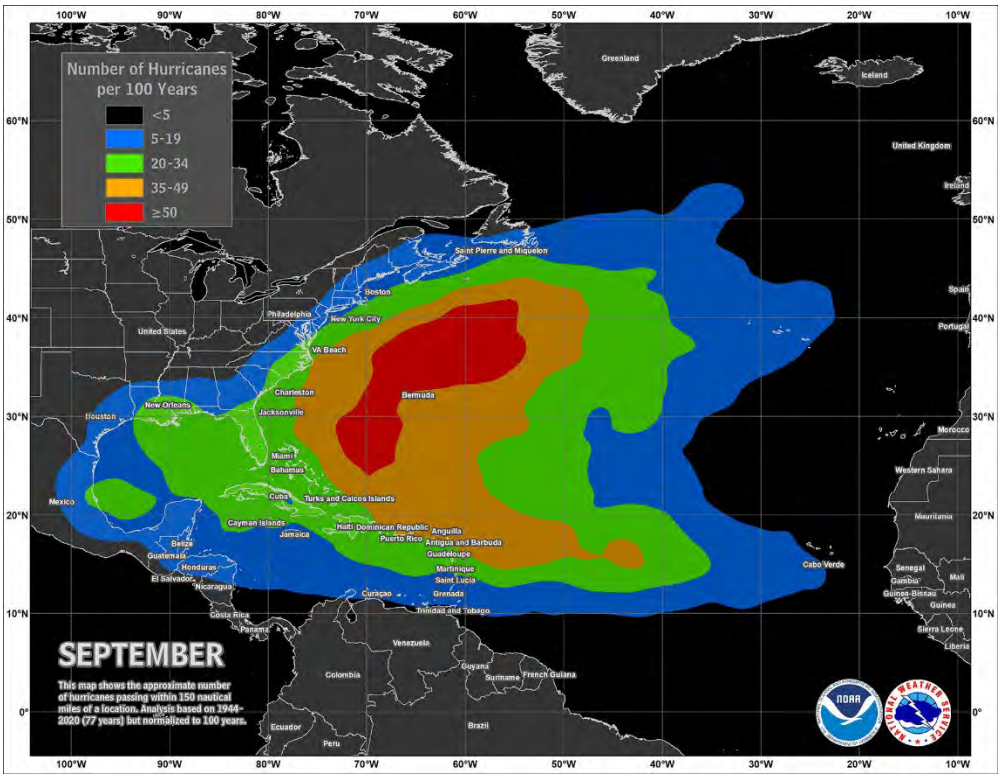

Figure 4-30 – Same as Figure 4-29, but for September (NHC).

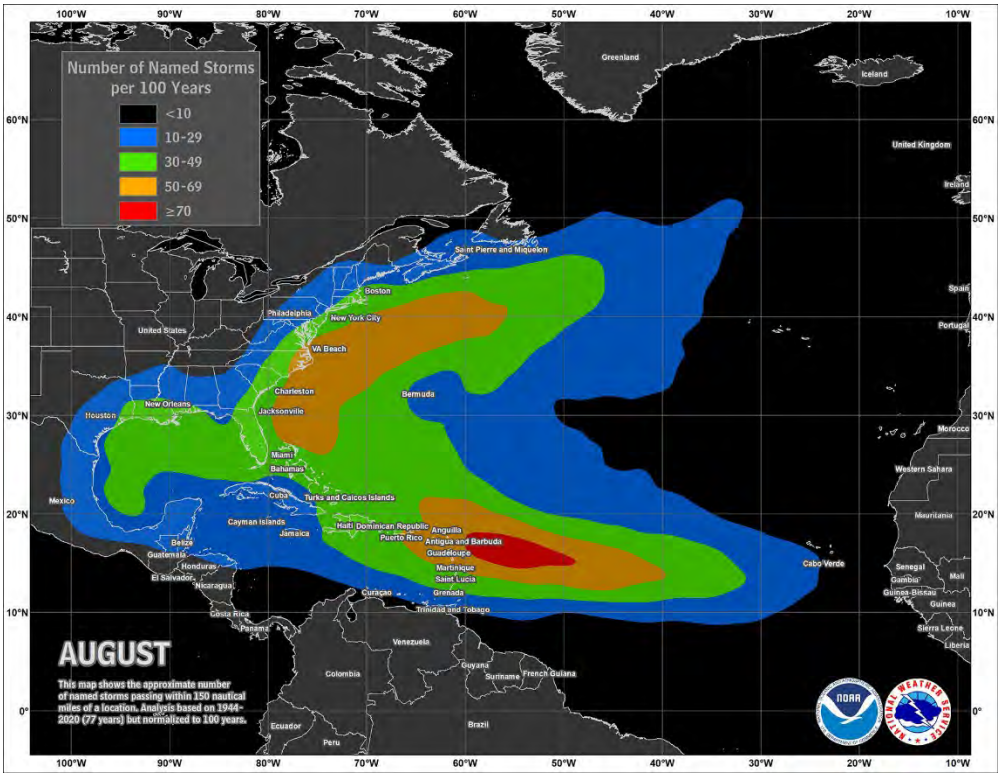

Figure 4-31 – Number of named storms per century during August (color shading). Colorbar shown in legend. Based on 77 years of data from 1944-2020 (NHC).

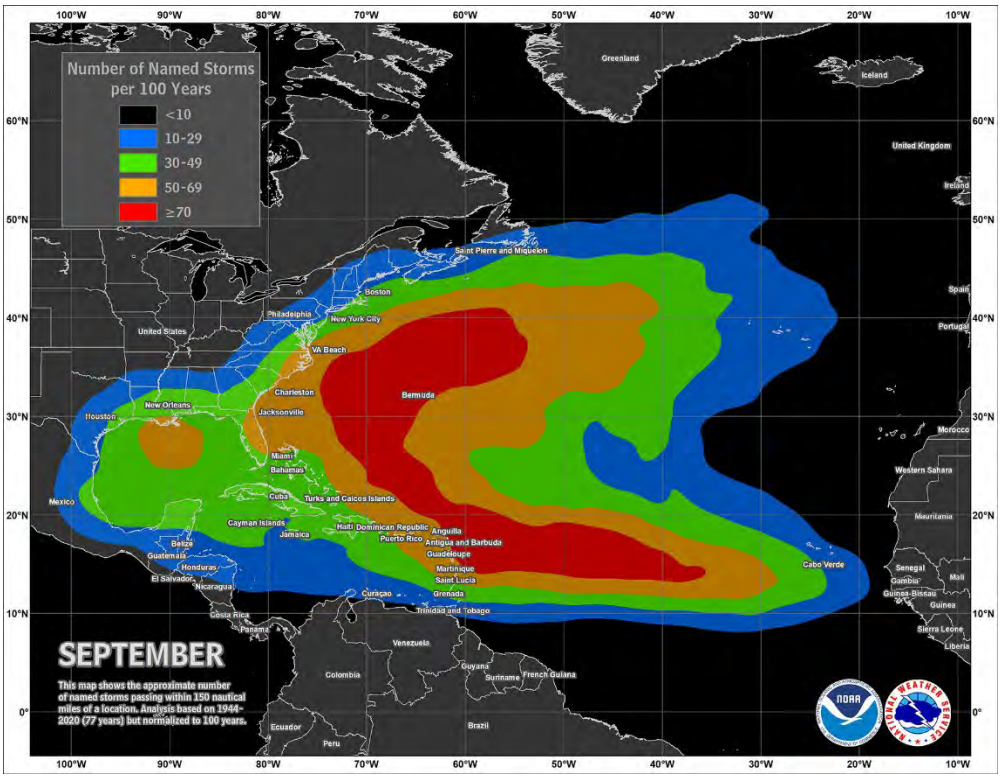

Figure 4-32 – Same as Figure 4-31, but for September (NHC).

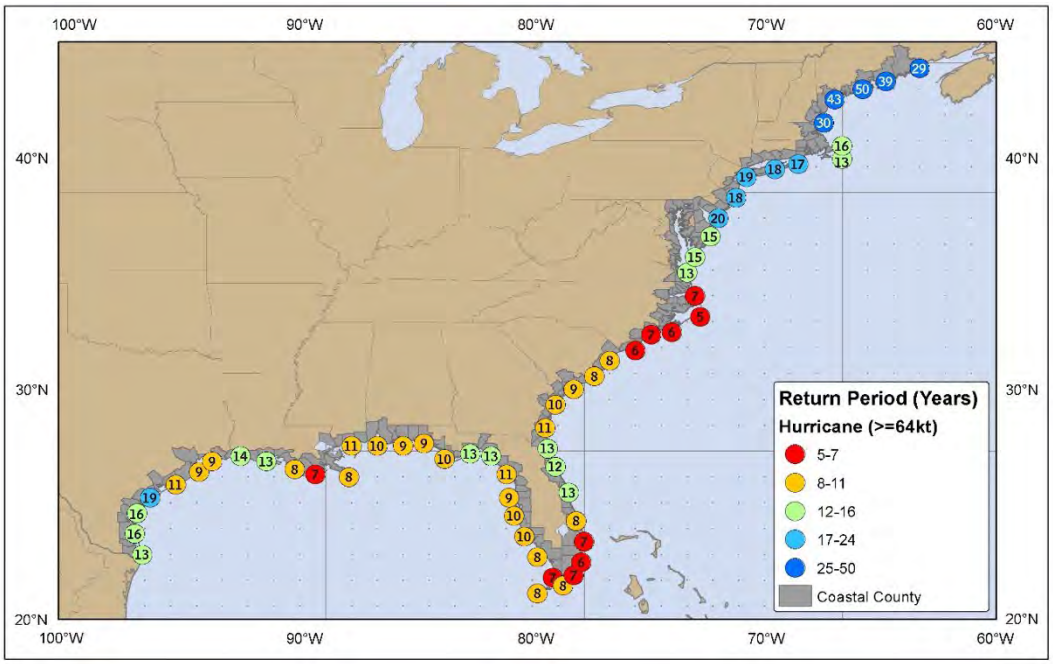

Figure 4-33 – Average number of years between hurricanes (storms with winds greater than 64 kts) along the gulf and east coasts of the United States (NHC).

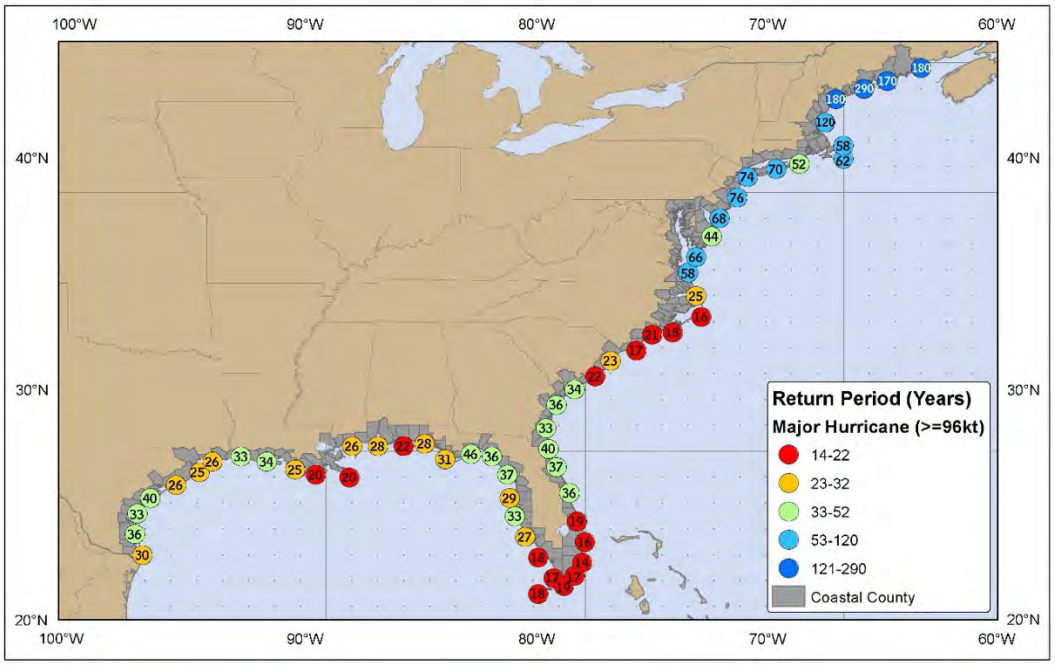

Figure 4-34 – Average number of years between major hurricanes (storms with winds greater than 96 kts) along the gulf and east coasts of the United States (NHC).

Between 2000-2021, 17 hurricanes occurred in the southern Mid-Atlantic Bight (Table 4-5 and Figure 4-35 through Figure 4-51). Of these, 11 made landfall and four were within 85, 140, 210, and 330 miles of the shore. The distance offshore was referenced to the southwest corner of the glider box [-75.3667, 35.5] since this was the closest point to shore within the box. Maximum wind speeds recorded at the NDBC Buoy 44095 never exceeded 70 mph. The maximum significant wave height for all storms was 7.2 meters (Hurricane Irene, 2011,

Category 4) which is below the five-year event (return period) value of 7.3 meters. The maximum wave period (12.2 seconds) was during Hurricane Earl in 2010, which was a Category 3. The maximum wind speed occurred during Hurricane Dorian in 2019, which was a Category 2.

Table 4-5 – Hurricanes in the Mid-Atlantic Bight between 2000-2021 based on historical hurricane data from National Hurricane Data Center, WIS data, NDBC data.

Year	Name	Date	Direction	Location	Category	Max Wind m/S	Peak Hs	Peak Ta	Storm event
2002	Gustav	Sep 10	NE	Within 10 miles of Outer banks, NC	TS to 1	18.1	5.08	7.85	>1
2003	Isabel	Sep 18	NW	Between Cape Lookout and Cape Hatteras, NC	2	22.2	N/A	N/A	n/a
2004	Alex	Aug 3	NNE	Within 10 miles of Outer banks, NC	1	17.3	4.01	7.12	>1
	Charley	Aug 15	NE	West of NC coast	1 to TS	15.8	2.72	7.12	>1
2005	Ophelia	Sep 15-16	NE	Stalled offshore Oregon Inlet, NC (~55 miles offshore)	1	13.1	3.95	8.44	>1
2010	Earl	Sept 3	NNW	~Offshore 85 miles	1 to2	N/A	6.90	12.24	3
2011	Irene	Aug 27	NNE	Near Cape Lookout, NC	1	21.4	7.19	8.94	4
2014	Arthur	Jul 3-4	NNE	Between Cape Lookout and Beaufort, NC	2	21.4	6.58	8.05	2
	Bertha	Aug 5	NE	~Offshore 140 miles	1 to TS	10.4	2.18	8.58	>1
2016	Hermine	Sep 6	NE	Nags Head, NC	TS	24.3	6.55	9.47	2
	Matthew	Oct 9	E	Turns eastward off Cedar Island	1	26.0	6.85	8.25	3
2017	Gert	Aug 15	NE	~Offshore 330 miles	1	10.5	2.43	9.52	>1
	Jose	Sep 19	N	~Offshore 210 miles	1	17.3	6.56	10.5	3
	Maria	Sep 27	E	~Offshore 140 miles	1	17.3	6.81	10.5	3
2018	Chris	Jul 9	NE	~Offshore 140 miles	2	13.8	3.5	8.1	>1
	Florence	Sep 13	NW	Landfall south of Morehead City, NC	2	13.0	4.78	10.75	3
2019	Dorian	Sep 6	NE	Landfall Outer banks, North Carolina	2	28.3	6.53	8.02	2

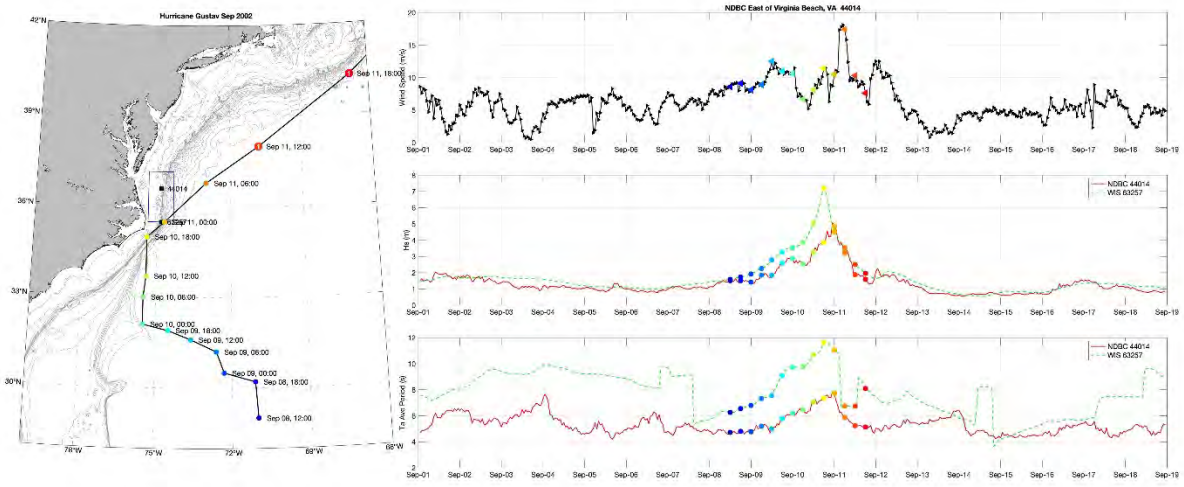

Figure 4-35 – September 2002 Hurricane Gustav map of storm path with dates and times of day (left panel); wind speed (m s^{-1}) versus date with colored dots indicate times shown in map on the left (top right panel); wave height (m) versus time (middle panel on right); average period (s) versus time (bottom panel on right panel). Time is 7-days before and 7-days after the storm. Wind and wave data is from NODC buoys (specified in legend) and WIS hindcast data. Blank panel indicates no data was available.

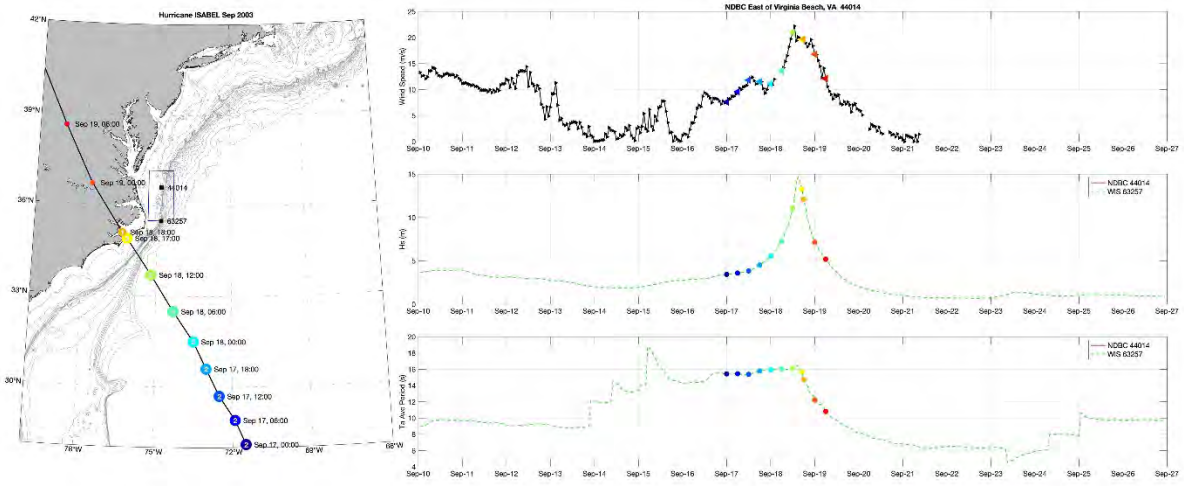

Figure 4-36 – Same as Figure 4-35 but for September 2003 Hurricane Isabel.

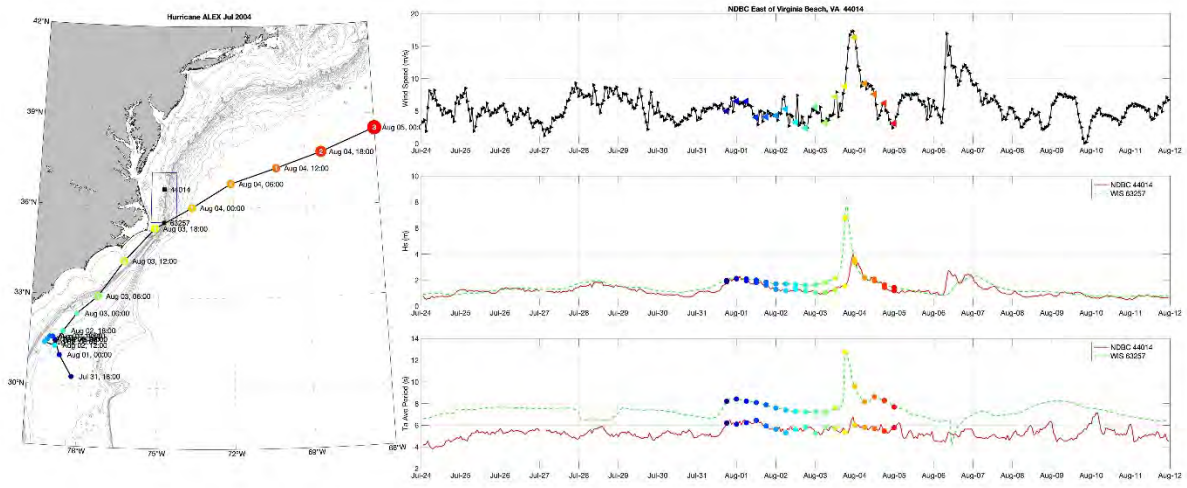

Figure 4-37 – Same Figure 4-35, but for August 2004 Hurricane Alex.

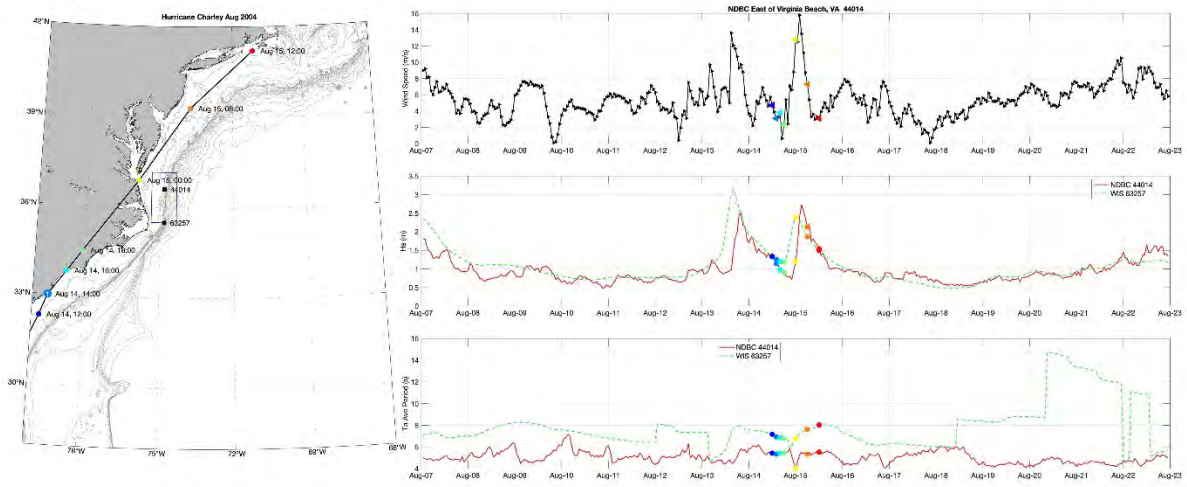

Figure 4-38 – Same Figure 4-35, but for August 2004 Hurricane Charley.

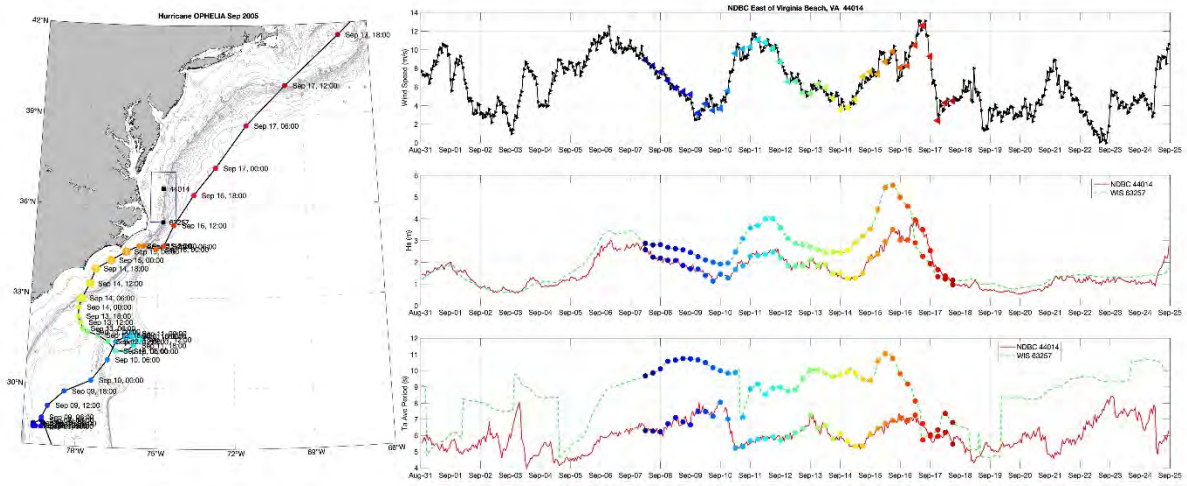

Figure 4-39 – Same Figure 4-35, but for September 2005 Hurricane Ophelia.

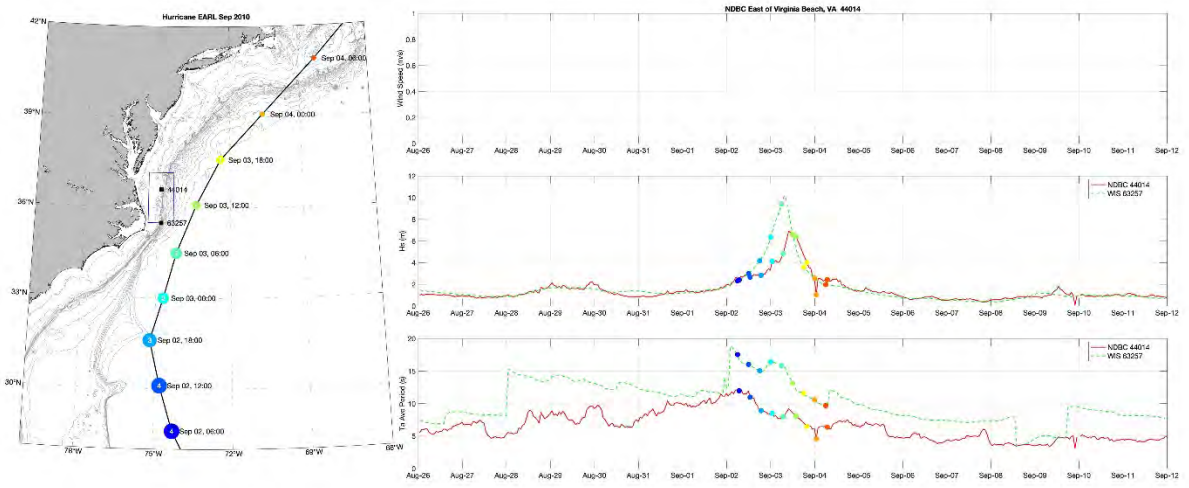

Figure 4-40 – Same Figure 4-35, but for September 2010 Hurricane Earl.

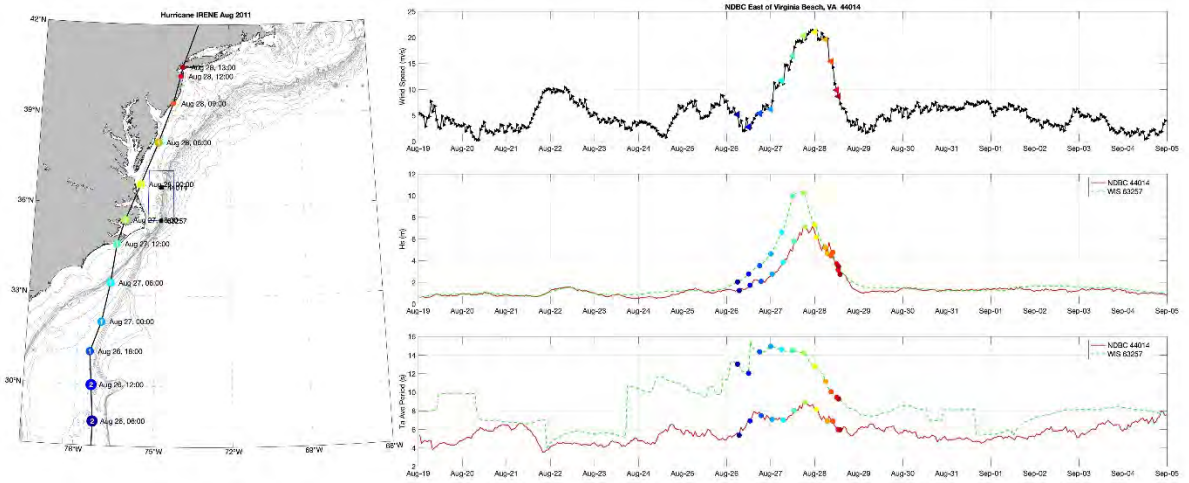

Figure 4-41 – Same Figure 4-35, but for August 2011 Hurricane Irene.

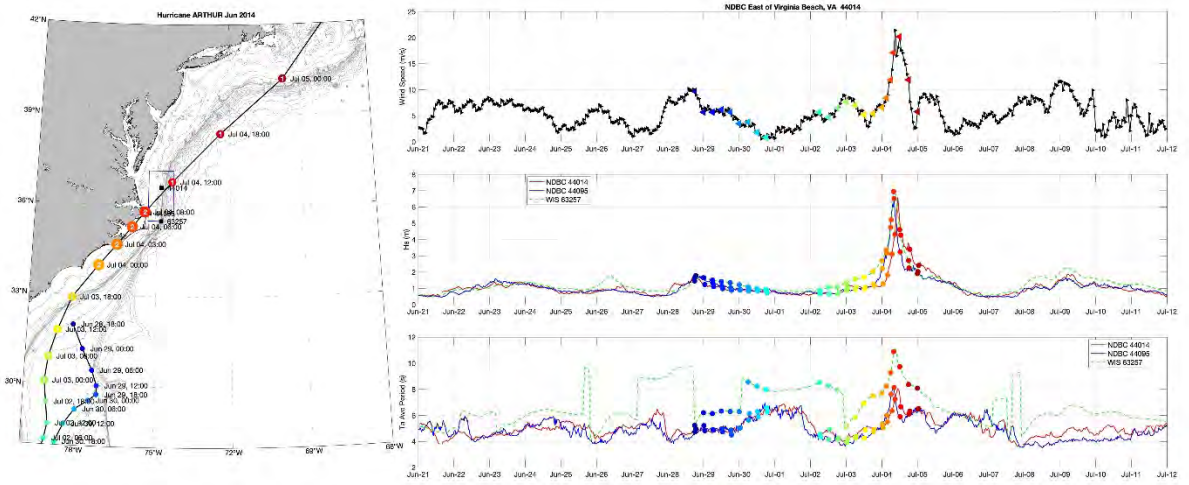

Figure 4-42 – Same Figure 4-35, but for June 2014 Hurricane Arthur.

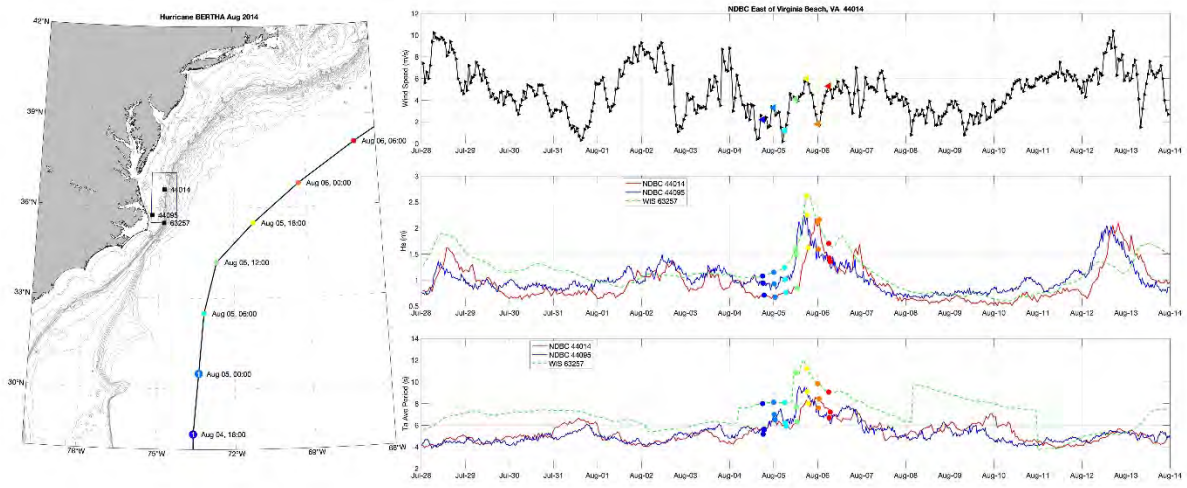

Figure 4-43 – Same Figure 4-35, but for August 2014 Hurricane Bertha.

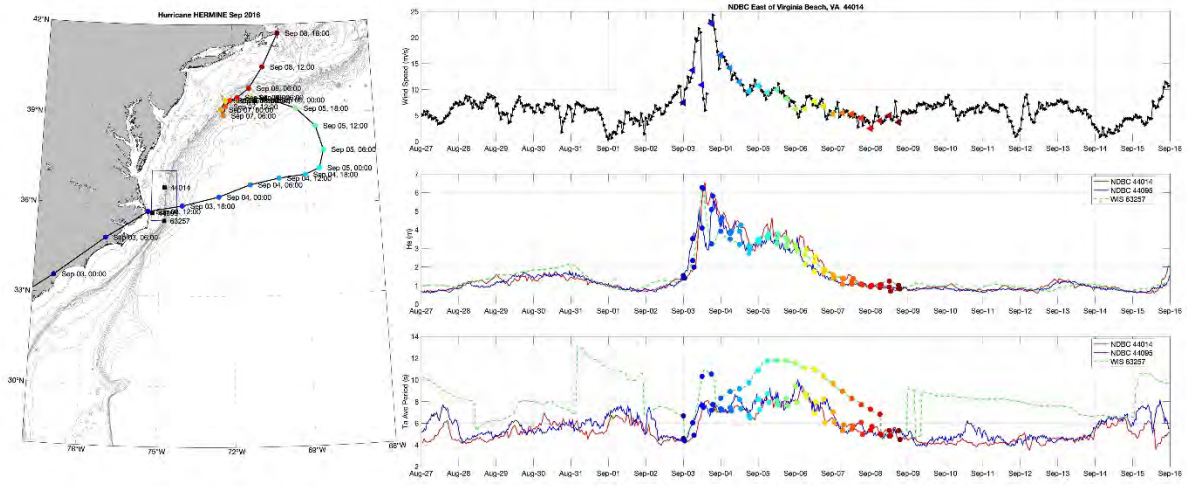

Figure 4-44 – Same Figure 4-35, but for September 2016 Hurricane Hermine.

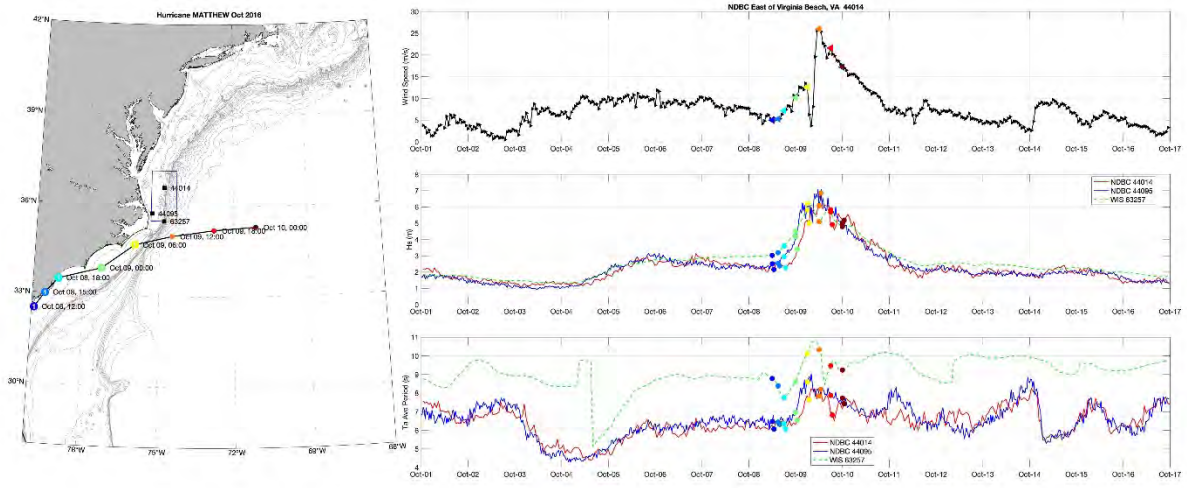

Figure 4-45 – Same Figure 4-35, but for October 2016 Hurricane Matthew.

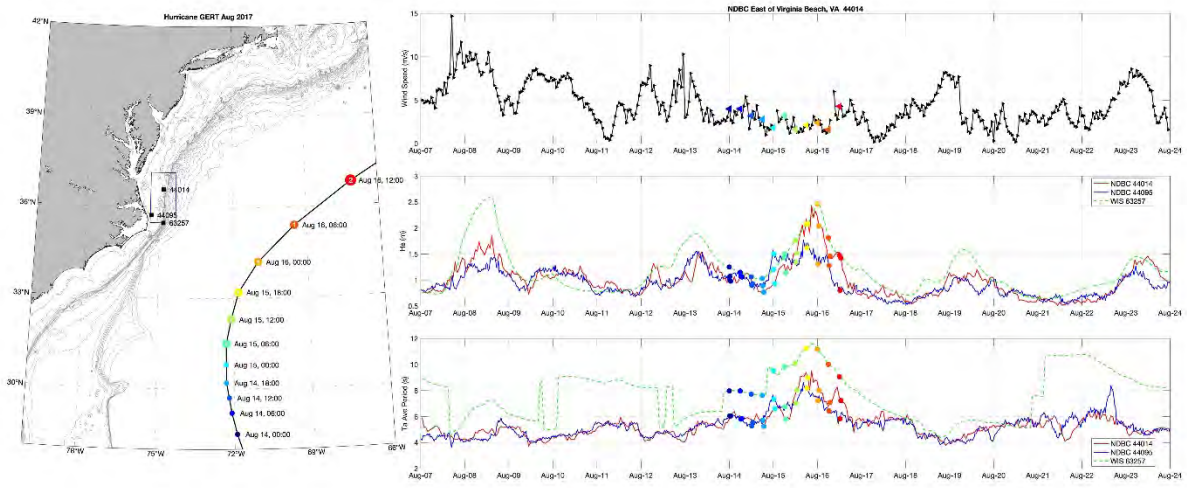

Figure 4-46 – Same Figure 4-35, but for August 2017 Hurricane Gert.

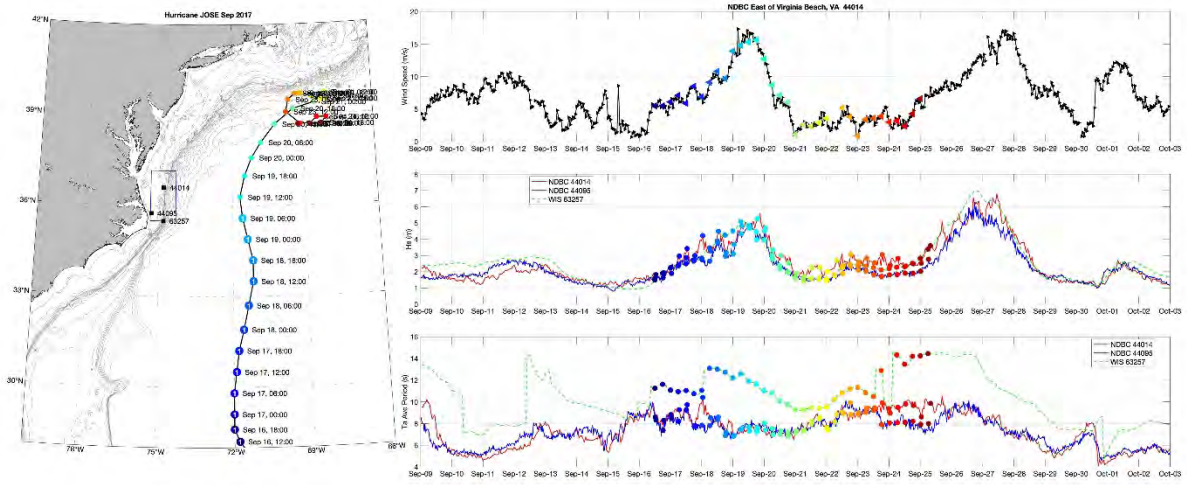

Figure 4-47 – Same Figure 4-35, but for September 2017 Hurricane Jose.

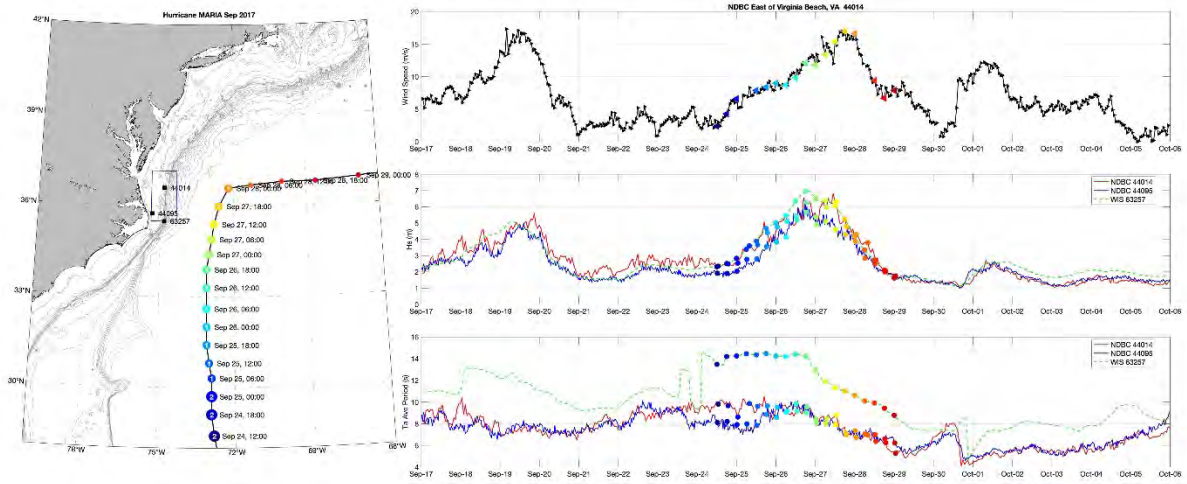

Figure 4-48 – Same Figure 4-35, but for September 2017 Hurricane Maria.

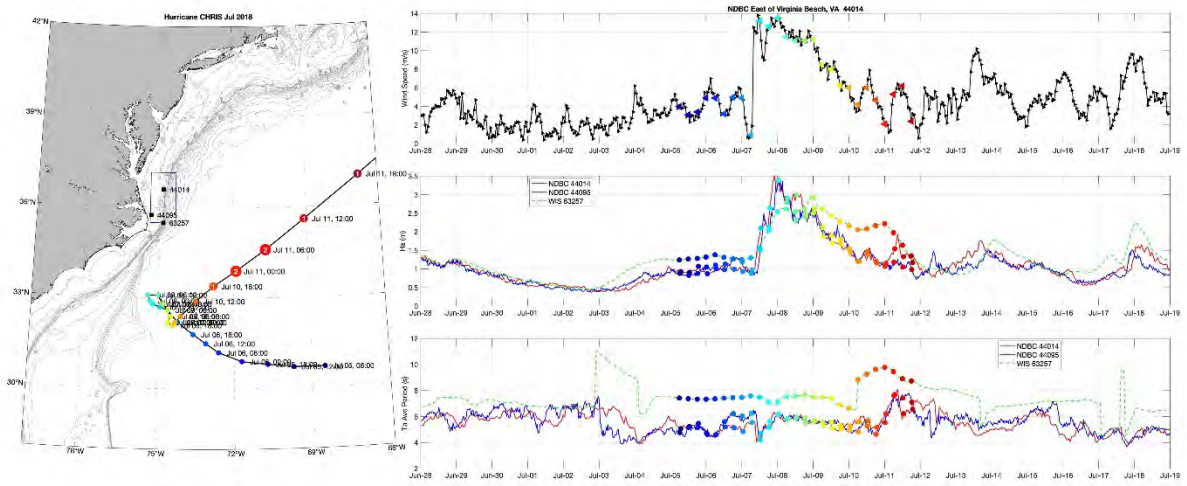

Figure 4-49 – Same Figure 4-35, but for July 2018 Hurricane Chris.

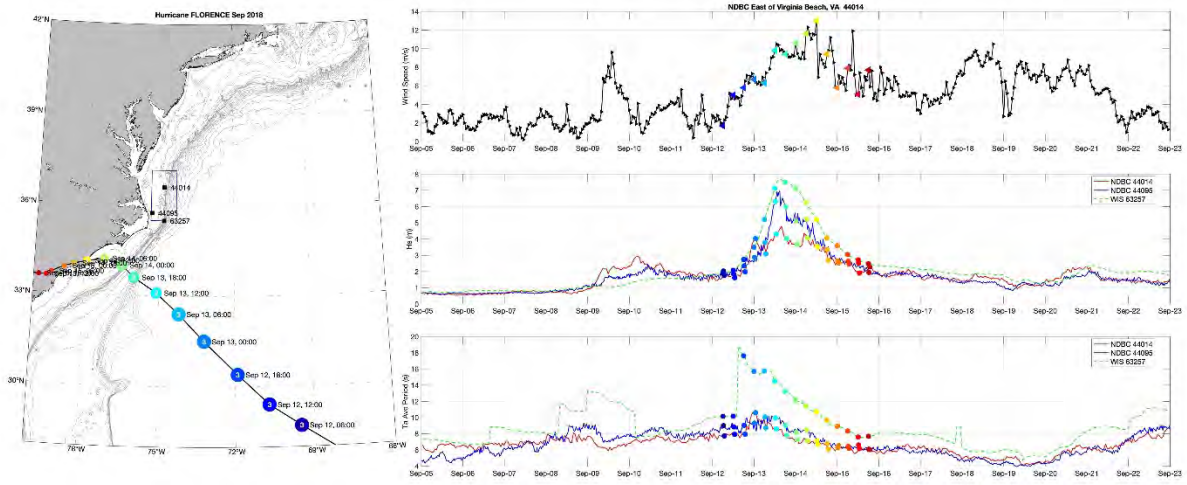

Figure 4-50 – Same Figure 4-35, but for September 2018 Hurricane Florence.

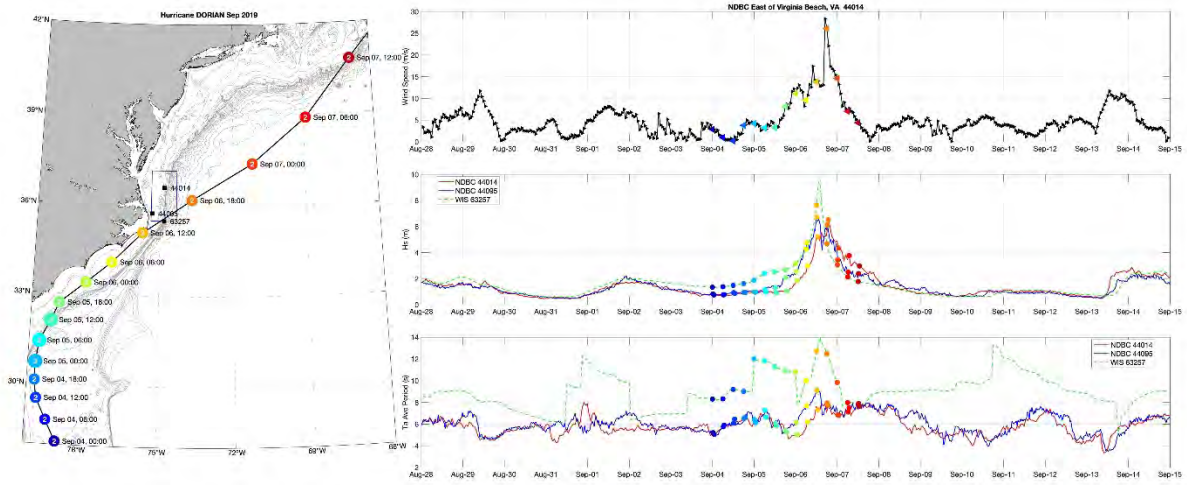

Figure 4-51 – Same Figure 4-35, but for September 2019 Hurricane Dorian.

Nor’easters

Nor’easters are massive storms generally without a clearly defined eye, but with a low-pressure core and winds circling to the right (i.e. counterclockwise). The warm air from the storm interacts with the cold air as it moves northeast. As these storms move northward, wave periods tend to stay long as swell continues to be generated from Greenland. Nor’easters can cause severe snowstorms, heavy rain, gale force winds, and excessive flooding.

Between 2000-2017, there were nine major nor’easters in the Mid-Atlantic Bight (Table 4-6). The maximum significant wave height was 7.3 meters during Winter Storm Grayson in 2018. The maximum wave period was 11.7 seconds, during Winter Storm Riley. The blizzard of 2018 (Jan 2-6) was a five-year storm event; all other storms were less than a five-year storm event. Note that the two longest wave periods were associated with slow-moving winter storms (Riley, 2018; Jonas 2016). The largest wave heights were associated with a winter storm (Grayson, 2018) and a hurricane (Ida, 2009).

Table 4-6 – Noteworthy Nor’easters in the Mid-Atlantic Bight between 2000-2021 based on historical data records. Wind and wave data from NDBC Buoy.

Year	Name	Date	Maximum wind speed m/a	Peak Hs	Peak Ta	Storm event
2003	President’s Day Storm II	Feb 14-19	16.3	5.77	8.6	1
2009	Nor’ Ida (remnants of Hurricane Ida in Gulf)	Nov 11-17	19	7.06	9.71	4
2010	Blizzard of 2010 (severe, long-lasting blizzard)	Dec 5-15	N/A	4.48	7.74	>1
2011	Blizzard of 2011 (first of two, back-to-back)	Jan 8-13	N/A	3.76	7.42	>1
2011	Blizzard of 2011 (second of two, back-to-back)	Jan 25-27	N/A	3.99	7.88	>1
2015	Blizzard of 2015	Jan 23-31	17.4	4.59	8.71	>1
2016	Winter Storm Jonas, Snowzilla, The Blizzard of 2016	Jan 19-29	19.3	6.13	10.32	2
2018	Winter Storm Grayson, Blizzard of 2018, Storm Brody	Jan 2-6	26.2	7.31	8.44	5
2018	Winter storm Riley (Nor’easter)	Mar 1-5	22.1	6.75	11.73	3

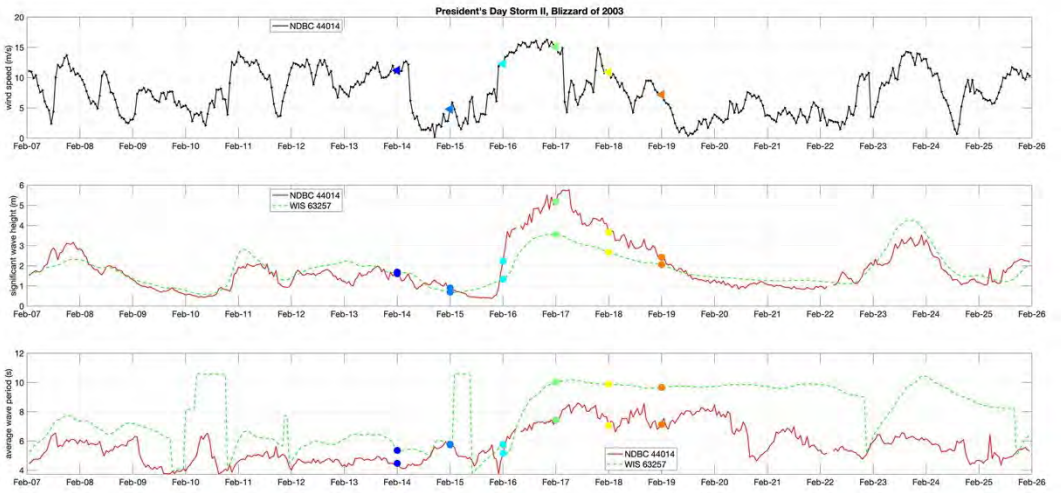

Figure 4-52 – 2003 President's Day Storm II Nor'easter wind speed (m s^{-1}) top panel; significant wave height (m) middle panel; wave period (sec) bottom panel. The figures span 7-days prior and 7-days post storm dates with colored markers marking the storm dates. The wind (black line) and wave (red line) data are from NDBC Station 44014. The green dashed line is hindcast data from the Wave Information Study (WIS). Blank panels indicate that no data were available.

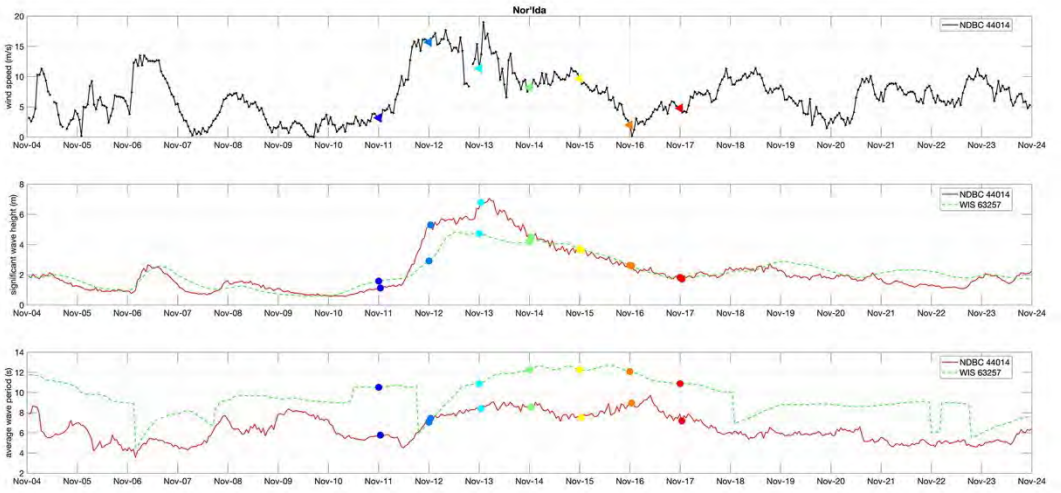

Figure 4-53 – Same as Figure 4-52, but for 2009 Ida Nor'easter.

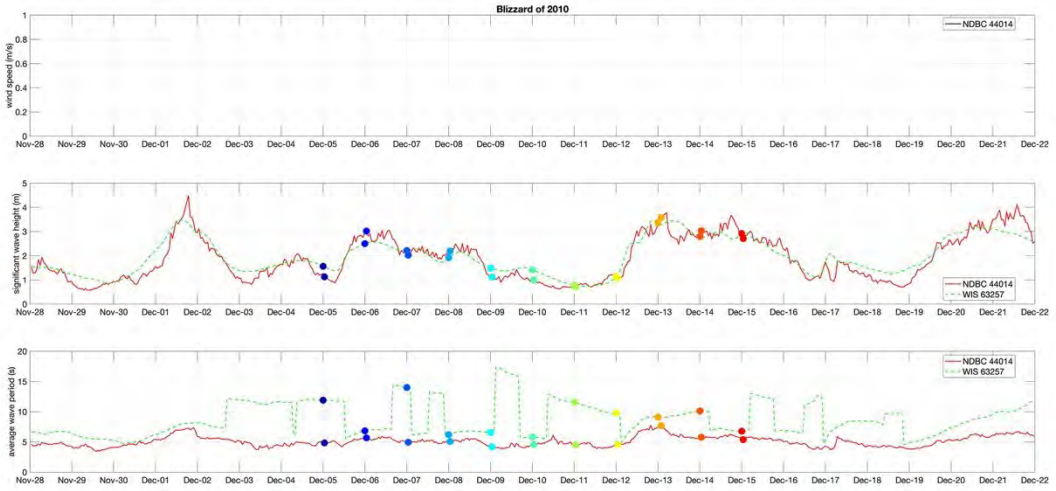

Figure 4-54 – Same as Figure 4-52, but for 2010 Blizzard.

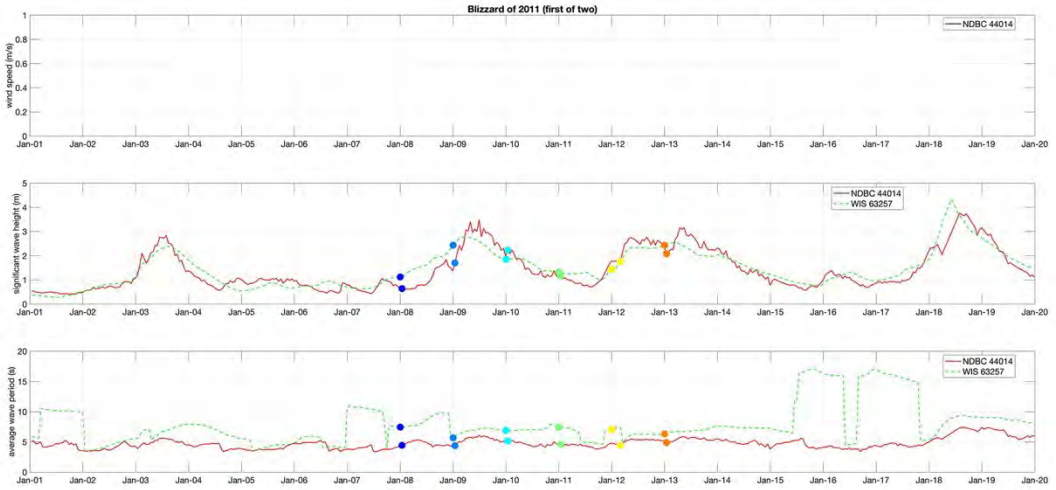

Figure 4-55 – Same as Figure 4-52, but for 2011 first Blizzard.

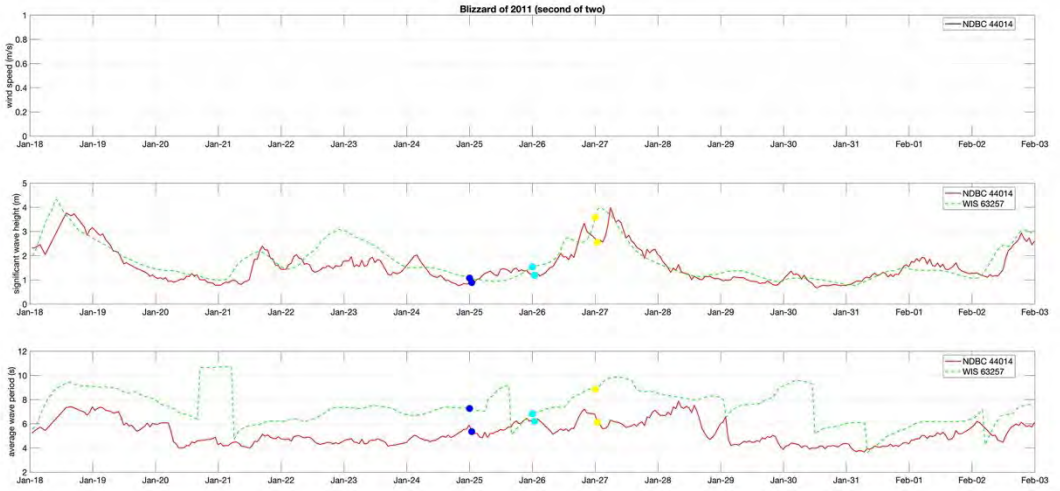

Figure 4-56 – Same as Figure 4-52, but for 2011 second Blizzard.

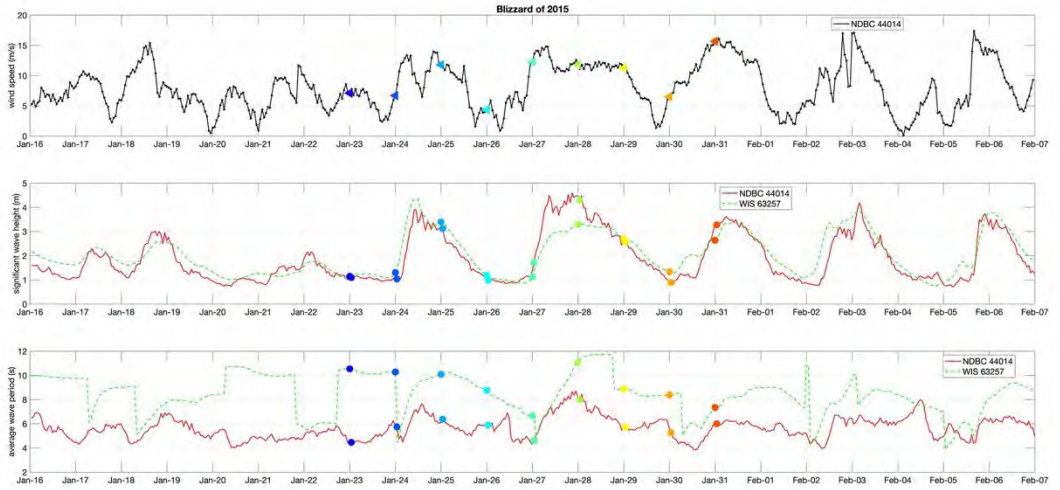

Figure 4-57 – Same as Figure 4-52, but for 2015 Blizzard.

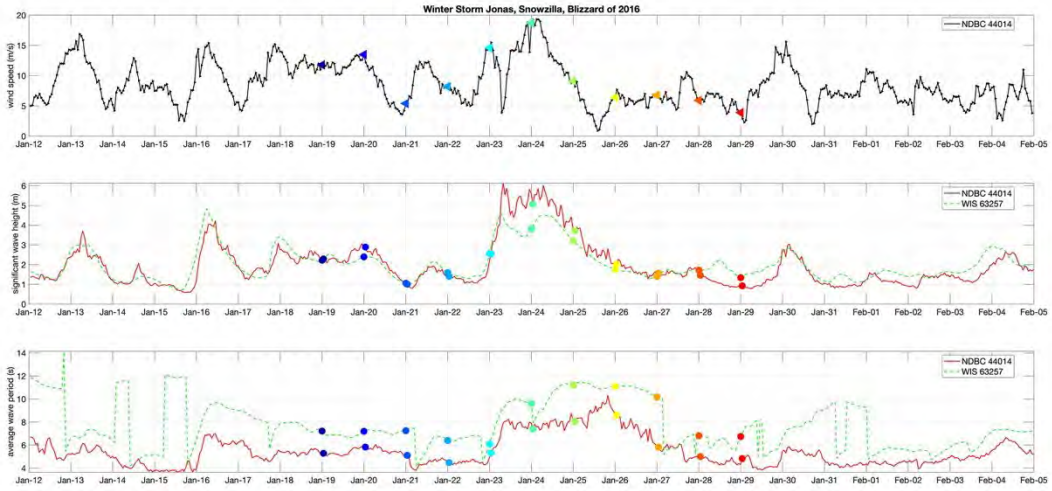

Figure 4-58 – Same as Figure 4-52, but for 2016 Winter Storm Jonas Blizzard, (also named Snowzilla).

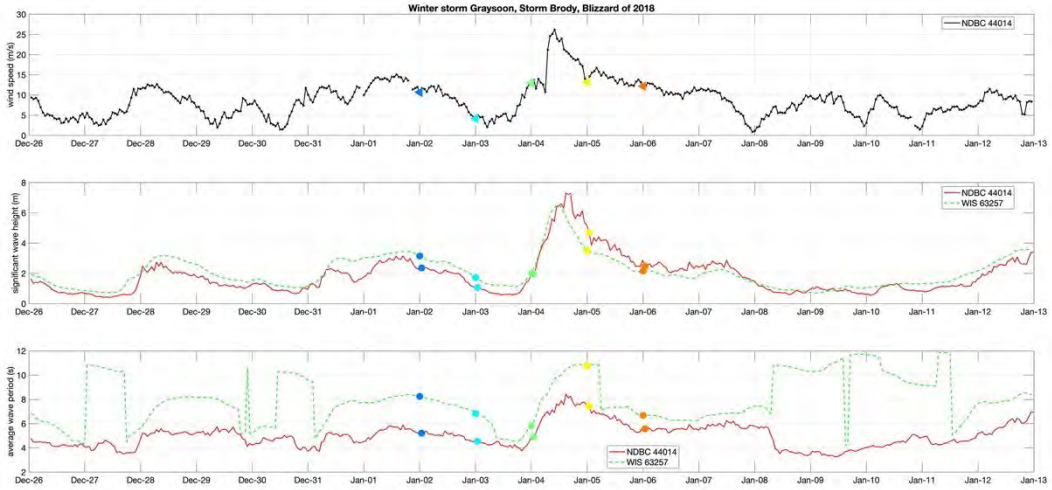

Figure 4-59 – Same as Figure 4-52, but for 2018 Blizzard Winter Storm Grayson (also named Storm Brody).

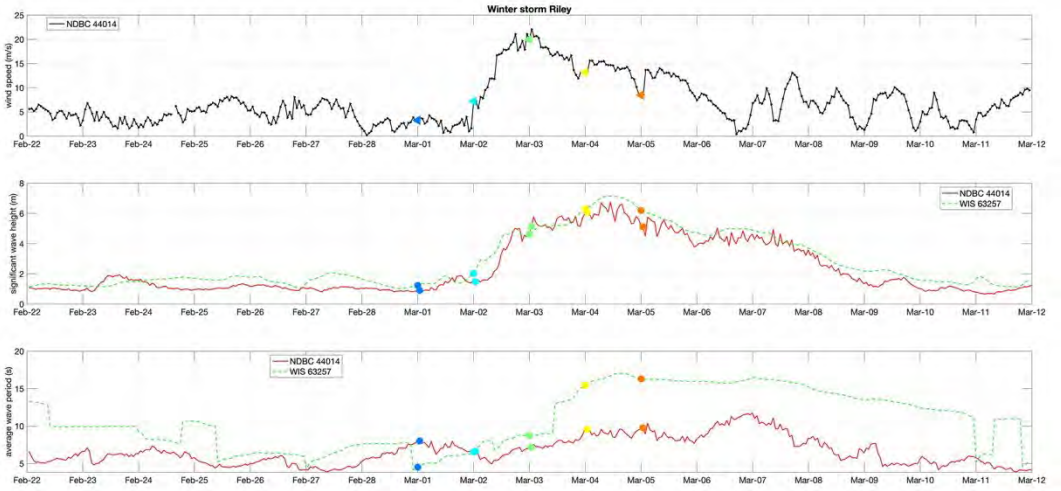

Figure 4-60 – Same as Figure 4-52, but for 2018 Nor'easter Winter Storm Riley.

It is worth noting that the PEACH AR-33 Cruise Report (Seim et al., 2018) stated that Buoys B1 and B2 were heavily damaged due to strong storms, particularly Winter Storm Riley (March 2018) and Hurricane Florence (September 2018), with a number of sensors damaged or missing. The PEACH Mooring report noted that mooring A3 moved downslope from 94 meters to 108 meters March 4, 2018 (during Winter Storm Riley). A disturbance in the bottom pressure of A1 also occurs March 4, 2018, although not as pronounced.

4.4. Solar radiation

Solar radiation (also known as shortwave radiation) data was available from NDBC Buoy #41035 located at inner Onslow Bay, NC, Figure 4-61 and Table 4-7. The data provided is the mean shortwave radiation (W/m^2) for the preceding hour with a sample frequency of 2Hz. As expected, the highest daily averaged values are in May and June; the lowest are December and January (Figure 4-62).

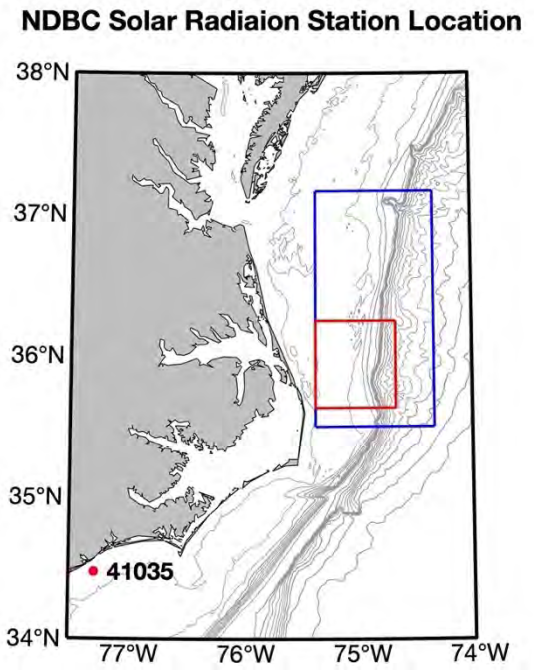

Figure 4-61 – NDBC Buoy 41035 location which provided shortwave solar radiation data for the site characterization.

Table 4-7 – Temporal and spatial information for NDBC Buoy 41035 and the reanalysis data from the Copernicus Climate Data Store (Hersbach, et al., 2018) used for the shortwave solar radiation data.

NDBC Buoy	Name	Location	Dates
41035	Onslow Bay Inner, NC	34.476 N, 77.280 W	Apr 1, 2006 - Sep 30, 2008 Apr 15, 2010 - Nov 30, 2010 Jan 1, 2011 - Aug 22, 2011
Reanalysis	Copernicus (CDS)	34.470 N, 77.300 W	Jan 1, 2006 - Dec 31, 2021

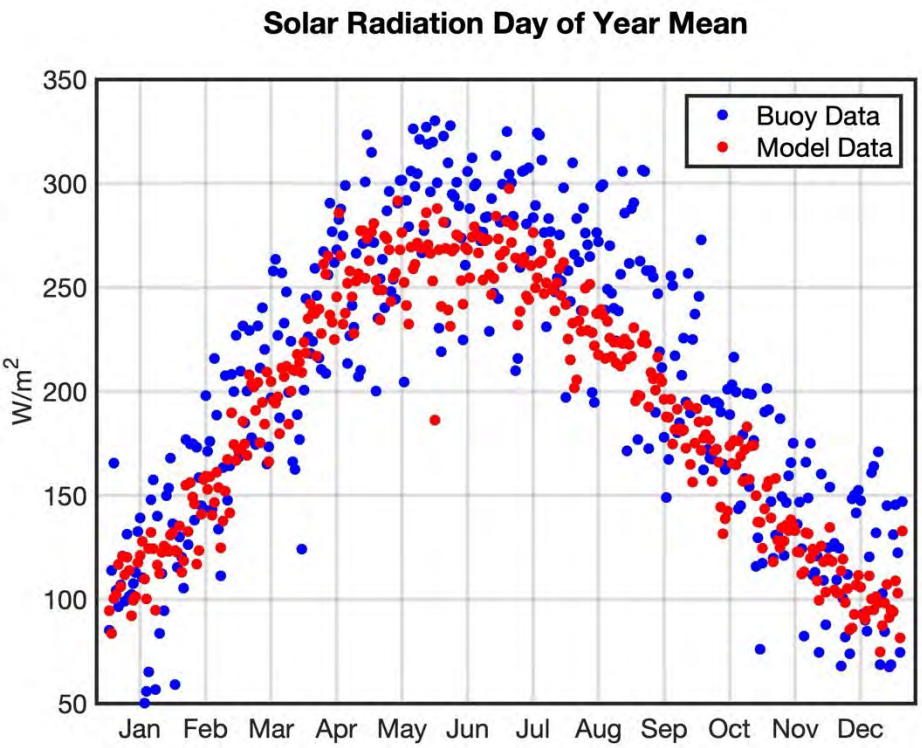

Figure 4-62 – Mean day of year for measured shortwave radiation (blue dots) and reanalysis shortwave radiation (red dots).

Mean one-hour surface downward shortwave radiation flux reanalysis data was downloaded from Copernicus Climate Data Store (Hersbach, et al., 2018). This parameter includes both direct and diffuse solar radiation. The reanalysis data has been mapped to a 0.25 deg x 0.25 deg grid. The data downloaded was from the closest location to Buoy Station 41035 (Table 4-7), starting January 1, 2006, until December 31, 2021. The model data follows the same trend of higher values in May and June and lowest values in December and January (Figure 4-63).

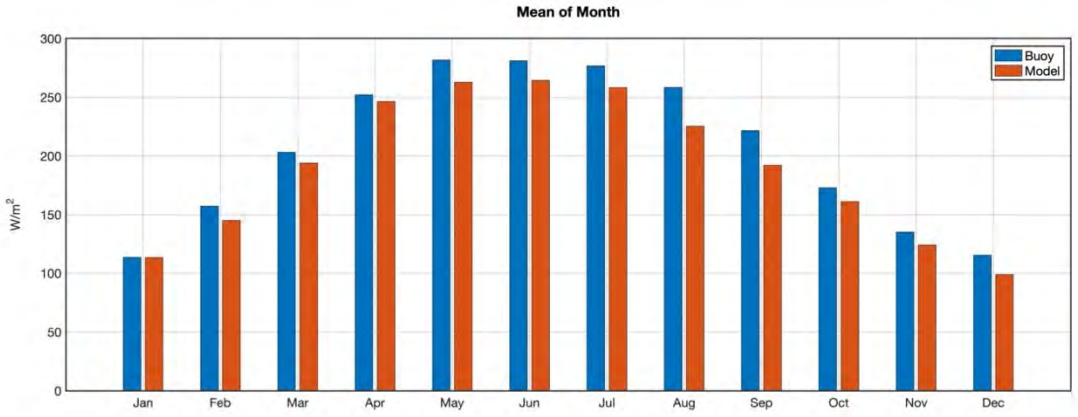

Figure 4-63 – Mean by month of year for measured shortwave radiation data (blue bars) and reanalysis shortwave radiation (red bars).

Directly comparing the measured data with the model data showed an 80% correlation between the two datasets (Figure 4-64). This high correlation supports using the reanalysis data for the site characterization. A sample of hourly data for the months of January and July of 2007 gives a sense of the good correspondence between measured and model radiation for shorter time scales (Figure 4-65).

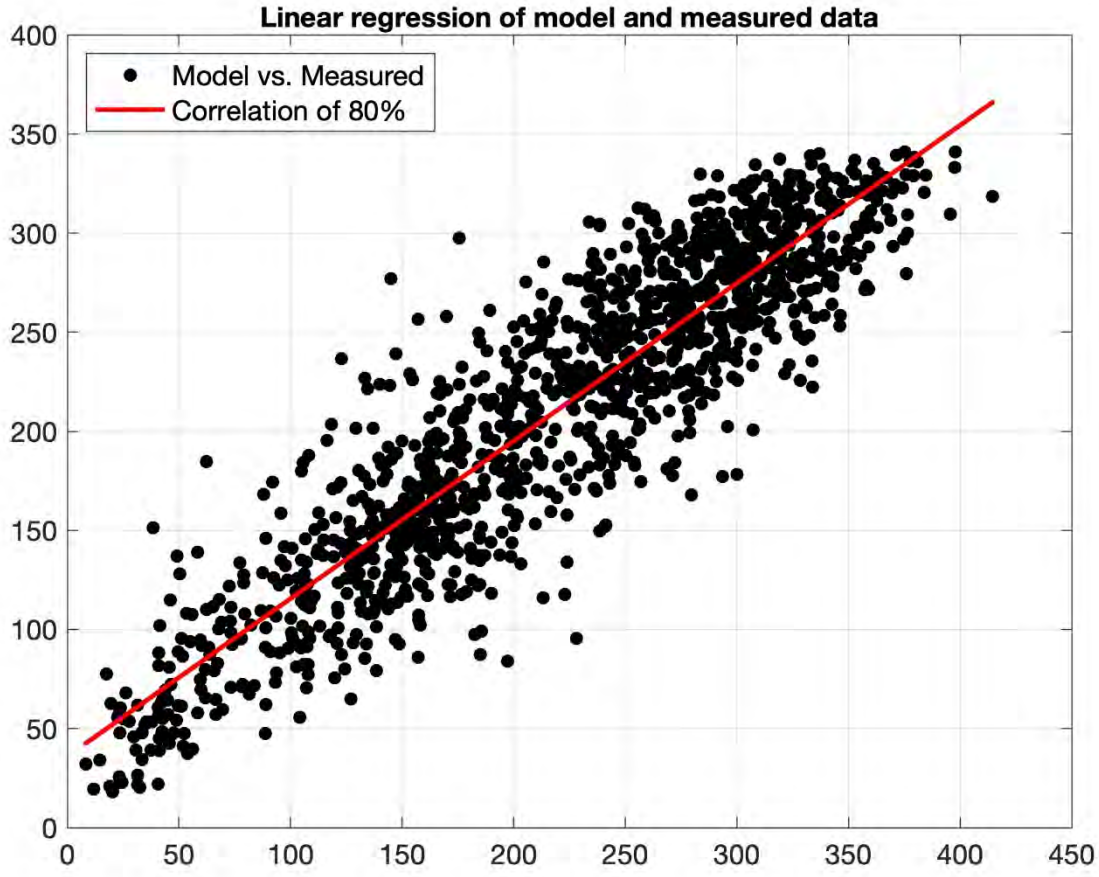

Figure 4-64 – Linear regression analysis comparing daily mean of measured shortwave radiation data from Buoy 41035 and daily mean of reanalysis shortwave radiation from the Copernicus Data Store (Hersbach, et al., 2018) for the same days. The data show an 80% correlation.

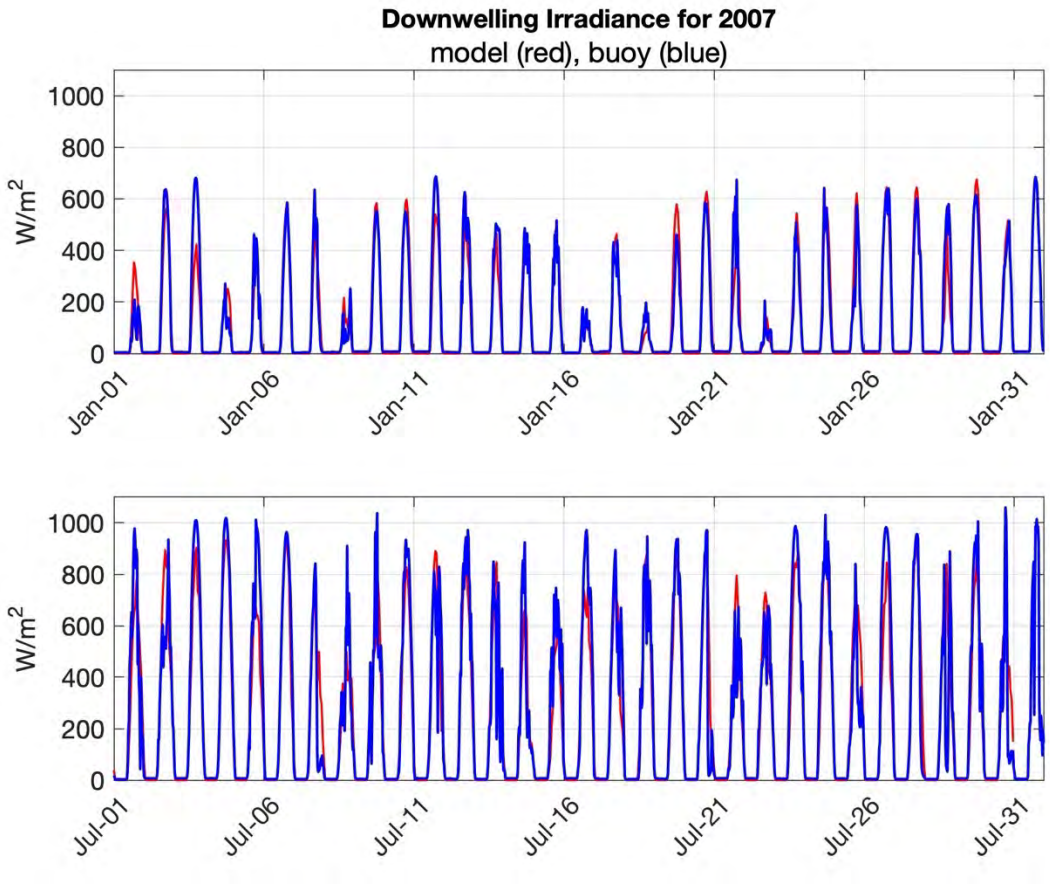

Figure 4-65 – Comparison of hourly downwelling solar irradiance for buoy data (blue) and reanalysis data (red) for the months of January 2007 and July 2007. As expected, the January values are lower on average than the July values.

5.0 References

Data Sources

Army Corps of Engineers, Wave Information Study, https://wis.erdc.dren.mil/

Coastal Data Information Program, https://cdip.ucsd.edu

GEBCO Compilation Group (2022) GEBCO 2022 Grid (doi:10.5285/e0f0bb80-ab44-2739-e053-6c86abc0289c)

Hersbach, H., Bell, B., Berrisford, P., Biavati, G., Horányi, A., Muñoz Sabater, J., Nicolas, J., Peubey, C., Radu, R., Rozum, I., Schepers, D., Simmons, A., Soci, C., Dee, D., Thépaut, J-N. (2018): ERA5 hourly data on single levels from 1959 to present. Copernicus Climate Change Service (C3S) Climate Data Store (CDS). (Accessed on 19-Dec-2022), https://doi.org/10.24381/cds.adbb2d47

NOAA National Centers for Environmental Information Bathymetric Data Viewer, Multibeam Bathymetry Mosaic, https://www.ncei.noaa.gov/maps/bathymetry/

NOAA National Centers for Environmental Information (2022). Coastal Relief Models (CRMs) [crm_vol2.nc]. NOAA National Centers for Environmental Information. https://doi.org/10.25921/5ZN5-KN44. Accessed 2022-08-19. (Formerly National Geophysical Data Center (NGDC))

NOAA National Data Buoy Center (1971). Meteorological and oceanographic data collected from the National Data Buoy Center Coastal-Marine Automated Network (C-MAN) and moored (weather) buoys (historic and real time solar radiation, wave, and wind data). NOAA National Centers for Environmental Information. https://www.ncei.noaa.gov/archive/accession/NDBC-CMANWx.

NOAA National Hurricane Center, https://www.nhc.noaa.gov/

NOAA Office of Coast Survey, Electronic Navigational Charts, Chart: US2EC02M, 'Cape Hatteras to Straits of Florida', scale 1:1,200,000, edition 43.0, August 4, 2023, https://charts.noaa.gov/InteractiveCatalog/nrnc.shtml

Ocean Data View (Schlitzer, Reiner, odv.awi.de, 2021)

Tozer, B, Sandwell, D. T., Smith, W. H. F., Olson, C., Beale, J. R., & Wessel, P. (2019). Global bathymetry and topography at 15 arc sec: SRTM15+. Distributed by OpenTopography. https://doi.org/10.5069/G92R3PT9. Accessed: 2022-08-18

U.S. Geological Survey Current Water Data for the Nation Database, online at URL: https://waterdata.usgs.gov/nwis/rt

U.S. Geological Survey East-Coast Sediment Texture Database, online at URL: http://woodshole.er.usgs.gov/project-pages/sediment/

World Ocean Database (https://www.ncei.noaa.gov/products/world-ocean-database)

Literature Cited

Berger, T. J., W. C. Boicourt, J. H. Churchill, P. Hamilton, R. J. Wayland, and D. R. Watts, 1994: A physical oceanographic field program offshore of North Carolina. Science Applications International Corporation Tech. Rep. MMS 94, 463 pp.

Buffitt, D., A. Plueddemann and S.N. White, 2023. CGSN Site Design: Pioneer Mid-Atlantic Bight Array, Ocean Observatories Initiative, Document Control No. 3210-00008, 28 pp.

Coles, S.G. (2001) An Introduction to Statistical Modeling of Extreme Values. Springer Series in Statistics. https://doi.org/10.1007/978-1-4471-3675-0

Conley, M.F., M.G. Anderson, L. Geselbracht, R. Newton, K.J. Weaver, A. Barnett, J. Prince and N. Steinberg. 2017. The South Atlantic Bight Marine Assessment: Species, Habitats and Ecosystems. The Nature Conservancy, Eastern Conservation Science. (SABMA_Report_26Dec2017.pdf, https://www.conservationgateway.org/ConservationByGeography/NorthAmerica/UnitedStates/edc/reportsdata/marine/sabma/sabma/Pages/default.aspx)

Glen Gawarkiewicz & Albert J. Plueddemann (2020) Scientific rationale and conceptual design of a process-oriented shelfbreak observatory: the OOI Pioneer Array, Journal of Operational Oceanography, 13:1, 19-36, DOI: 10.1080/1755876X.2019.1679609

Haines, S., M. Muglia, F. Bahr, B. Hogue, P. Taylor, III, N. DeSimone, G. Matthias, 2022. Mooring Data Report for the Processes driving Exchange at Cape Hatteras (PEACH) Project. Department of Marine Sciences, University of North Carolina. Technical Report. https://zenodo.org/record/6390566#.ZCRpBezML9s

Lentz, S., M. Carr, and T. H. C. Herbers, 2001. Barotropic Tides on the North Carolina Shelf. *Journal of Physical Oceanography*, Volume 31, Pages 1843–1859, https://doi.org/10.1175/1520-0485(2001)031<1843:BTOTNC>2.0.CO;2.

Lentz, S. J., 2008a. Observations and a Model of the Mean Circulation over the Middle Atlantic Bight Continental Shelf. *Journal of Physical Oceanography*, Volume 38, Issue 6, Pages 1203–1221, https://doi.org/10.1175/2007JPO3768.1.

Lentz, S. J., 2008b. Seasonal Variations in the Circulation over the Middle Atlantic Bight Continental Shelf. *Journal of Physical Oceanography*, Volume, 38, Issue 7, Pages 1486–1500, https://doi.org/10.1175/2007JPO3767.1.

Lentz, S. J., M. Fewings, P. Howd, J. Fredericks, and K. Hathaway, 2008. Observations and a Model of Undertow over the Inner Continental Shelf. *Journal of Physical Oceanography,* Volume 38, Issue 11, Pages 2341–2357, https://doi.org/10.1175/2008JPO3986.1.

McDougall, T.J. and P.M. Barker. Getting started with TEOS-10 and the Gibbs Seawater (GSW) Oceanographic Toolbox, 28pp., SCOR/IAPSO WG127, ISBN 978-0-646-55621-5 (2011).

McMullen, K.Y., Paskevich, V.F., and Poppe, L.J., 2014, GIS data catalog (ver. 3.0, November 2014), in Poppe, L.J., McMullen, K.Y., Williams, S.J., and Paskevich, V.F., eds., USGS east-coast sediment analysis: Procedures, database, and GIS data, U.S. Geological Survey Open-File Report 2005-1001, available online at http://pubs.usgs.gov/of/2005/1001/.

Roarty, H., S. Glenn, J. Brodie, L. Nazzaro, M. Smith, E. Handel, et al. (2020). Annual and seasonal surface circulation over the Mid-Atlantic Bight Continental Shelf derived from a

decade of High Frequency Radar observations. *Journal of Geophysical Research: Oceans,*125, e2020JC016368. https://doi.org/10.1029/2020JC016368

Sandwell, D.T., A.B. Watts, P. Wessel, and W.H.F. Smith (2019). The Marine Gravity Field: From Ships to Satellites, *AGU Fall Meeting Abstracts*, December 2019, https://ui.adsabs.harvard.edu/abs/2019AGUFM.G54A..04S

Seim, H.E. D. Savidge, M. Andres, J. Bane, C. Edwards, G. Gawarkiewicz, R. He, R.E. Todd, M. Muglia, J. Zambon, L. Han, and S. Mao, 2022. Overview of the Processes Driving Exchange at Cape Hatteras Program. *Oceanography*, 35(2), 6-17. https://doi.org/10.5670/oceanog.2022.205

Seim, H., M. Andres, P. Robbins, S. Haines, C. Edwards, J. Zambon, F. Bahr, C. Clayson, J. Edson, M. Muglia (2018) AR-33 Cruise Report: PEACH Array Recovery Cruise, November 16-28, 2018

Thomas N., A. P. Pertiwi, D. Traganos, D. Lagomasino, D. Poursanidis, S. Merono, and L. Fatoyinbo, 2021. Space-Borne Could-Native Satellite-Derived Bathymetry (SDB) models using ICESat-2 and Sentinel -2., *Geophysical Research Letters*, https://doi.org/10.1029/2020GL092170

Tozer, B., D.T. Sandwell, W.H.F. Smith, C. Olson, J.R. Beale, & P. Wessel, 2019. Global bathymetry and topography at 15 arc sec: SRTM15+. *Earth and Space Science*, 6, 1847– 1864. https://doi.org/10.1029/2019EA000658

Wallace, E. J., L.B. Looney, & D. Gong, 2018. Multi-decadal trends and variability in temperature and salinity in the Mid-Atlantic Bight, Georges Bank, and Gulf of Maine. *Journal of Marine Research*, 76, 163–215. https://scholarworks.wm.edu/vimsarticles/1860